Master's thesis

NTNU
Norwegian University of Science and Technology
Faculty of Engineering
Department of Civil and Environmental Engineering

Agnete Rogstad

Empirical and Numerical Analysis of the Retrogression in the Gjerdrum Landslide

Master's thesis in Civil and Environmental Engineering
Supervisor: Gustav Grimstad
Co-supervisor: Quoc Anh Tran
June 2022

NTNU
Norwegian University of Science and Technology

Agnete Rogstad

Empirical and Numerical Analysis of the Retrogression in the Gjerdrum Landslide

Master's thesis in Civil and Environmental Engineering
Supervisor: Gustav Grimstad
Co-supervisor: Quoc Anh Tran
June 2022

Norwegian University of Science and Technology
Faculty of Engineering
Department of Civil and Environmental Engineering

NTNU
Norwegian University of
Science and Technology

Preface

This master's thesis is written during spring 2022 for the Geotechnical Division at the Norwegian University of Science and Technology (NTNU). The project was proposed by Gustav Grimstad and Quoc Anh Tran.

Trondheim, 2022-06-10

Agnete Rogstad

Acknowledgment

I would like to thank my supervisor, Gustav Grimstad, for great help with this thesis. He has provided suggestions, guidance and fruitful discussions whenever needed. Furthermore, my co-supervisor, Quoc Anh Tran, has provided immense help to run the MPM simulations, and has been of great overall support. I would also like to thank Ivan Depina for help with the shear strength distribution for the 3D MPM simulations, and Fabricio Fernández (Pontifical Catholic University of Rio de Janeiro) for help with the numerical geometry for the 3D MPM simulations. Lastly, I greatly appreciate the help from Ellen Davis Haugen (Norwegian Water Resources and Energy Directorate) for providing data for the soil layering in Gjerdrum.

A.R.

Abstract

A large sensitive clay landslide occurred on the 30th of December 2020 in Ask in Gjerdrum. Ten people and an unborn child lost their lives, and the slide caused extensive damage to buildings and infrastructure. As a measure to prevent sensitive clay slides, quick clay hazard zones are defined based on the estimated retrogression of potential slides. The larger area of the retrogression extent is defined to be, the larger area will be subjected to restrictions on the construction of buildings and other measures. Therefore, it is desirable to find a balance between the cost of a conservative retrogression extent and the cost to define a more precise retrogression extent. This thesis evaluates empirical and numerical methods to determine the retrogression of the Gjerdrum slide. Furthermore, it determines how the level of detail in the soil layering and the shear strength degradation parameters in the material model affect the retrogression.

Three different levels of detail in soil layering have been used for the empirical criteria. The first one only takes the terrain into account. The second one takes the terrain and bedrock into account. Lastly, the third criterion takes the terrain, bedrock, and sensitive clay layer into account. The Material Point Method is the chosen numerical method because it is suitable for large deformations. The areas defined by the retrogression distances from the empirical criteria are compared to the extent of the slides from the 3D Material Point Method simulations. Two different levels of detail in soil layering were used for the simulations. In addition, 2D Material Point Method simulations were run to investigate the effect of the remolded undrained shear strength, $s_{u,r}$, and the shear strain at 95 % reduced shear strength, γ_{95}.

The 2D simulations showed that γ_{95} affected the retrogression distance. The retrogression was largest for γ_{95} equal to 1. However, γ_{95} equal to 4 gave a longer retrogression distance compared to γ_{95} equal to 2. The retrogression distance was constant for different values of $s_{u,r}$. It should be noted that the retrogression distance mainly appeared controlled by the extent of the sensitive clay layer.

For the 3D simulations, the least detailed soil layering gave the best results. However, the slide extent was larger than in Gjerdrum, and it is considered a conservative approach. The simulations that took the sensitive clay layer into account, showed an initial failure in the slope west of Holmen where the initial slide is believed to have occurred. The simulated slide did not develop into a retrogressive slide because the slide masses had low mobility. Further investigations are recommended to examine if a change in sensitivity parameters or the numerical geometry of the sensitive clay layer gives a different extent of the slide. For the empirical criteria, the most detailed soil layering gave the best results. This criterion corresponded almost precisely to the extent of the Gjerdrum slide. The criterion that took terrain and bedrock into account, corresponded quite well with the equivalent 3D simulation. The most conservative empirical criterion overestimated the retrogression of the Gjerdrum slide. Taking into consideration the necessary resources to perform a Material Point Method simulation, the empirical criteria appear to be the most favorable way to determine the retrogression extent of the Gjerdrum slide.

Sammendrag

Den 30. desember 2020 gikk det et stort kvikkleireskred på Ask i Gjerdrum. Ti personer og et ufødt barn mistet livet, og skredet forårsaket store skader på bygninger og infrastruktur. For å forhindre slike skredhendelser er det opprettet kvikkleiresoner basert på mulig utstrekning til potensielle skred. Jo større utstrekning sonen defineres til å ha, desto større områder blir omfattet av restriksjoner på byggearbeider. Det er ønskelig å finne en balanse mellom kostnaden av en større sone sammenlignet med kostnadene ved å definere en mer presis mulig skredutbredelse. Denne oppgaven evaluerer empiriske og numeriske metoder for definere skredutbredelsen for skredet i Gjerdrum. Videre undersøker den hvordan ulik lagdeling og skjærstyrkeparametre påvirker retrogresjonslengden.

Tre ulike detaljnivåer av lagdeling er benyttet for de empiriske kriteriene. Det første kriteriet tar kun hensyn til terrenget. Det andre kriteriet tar hensyn til terrenget og grunnfjellet. Til slutt tar det tredje kriteriet hensyn til terrenget, grunnfjellet og plassering og utbredelse av kvikkleirelaget. Skredutbredelsen definert av retrogresjonslengdene sammenlignes med utbredelsen av de simulerte 3D-skredene ved bruk av *Material Point Method*. For simuleringene er de to siste detaljnivåene av lagdelingen benyttet. I tillegg er det kjørt 2D analyser for å undersøke effekten av den omrørte udrenerte skjærstyrken, $s_{u,r}$, og skjærtøyning når styrken er 95 % redusert, γ_{95}.

2D simuleringene viste at γ_{95} påvirket retrogresjonslengden. Lengden var størst når γ_{95} var lik 1. γ_{95} lik 4 ga en lengre retrogresjonslengde enn γ_{95} lik 2, noe som var uventet. Retrogresjonslengden var lik for ulike verdier av $s_{u,r}$. Det er viktig å påpeke at utbredelsen av kvikkleirelaget så ut til å være den mest styrende faktoren for retrogresjonslengden.

For *Material Point Method*-simuleringene ga den minst detaljerte lagdelingen det beste resultatet. Likevel ga den en utbredelse som var større enn skredet i Gjerdrum, og det kan derfor regnes som en konservativ tilnærming. Simuleringene som tok hensyn til kvikkleirelaget viste at initialskredet gikk ved Holmen, slik som for skredet i Gjerdrum. Skredet i simuleringen utviklet seg ikke til et retrogressivt skred fordi skredmassene hadde av mobilitet. Videre analyser for å undersøke om en endring i sensitivitetsparametrene eller en annen numerisk geometri av kvikkleirelaget gir en annen skredutbredelse er anbefalt. For de empiriske kriteriene ga den mest detaljerte lagdelingen det beste resultatet. Dette kriteriet viste en svært god tilnærming til utbredelsen av skredet i Gjerdrum. Det andre kriteriet som tok hensyn til terreng og grunnfjell hadde en utbredelse som samsvarte godt resultatet fra den tilsvarende simuleringen. Det mest konservative empiriske kriteriet overestimerer utbredelsen av skredet. Tatt i betraktning ressursbruken som kreves for å kjøre *Material Point Method*-simuleringer fremstår de empiriske kriteriene som bedre egnet for å definere skredutbredelsen i Gjerdrum.

Contents

List of Figures

List of Tables

List of Acronyms

DTM Digital Terrain Model.

FEM Finite Element Method.

GIMP Generalized Interpolation Material Point Method.

MPM Material Point Method.

NIFS Natural hazards: Infrastructure, Floods and Slides.

NTNU Norwegian University of Science and Technology.

NVE Norwegian Water Resources and Energy Directorate.

OCR Over Consolidation Ratio.

List of Symbols

Latin letters

Symbol	Description	Unit
a	Attraction	kPa
b	Depth of sensitive clay layer above critical surface	m
c	Cohesion	kPa
D	Depth from terrain to critical surface	m
E	Young's modulus	MPa
E_u	Undrained Young's modulus	MPa
G	Shear modulus	MPa
H	Slope height	m
I_L	Liquidity index	-
I_P	Plasticity index	-
K	Bulk modulus	MPa
L	Retrogression distance	m
N_s	Janbu's stability number	-
Q	Quickness	%
S_t	Sensitivity	-
s_u	Undisturbed undrained shear strength	kPa
$s_{u,ref}$	Reference undisturbed undrained shear strength	kPa
$s_{u,r}$	Remolded undrained shear strength	kPa
w_L	Liquid limit	%

Greek letters

Symbol	Description	Unit
ε	Normal strain	-
γ	Bulk unit weight	-
γ	Shear strain	-
γ_e	Shear strain at maximum shear stress	-
γ_{95}	Shear strain at 95 % reduced shear strength	-
ν	Poisson's ratio	-
ν_u	Undrained Poisson's ratio	-
σ	Normal total stress	kPa
σ'	Normal effective stress	kPa
σ_1	Highest principal stress	kPa
σ_1	Lowest principal stress	kPa
τ	Shear stress	kPa
τ_f	Shear strength	kPa
φ	Friction angle	$^\circ$
ψ	Dilatancy angle	$^\circ$

Chapter 1

Introduction

This chapter will discuss the background and context of the thesis. Furthermore, the chapter describes the objectives of the research, the approach, and its limitations. A structure of the thesis is also given.

1.1 Background

Large quick clay landslides are of great interest due to the risk of tremendous damage. Retrogressive slides, which develop backward or sideways from the initial slide, often cover large areas and have slide debris that can flow several kilometers. When such slides happen in urban areas, they can cause extreme damage to people, buildings, and infrastructure. The abrupt behavior and lack of warning signs increase the threat of quick clay landslides. This has caused a great interest in understanding the behavior of quick clay and investigating quick clay landslides, in order to improve the hazard and risk management.

After the Rissa landslide in 1978 (Gregersen, 1981), Norway started a national mapping program to detect areas where large quick clay slides may happen. The main objective of the national mapping is to define areas, quick clay hazard zones, where precautions can be made to avoid triggering landslides. To define a hazard zone, the potential extent must be evaluated. The determination of potential retrogression is based on empirical methods, which have been developed over several years. Due to the precautions necessary for construction work in hazard zones, it is desirable to limit these areas as much as possible without compromising on safety.

In addition to empirical criteria, numerical analysis can be used to estimate the extent of sensitive clay landslides and their development. The Finite Element Method (FEM) has been used to calculate the critical failure surface in slope stability. The FEM is not suitable for large deformations due to the mesh distortion and is therefore not suitable to calculate the post-failure of sensitive clay landslides. To simulate the behavior of sensitive clay landslides both pre-failure and post-failure, a robust numerical technique is required. Particle-based methods such as the Material Point Method (MPM) avoid mesh

distortion. If combined with an appropriate constitutive soil model, it can simulate both a solid-like and fluid-like material behavior. The MPM has been used for several 2D analyses of former landslides to calculate both retrogression and run-out. Recent studies include landslides in Wangjiayan, China (Li et al., 2016), Vajont, Italy, and Tokai-Hokuriku Expressway, Japan (Llano-Serna, Farias, and Pedroso, 2016) and Sainte-Monique, Canada (Tran and Sołowski, 2019). A 3D simulation of the run-out of the Hongshiyan landslide has also been performed (Xu et al., 2018), with a pre-defined detachment area.

Both empirical and numerical estimation of the extent of the slide requires knowledge about the area and soil profile. However, the empirical criteria used in Norway can be performed with only the terrain elevation or with the soil layering and calculation of a critical failure surface (Norwegian Water Resources and Energy Directorate, 2019). On the other hand, an MPM simulation of a slide requires extensive knowledge about soil layering and soil parameters in the study area. An MPM simulation also demands high computational capacity. For both methods, different levels of detail in soil layering will presumably affect the retrogression distance, yet it is unknown to what extent. If a less detailed soil layering gives a sufficiently good approximation, it reduces the need for extensive ground investigations. A balance must be made between the resources used to define a smaller, more precise retrogression extent, and to define a too conservative potential retrogression using fewer resources.

The development of a slide in an MPM simulation highly depends on the constitutive soil model. The continuum material model needs to replicate the natural behavior of the soil as accurately as possible. Sensitive clay inhabits a strain softening effect after being loaded to peak strength. This is tightly coupled with the progressive failure in sensitive clay slides. The strain softening is both controlled by how fast the shear degradation happens, and by the remolded shear strength. Wang, Vardon, and Hicks (2016) show that the development of the retrogressive failure and the retrogression extent are dependent on the softening and the residual strength. Thus, the strain softening parameters chosen for the analysis can greatly affect the outcome. A further investigation of how the strain softening affects an MPM simulation with a specified sensitive clay layer may give valuable insight to establish reasonable strain softening parameters.

To examine the difference between empirical methods and an MPM simulation, and what factors control the development and retrogression, it is useful to investigate an actual slide. A large sensitive clay landslide occurred on the 30th of December 2020 in Ask in Gjerdrum. An initial slide developed into a large retrogressive slide with a slide crater of 12 000 m^2 (Ryan et al., 2021). Ten people and an unborn baby lost their lives. Numerous buildings were destroyed, and infrastructure was damaged. After the slide, both Multiconsult and the Norwegian Geotechnical Institute (NGI) have performed ground investigations and laboratory testing in the area. Furthermore, on assignment from the Norwegian Water Resources and Energy Department (NVE), Multiconsult has developed a 3D soil layering model (Leapfrog model). This results in extensive knowledge about the soil layering and available information about the slide.

1.2 Aim and Objectives

This master's thesis aims to investigate which method, the MPM or the empirical criteria, gives the most correct retrogression distance and extent of the Gjerdrum landslide. Furthermore, to investigate how material parameters and levels of detail in soil layering affect the retrogression distance and development of the Gjerdrum landslide.

The main objectives are:

- To compare retrogression distances and development of the slide from the MPM simulations and the empirical criteria to the Gjerdrum landslide.
- To compare how the level of detail in soil layering affects the retrogression in the MPM simulations and the empirical criteria.
- To evaluate the effect of the shear strength parameters, $s_{u,r}$, S_t, and γ_{95}, on retrogression distance and slide development in the MPM simulations.

1.3 Approach

To investigate the potential retrogression in Gjerdrum, information about the soil properties and soil layering is retrieved from relevant reports and the Leapfrog model by Multiconsult. A sensitivity analysis on the parameters γ_{95} and $s_{u,r}$ is performed to evaluate the effect of shear strength material parameters on retrogression distance and slide development. Due to the complexity and higher uncertainty in a 3D MPM analysis, than a 2D MPM analysis, the latter is chosen. The 2D profile is taken from the slope east of Tistilbekken up to Holmen. The initial slide is believed to have taken place here. Either the remolded shear strength or the strain rate when the clay has lost 95 % shear strength is varied. All other parameters are kept constant.

3D MPM simulations are performed to compare how different level of detail in soil layering affects retrogression. Two different soil layering profiles are evaluated. One simulation only accounts for the terrain and bedrock elevation and assumes all masses in between as sensitive clay. The other simulation accounts for the terrain and bedrock elevation and the placement of a sensitive clay layer. All non-specified material between the terrain and the bedrock is defined as non-sensitive clay. The latter simulation is run with the non-sensitive clay layer as perfectly plastic and with a semi-brittle behavior to give a more realistic approach of the soil.

The clay is modeled on a total stress basis. Hence the simulations are performed without a groundwater level, and no pore pressure change is simulated. Furthermore, the slope fails under self-weight for both the 2D and 3D analyses. Meaning that no additional triggering mechanism is necessary. However, for the 2D simulations, the slope fails when the parameters are shifted from drained to undrained. All simulations are run without a predefined detachment area. Therefore, no material will move before an

initial failure occurs.

To compare the 3D MPM simulation with simpler methods to define retrogression, three empirical criteria are used. The first criterion only accounts for terrain elevation, while the second accounts for terrain and bedrock elevation, and the third one accounts for terrain and bedrock elevation and placement of the sensitive clay layer. As the empirical criteria can only be used perpendicular to the contour lines, several profiles are used to determine the retrogression potential for the whole area.

1.4 Limitations

The data used as a basis for the simulations and the empirical criteria are retrieved directly from available reports and the Leapfrog model. It is not performed a thorough critical evaluation of the data and they are used directly for the analyses. Multiconsult (2022) describes the uncertainty of the Leapfrog model. The uncertainty is high in some areas due to few ground investigations, yet this is not discussed further in this thesis. In addition, the interpreted shear strength profiles from Multiconsult (2021a) are used directly. These data are based on interpretations, and they are further simplified and adjusted.

Due to the uncertainty, simplifications, and adjustments of the data, it is important to interpret and use the results keeping the uncertainty in mind.

The analyses have only been performed for the specific area in Gjerdrum where the slide took place. The different topography and different soil layering in other areas might play a significant role for the retrogression. Therefore, the conclusions from this area in Gjerdrum cannot without further evaluation be generalized to apply to other areas.

1.5 Structure

The rest of the thesis is structured as follows:

- **Chapter 2** is a literary review on quick clay and sensitive clay landslides.
- **Chapter 3** presents the Material Point Method and the constitutive material model.
- **Chapter 4** presents the landslide in Gjerdrum.
- **Chapter 5** describes the methods used in the calculations.
- **Chapter 6** presents the results from the calculations.
- **Chapter 7** discusses the findings and results.
- **Chapter 8** concludes and presents recommendations for further work.

Chapter 2

Quick Clay and Quick Clay Landslides

This chapter describes what quick clay is, and how it behaves. Firstly, the geotechnical definition of brittle material and quick clay is explained. Secondly, to understand the behavior of quick clay, the formation of quick clay and its structure are briefly presented. The post-failure behavior, hereby the strain softening effect is in focus. Furthermore, quick clay landslides and in particular retrogressive slides are presented. Criteria to develop retrogressive slides and factors that control retrogression are discussed. Lastly, empirical relations to determine retrogression distances in quick clay mapping in Norway are presented.

2.1 Geotechnical Definition of Brittle Material and Quick Clay

Soils are classified as clay if they contain 15 % particles smaller than 2 µm (Norwegian Geotechnical Society, 2011). Brittle material and quick clay are, according to Norwegian practice, defined by remolded undrained shear strength, $s_{u,r}$. If a soil has $s_{u,r} < 2$ kPa given NS8015 (1.27 kPa given ISO 17892-6:2017), it is considered as brittle material (Norwegian Water Resources and Energy Directorate, 2019). The most extreme version of brittle material is quick clay, which is defined by $s_{u,r} < 0.5$ kPa given NS8015 (0.33 kPa given ISO 17892-6:2017). Due to its structure, brittle material and quick clay are strong when the soil is intact, but can become liquefied when being loaded above its peak strength.

In addition to the current geotechnical definition of brittle material and quick clay by $s_{u,r}$, other parameters are also relevant to indicate quick clay. Common indicators include a water content above the liquid limit, w_L. This corresponds to a liquid index, I_L, above 1. A high sensitivity, S_t, and a low salt content can also be an indication of quick clay.

In this thesis, the term sensitive clay is also used to describe clay that experiences a significant reduction of undrained shear strength after loaded above its peak undrained shear strength.

2.2 Formation and Structure of Quick Clay

Quick clay can be found in Norway, Sweden, Canada, Alaska, Finland, and northern Russia. During the last ice age, Weichselian, these areas were covered by ice shields. When the glacier advanced and withdrew, large amounts of sediments were eroded. During and after deglaciation, these sediments were transported and sedimented. Clay particles are too small to deposit in the fluvial environment and were transported to the seawater.

As clay particles normally have a net negative electrical charge, they will seek to obtain a neutral charge (Mitchell and Soga, 2005). When these particles are suspended in saline water, the surface of the clay minerals will therefore adsorb cations from the saline water. The abundant cation in the seawater is sodium (Na^+). Thus, this is the abundant cation bound to clay minerals. Together with the negatively charged clay mineral surface, the cations make the electrical double layer. The particles' electrical double layer will function as a repulsive force between the particles. Depending on the number of cations bound to the surface, the thickness of the electrical double layer will increase or decrease. This also applies to the repulsive forces between the particles. Attractive forces between the particles stem from van der Waals forces between the atoms in the particles. The attractive forces will cause the clay particles to flocculate and create larger particles. On the other hand, the repulsive forces between similar charges will ensure that the distance between the particles is the largest possible. The edges of the flaty clay particles may have a different charge than the face surface. Depending on the surface charge the structure is built of clay particles with edge-to-face or edge-to-edge. This will give a "card house"-structure and a high void ratio which allows a high water content.

After the ice age, the formerly oppressed land was subjected to isostatic uplift. Marine clay deposits became present above the current sea level. The clay is then subjected to leaching, where groundwater flow removes ions from the pore water. This increases the thickness of the diffuse double layer and the repulsive forces between the particles (Rankka et al., 2004). The clay still has the same structure but can collapse if loaded above its peak shear strength. Due to the low permeability of the clay, this process can take thousands of years. Quick clay is not only dependent on low salt content, but it is also dependent on the ions in the pore water (Rankka et al., 2004). Thus, other factors may influence the ion composition in the pore water such as chemical weathering or organic material. The groundwater can also add ions that make the clay more stable. This process can cause the clay to return from quick clay to stable clay.

2.3 Behavior of Quick Clay

Quick clay is non-linear elastic before failure. Compared to non-sensitive clay quick clay has the same behavior and strength before failure. Hence, the interesting aspect of quick clay is its post-failure behavior.

The quick clay has a viscoplastic behavior. When the quick clay is loaded above its maximum shear strength, the inter-particle repulsive forces in the clay are no longer strong enough to retain the structure of the clay, and it collapses. This will lead to a considerable decrease in the undrained shear strength as the accumulated plastic shear strain increases. This is known as the strain-softening effect, and is illustrated in Figure 2.1. The remolded clay will liquefy, and the clay particles will "flow" in their pore water.

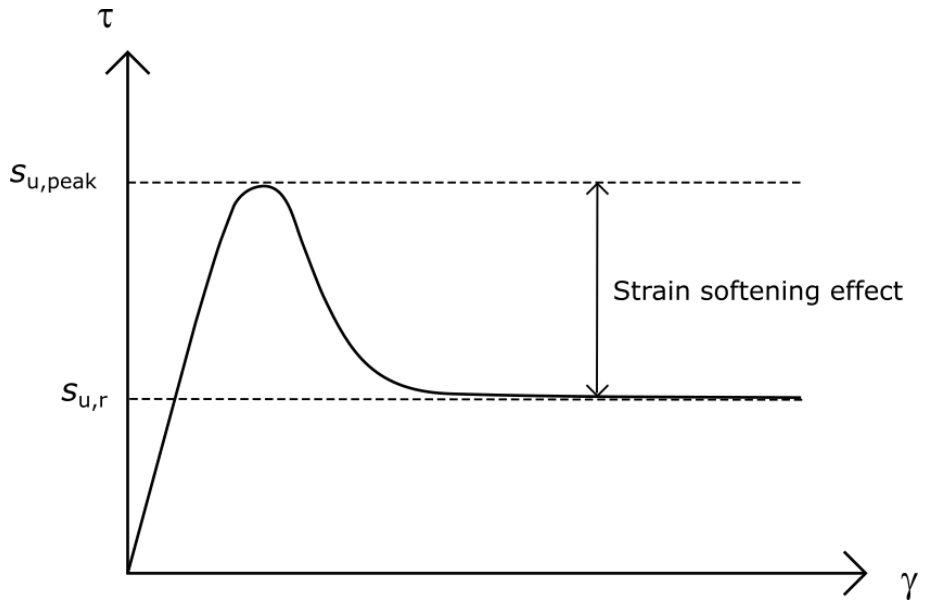

Figure 2.1: Strain softening effect in sensitive and quick clay.

Quick clay normally either has a Bingham plastic behavior or a shear-thinning behavior (Torrance, 1999). Both material behaviors show a reduction of viscosity when the shear strain rate increases. This leads to an increase in the shear strength. The shear strength of the soil during flow will therefore be lower than the peak undrained shear strength. However, the shear strength will be higher than the remolded shear strength measured in the laboratory.

The strain softening effect is tightly coupled with progressive failure in slopes. Skempton (1964) describes the process of progressive failure. If any particular point in a slope passes the peak shear strength, the strength will decrease toward a residual strength. This will pass additional stress to nearby points, which causes these points to pass the peak strength. According to this method, the failure will progress in the slope until the strength along the whole failure surface is reduced to a residual strength. This process is

illustrated in Figure 2.2 where a circular failure surface develops. There is little to no movement in the slope until the failure surface is fully developed.

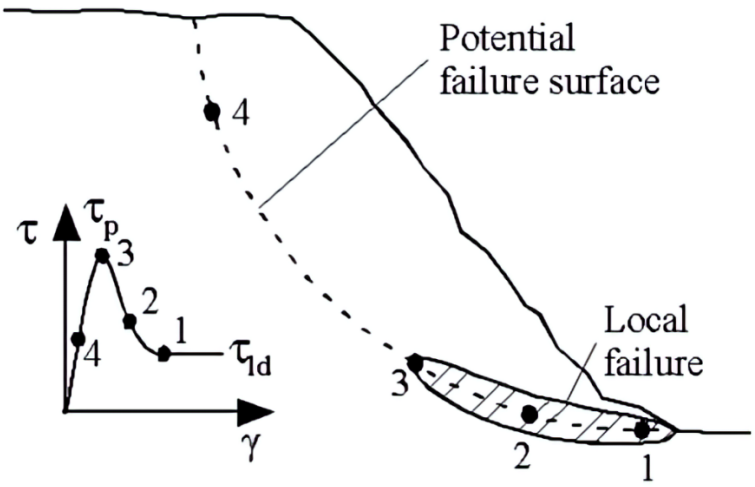

Figure 2.2: Progressive failure along a circular failure surface (from Locat et al., 2011)

2.4 Quick clay Landslides

2.4.1 Quick lay Landslide Types

There are four relevant slide mechanisms for quick clay (Varnes, 1978; Karlsrud, Aas, and Gregersen, 1984; Hungr, Leroueil, and Picarelli, 2014). Several types of slide mechanisms can occur in one landslide (Karlsrud, Aas, and Gregersen, 1984), such as for the Rissa landslide in Norway (Gregersen, 1981).

- Single rotational slide
- Multiple retrogressive slide or flowslide
- Translational slide or flake slide
- Lateral spread

Retrogressive landslides were first described by Bjerrum (1954), who states that a retrogressive slide will start with a single rotational initial slide. The clay will remold and flow out of the crater. This leaves an unstable back scarp, and a new rotational slide will happen. The slide will continue to develop in a retrogressive manner, shown in Figure 2.3a, until the propagation stops due to a lack of sensitive material or a stable back scarp. Retrogressive slides are sometimes denoted flowslides, which refer to the velocity and mobility of the slide debris. Hungr, Leroueil, and Picarelli (2014) characterizes flowslides by very to extremely rapid flow of liquefied quick clay and complete depletion of the source area. The original terrain in a flowslide can experience large displacements due to the viscosity of the remolded quick clay.

Flowslides can often have a characteristic bottle-neck shape, such as in the Ullensaker slide in Norway (Bjerrum, 1954).

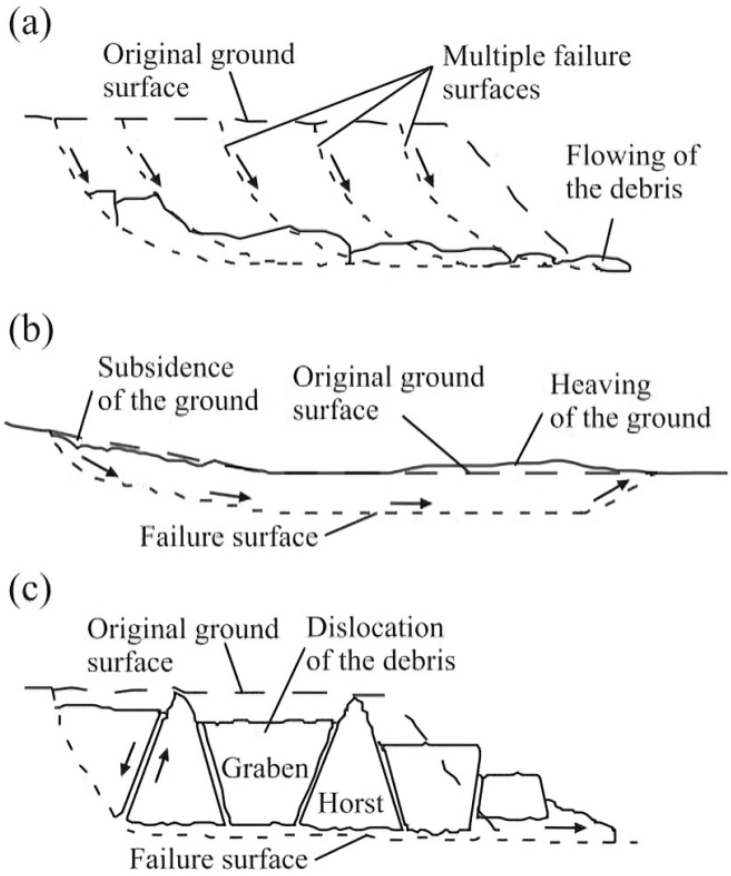

Figure 2.3: Three types of quick clay landslides: a) multiple retrogressive slide, b) translational slide, and c) lateral spread (from Locat et al., 2011).

Flake slides are characterized by a cohesive layer of insensitive clay and a dry crust that slides on a thin layer of remolded quick clay. The failure surface is often parallel to the ground or follows faults or joints (Cruden and Varnes, 1996). This slide type is common for gentle slopes with thin layers of quick clay. Flake slides can be either upwards or downwards progressive depending on where the local initial failure happens. Figure 2.3b shows a downwards progressive failure.

Spreads have distinctive horst and graben shapes, see Figure 2.3c. The grabens will often have an almost horizontal, flat surface, while horsts are sharp wedges. Spreads have formerly been viewed as retrogressive, but Quinn et al. (2007), Quinn et al. (2011), Locat et al. (2011), and Locat, Leroueil, and Jostad (2014) propose that spreads are a result of upwards progressive failure from the toe of the slope and that the entire failure surface is developed before any significant movement. Spreads are generally smaller than flowslides (Locat et al., 2017), and have a higher $s_{u,r}$ than found for flows (Geertsema, Cruden, and Schwab, 2006).

2.4.2 Criteria for Retrogressive Landslides

Tavenas et al. (1983) describes five criteria for retrogressive slide development:

An initial slide

Without an initial slide, there is no risk of retrogressive slide development. An initial slide is triggered by a change in slope stability. The triggering factors can be divided into human activities and natural causes. Human activities may include excavation in the toe or filling at the crest, disturbance due to construction work, or deforestation. Natural causes can be erosion of the toe, increased pore pressure, or earthquakes.

Continued back scarp failure

To develop into a retrogressive slide, several failures must occur. After the initial slide, the back scarp needs to be unstable such that a new slide will happen. Bjerrum (1954) states that the retrogressive development will continue until the back scarp is stable. Janbu's stability number, $N_s = \gamma H / s_u$ is often used to characterize the stability of a slope. Here is γ the bulk unit weight of the soil, H is the height of the back scarp and s_u is the average undrained shear strength. Mitchell and Markell (1974) describes a stability number higher than 6 for retrogressive slides for Canadian soils. For Norwegian soils Geertsema and L'Heureux (2014) states that the threshold value for retrogressive slides is likely larger than 6, while Thakur et al. (2014) argues that the threshold value is 4.

The remolded clay must be liquid enough to flow

An unstable back scarp is not obtained unless the slide debris partly moves away from the slide crater. The mobility of the remolded clay and slide debris must therefore be such that they flow out of the crater. According to Tavenas et al. (1983), Lebuis and Rissman (1979) suggests that $s_{u,r} < 1kPa$ and $I_L > 1.2$ for retrogressive slides to develop. This coincides with the criteria recommended by the Norwegian Water Resources and Energy Directorate (2019) in *NVE Guidelines 2019/01*. Thakur et al. (2013) defines a mobility parameter, quickness (Q), to assess the potential for flowslides. Based on this, $Q > 15\%$ and $s_{u,r} < 1$ kPa is defined as the upper limit for development of a retrogressive slide.

The potential energy must be high enough to remold the clay

The potential energy is a function of the slope height and soil density (Tavenas et al., 1983). Thakur et al. (2014) describes that to remold intact soil material a certain amount of energy is needed. Per volume unit, this can be quantified by the area under the shear stress-strain curve. To fully liquefy the clay, the potential energy needs to be higher than the remolding energy for the total clay volume.

Favorable Topography

The topography must allow the slide debris to flow out of the slide crater.

2.4.3 Factors that Control Slide Development and Retrogression

Numerous factors will affect the slide development and extent of retrogression. These can be divided into three categories:

- Topographic conditions, such as slope inclination, slope height, and surrounding areas
- Geological and geotechnical aspects such as extent and depth of quick clay layer, depth from terrain to quick clay layer, and depth to bedrock
- Material parameters such as undisturbed shear strength, remolded shear strength, the liquidity index, the plasticity index, soil density

Some of these aspects will be discussed further in the following paragraphs.

The topography in the area around the slide will impact whether the slide debris can flow out of the slide crater, and how fast the crater is depleted. If the debris is left in the pit, it will stabilize the back scarp and prevent further retrogression. Tavenas et al. (1983) describes that large retrogression is more likely to occur in steep areas and for valleys or wide rivers, than for flat terrain or narrow valleys.

The depth and extent of the quick clay layer are important factors for the slide mechanism. As described above, a thin layer will more probably lead to a translational slide mechanism than a retrogressive slide. If the quick clay layer is deep, it is more unlikely that the failure surface from an initial slide will propagate into the quick clay and lead to a large landslide. However, an initial slide that does not propagate into quick clay may expose a quick clay layer behind the slope that may lead to a quick clay landslide. *NVE Guidelines 2019/01* uses a ratio of b/D larger than 40 % to define a potential retrogressive landslide, where b is the depth of the quick clay layer above the critical failure surface, and D is the depth from the terrain to the computed failure surface.

When a retrogressive slide has developed, it will not stop until there is no more quick clay or the back scarp is stable (Bjerrum, 1954). Hence, the maximum retrogression distance is defined by the extent of quick clay. The slide often stops before it reaches the outer boundary of quick clay due to other factors. The stability of the back scarp is often described by Janbu's stability number, as described above. A higher stability number is related to a longer retrogression distance, see Figure 2.4.

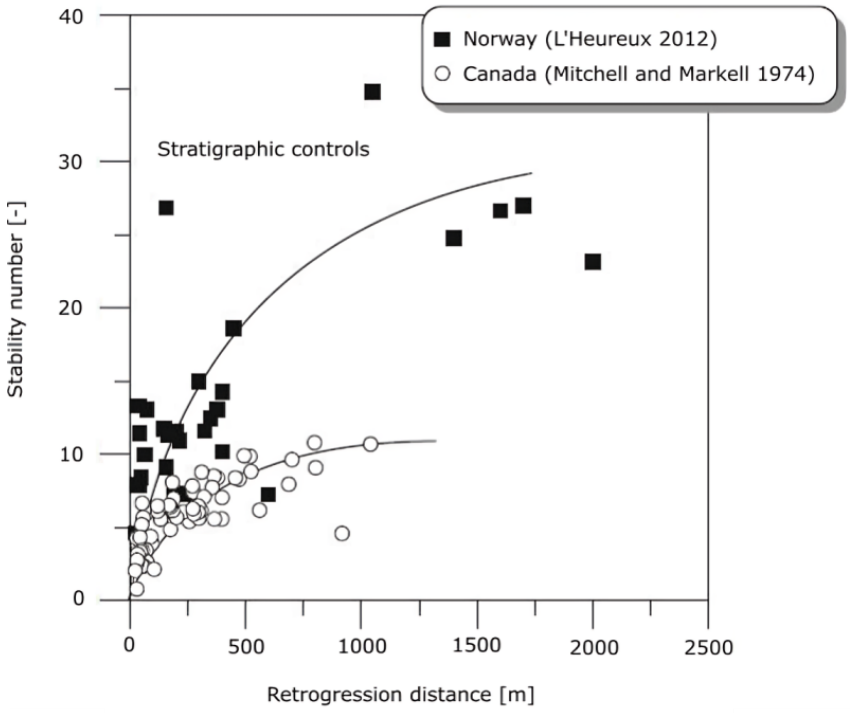

Figure 2.4: Retrogression distance versus stability number for Canadian and Norwegian slides (from Geertsema and L'Heureux, 2014).

L'Heureux (2012) states that the extent of retrogression is among others, governed by to what degree the remolded debris can flow out of the slide crater. In addition to the topography, this is controlled by the viscosity and the mobility of the remolded clay. The mobility of the slide debris is often characterized by the remolded shear strength, the sensitivity, and the liquidity index. Thakur et al. (2014) show that the retrogression distance increase for decreasing remolded shear strength, see Figure 2.5. This is supported by L'Heureux (2012), who states that extensive retrogression occurs when the remolded shear strength is less or equal to 0.5 kPa. He further shows a strong correlation with increased sensitivity for decreasing remolded shear strength or increasing liquidity index.

The flow behavior of remolded quick clay can also be assessed with the quickness parameter (Thakur et al., 2013). Quickness tests performed on clay with different remolded shear strength, shows that the registered collapse of the soil was nearly negligible when $s_{u,r} > 1$ kPa, while $s_{u,r} < 0.2$ kPa appeared as a soup (Thakur et al., 2013). On the other hand, Thakur and Degago (2012) show that clay with 0.5 kPa $< s_{u,r} < 1$ kPa were semisolid in nature and not as liquid as originally thought. Based on the landslides studied in Thakur et al. (2013), $Q > 25$ % (or $s_{u,r} < 0.5$ kPa) is related to a retrogression distance larger than 250 m.

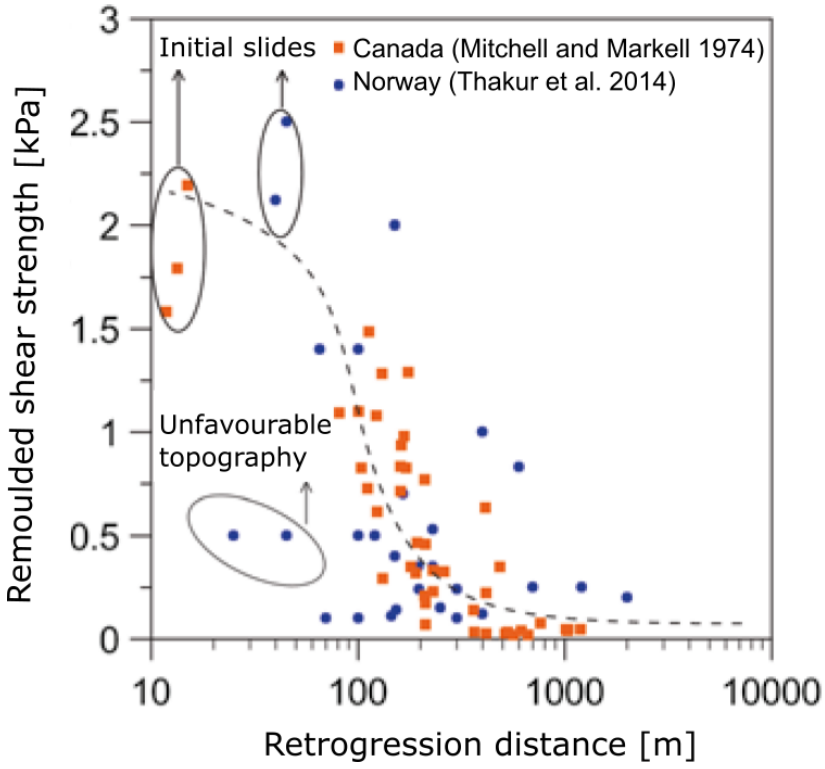

Figure 2.5: Retrogression distance versus remolded shear strength for Canadian and Norwegian slides (from Thakur et al., 2014).

2.4.4 Quick Clay Mapping in Norway and Empirical Relations Used to Determine Retrogression Distance

Construction work in areas with sensitive and quick clay needs to be done with precaution. In Norway, NVE has established quick clay hazard zones. *NVE Guidelines 2019/01* describe how to investigate and take into consideration the danger for sensitive clay slides in order to build safely. A quick clay hazard zone is established where ground investigations show sensitive clay, and the boundaries of the zone are determined based on *NVE Guidelines 2019/01*.

After delimiting the potential areas of marine clay and slopes with height and inclination susceptible to landslides, the extent of potential slides is determined by empirical relations. These relations are based on the work by Aas (1979) and Gregersen (2008) and have been further developed into the current empirical criteria in *NVE Guidelines 2019/01*. The chosen criterion depends on the slide mechanism, which is determined based on the diagram in Figure 2.6. Given a retrogressive slide mechanism, there are three empirical criteria to define the potential extent of an initial slide. *NVE Guidelines 2019/01* only provides criteria for the development of the slide normal to the contour lines. Engineering judgment and factors such as topography is used to determine the potential retrogression along the contour lines.

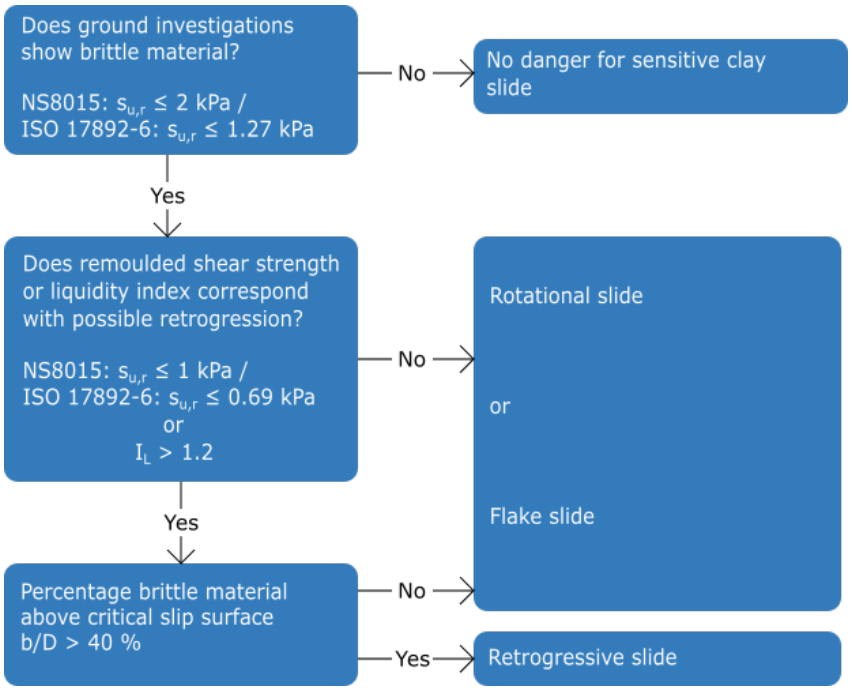

Figure 2.6: Flow chart for determination of slide mechanism (from *NVE Guidelines 2019/01*).

D is the depth from terrain to the critical failure surface, and b is the depth of the quick clay above the critical failure surface.

1:15 Method

This is the most conservative approach for determining the retrogression distance. The length is determined based on a distance that is 15 times the slope height normal to the contour lines. The length can be adjusted where the ground investigations do not show any brittle material. This criterion can be used without thorough knowledge about the soil layering, depth to bedrock, or stability analysis. L'Heureux (2012) shows that several slides have $L/H > 15$, and claims that this criterion should be used with care to delimit the extent of a potential landslide in quick clay.

NGI Method

The NGI method is based on the soil layering and calculation of the critical slip surface for an initial slide. A 1:15 line is drawn from the bottom of the critical surface through the sensitive material. When the line hits the outline of the sensitive material, a 1:3 or 1:2 line is drawn up to the terrain. If the critical surface is deep or no stability analysis has been performed, the 1:15 line should start at a maximum of $0.25H$ below the slope toe. Unless the overlaying material of the quick clay is shallow, this method will give a smaller detachment area than the 1:15 method.

NIFS Method

The NIFS method was developed during the Natural Hazards, Infrastructure, Floods, and Landslides project (NIFS). The method is based on several geometrical and geotechnical criteria and previous landslide activity in the area (Aunaas et al., 2016). Similar to the NGI-method, this method uses the critical slip surface. The score is then given by the b/D ratio at two different places in the slope, the distance from the toe of the slope to the quick clay layer, the possibility for debris flow out of the area, former landslide activity in the area, and the ratio $s_u/\gamma D$. A score is obtained based on the criteria listed above. This score corresponds to the L/H ratio for the detachment area. The highest possible score is 24, but due to the scoring method, most slopes will obtain 15 at maximum.

Chapter 3

Material Point Method and Material Model

This chapter will present the Material Point Method and its algorithm. Some important strengths and shortcomings of the method regarding landslide modeling will be discussed. The differences between the FEM and the MPM will be presented. Furthermore, the constitutive material model used in the MPM simulations will be described. The theory of the failure criterion is presented, as well as the relations for the shear strength. A complete list of input parameters is also given.

3.1 The Material Point Method

3.1.1 Introduction

The Material Point Method is a development of the particle-in-cell (PIC) method developed by Harlow (1964). Due to a problem with excessive energy dissipation, the Fluid Implicit Particle method (FLIP) was introduced by Brackbill and Ruppel (1986) and Brackbill, Kothe, and Ruppel (1988). MPM was then proposed as an alternative for solid mechanics, as PIC and FLIP were mostly applied to fluid dynamics. Sulsky, Chen, and Schreyer (1994) and Sulsky, Zhou, and Schreyer (1995) first introduced the method, and it was named the Material Point Method by Sulsky and Schreyer (1996). MPM have since been further developed into different versions such as, among others, the Generalized Interpolation Material Point Method (GIMP) (Bardenhagen and Kober, 2004), the Convected Particle Domain Interpolation (Sadeghirad, Brannon, and Burghardt, 2011), the Improved Material Point Method (Sulsky and Gong, 2016), the B-spline Material Point Method (Steffen et al., 2008). The GIMP as encoded in the Uintah software (http://uintah.utah.edu), is used for the simulations in this thesis.

The MPM has been used for different geotechnical problems, including modeling landslides. Both former

landslides and more idealistic approaches have been investigated. Wang, Vardon, and Hicks (2016) show an idealistic slope that fails under its self-weight, for a Von-Mises material model with softening. These simulations show that the MPM is suitable to model retrogressive behavior of a landslide. Wang, Vardon, and Hicks (2016) further show that the results depend on the softening parameters. The MPM has also shown good approximations with former slides, such as the landslide in Sainte-Monique, Canada (Tran and Sołowski, 2019).

3.1.2 Method and Algorithm

MPM is a numerical method that can simulate the behavior of continuum materials. The material is represented by a discrete number of material points or Lagrangian particles (De Vaucorbeil et al., 2020). The area of the continuum material and surrounding area is discretized by a fixed Eulerian background grid. The material points can move freely over the background grid. Due to this, MPM is a particle-based method and is generally viewed as meshless or meshfree. All of the material points store history-dependent internal state variables for the nearest surrounding material (Zhang, Chen, and Liu, 2017). The grid stores no permanent information (Sulsky, Zhou, and Schreyer, 1995). Necessary internal state variables depend on the chosen constitutive model for the material.

Initial conditions and material properties are defined for the material points before the simulation. The simulation runs for a predefined amount of time and number of time steps. The MPM algorithm is performed for each time step, and can be divided into four stages shown in Figure 3.1 below:

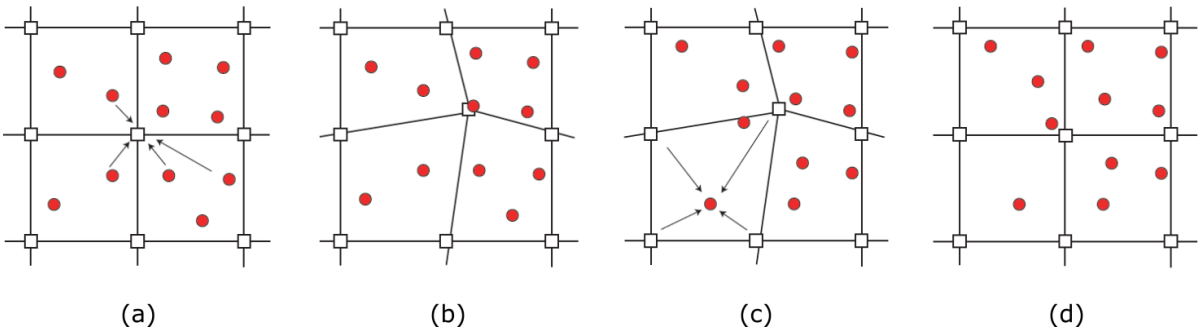

Figure 3.1: Illustration of MPM algorithm with a) particle to grid, b) grid updating, c) rid to particle and d) grid resetting (modified from De Vaucorbeil et al., 2020).

The first step of the algorithm is to extrapolate material properties from each particle to the background grid nodes (Figure 3.1a). Secondly, the momentum equations are solved in their weak form for the grid nodes and the grid is updated (Figure 3.1b). The third step extrapolates the nodal solution from the grid nodes to the particles and updates the particles with position, velocity, and stress among others (Figure 3.1c). Lastly, the grid is reset to its original state (Figure 3.1d).

3.1.3 Strengths and Shortcomings

The absence of mesh distortion is one of the most important advantages of using the MPM in geotechnical engineering. If a Lagrangian mesh was used solely, where material points moved with the mesh, it would either require considerably small time steps or become twisted for large deformations (Sulsky, Zhou, and Schreyer, 1995). A fixed Eulerian grid that resets for each time step prevents such problems. The MPM is therefore highly suitable for simulating large deformations. The ability to simulate large strain problems is advantageous for modeling landslides and several other geotechnical problems with large deformations. The MPM can model pre-failure, failure, and post-failure of a landslide.

The MPM has several challenges regarding stability and accuracy. One of them is instability due to cell crossing (Bardenhagen and Kober, 2004). Due to a non-smooth interpolation function, material points that cross element boundaries in the grid will lead to a sudden change in stress. However, this problem is reduced in the GIMP which utilizes smoothed grid basis functions. More recent formulations of the MPM also reduce this numerical error.

The output of the MPM simulation depends greatly on the chosen grid size and the number of material points in each element. Tran and Sołowski (2019) show that a decrease in grid density gave a longer run-out for a simulation of the Saint Monique landslide, while the retrogression distance is constant. When the grid size was reduced, the number of material points was increased. Adding the shear band thickness to the constitutive model can reduce the dependency of the grid density (Tran and Sołowski, 2019). Further, Tran and Sołowski (2019) show that the orientation of the grid also impacted the shear bands in the simulation.

3.1.4 Differences between FEM and MPM

The Finite Element Method (FEM) and the MPM have several important differences, in addition to several similarities. The differences are concentrated on to highlight the possible advantages to use the MPM instead of the FEM.

The main difference between the FEM and the MPM is that the numerical integration is performed at the Gauss points in the FEM, but at the material points in MPM. The other most important difference between the FEM and the MPM is the mesh. In the FEM, the computational mesh attaches to the material and will be deformed as the material gets deformed. While in the MPM, the material is independent of the mesh (Eularian mesh), as the grid is reset for every time step. Figure 3.2 illustrates how the material points in the MPM move freely over the grid, while the integration points in the FEM are fixed within the grid.

As the grid does not carry any information in the MPM, mass and momentum must be mapped from the particles to the grid nodes at the beginning of each time step, and back at the end of each time step (Zhang, Chen, and Liu, 2017). This is not necessary for the FEM as the mass and momentum are carried

by the mesh nodes, and do not need to be recalculated. In addition, the MPM requires a calculation of the velocity and position of the particles as these are not attached to the mesh. The MPM often has a greater number of particles in each grid cell, which requires additional calculation compared to the FEM (Zhang, Chen, and Liu, 2017). To sum up, these differences will lead to a higher computational cost by using the MPM compared to the FEM. Thus, to solve large problems the MPM will require a considerably computational capacity. Therefore, the MPM is less accessible to use than the FEM.

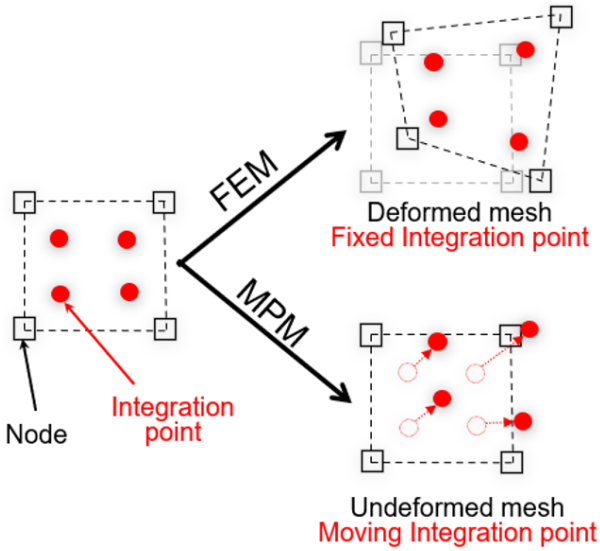

Figure 3.2: Illustration of difference between integration points in the FEM versus the MPM.

In the FEM, the deformation of the mesh leads to a decrease in time step size (Zhang, Chen, and Liu, 2017). Thus, as the deformation increases, the number of time steps must be increased. An increased number of time steps require greater capacity and takes additional time, which makes the efficiency decrease. For small deformations, this does not have a large impact since the time step size does not reduce remarkably. However, for large deformations, this leads to better efficiency for the MPM than the FEM.

Both the FEM and the MPM utilize the weak form formulation of shape functions. The accuracy difference between the MPM and the FEM is dependent on the weak form integration over the Gauss points in the FEM and particles in the MPM (Zhang, Chen, and Liu, 2017). In the FEM, the Gauss quadrature leads to accurate integration over the Gauss points. The arbitrary position of the particles in the MPM leads to a lower accuracy (Tran and Sołowski, 2019). In addition, the original MPM formulation has a reduced accuracy due to cell-crossing errors, as presented above. On the other hand, the FEM is less accurate for large deformations due to the mesh distortion.

To sum up, the MPM is more efficient and accurate for large deformations, while the FEM is more suitable for small deformations. Since landslides will generate large deformations after failure, the FEM

is not suitable for modeling post-failure behavior. The MPM is more relevant when modeling pre-failure, failure, and post-failure of a sensitive clay mechanism.

3.2 Constitutive Material Model

3.2.1 Failure criteria

The constitutive model is based on the Mohr-Coulomb material model. This is a fairly simple linear elastic-perfectly plastic material model with few input parameters.

The failure criterion in Mohr-Coulomb is defined as

$$\tau_f = c + \sigma' tan(\varphi) = (\sigma' + a)tan(\varphi), \tag{3.1}$$

where c is the cohesion, σ' is the normal effective stress, a is the attraction and φ is the friction angle.

If $\varphi = 0$, then $\tau_f = c = s_u$ and the Mohr-Coulomb failure criterion reduces to the Tresca failure criterion. The Tresca failure criterion is normally used for undrained analysis and is defined as

$$\tau_f = \frac{\sigma_1 - \sigma_3}{2} = s_u, \tag{3.2}$$

where σ_1 and σ_3 is respectively the largest and smallest principal stresses and s_u is the undrained shear strength. The failure criterion is therefore independent of the normal stress. Both failure criteria is illustrated in Figure 3.3:

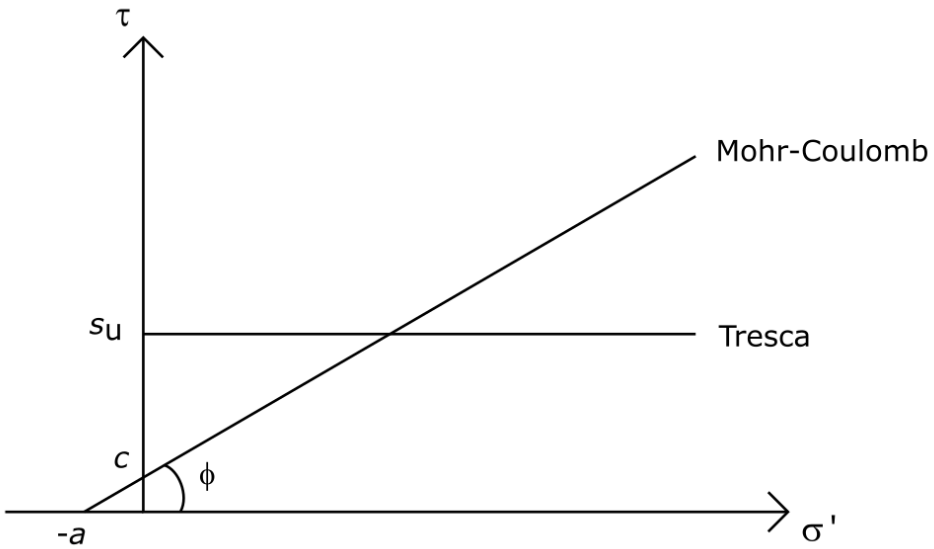

Figure 3.3: The Mohr-Coulomb and Tresca failure criterion.

The clay is modeled undrained and uses $\varphi = 0$ which implies a Tresca failure criterion. The dry crust is considered drained and is modeled by the Mohr-Coulomb failure criterion.

3.2.2 Shear strength

The soil is modeled as linear elastic until failure is reached. This elastic behavior is defined by Hooke's law:

$$\sigma = E \cdot \varepsilon, \tag{3.3}$$

where E is Young's modulus, σ is the normal stress and ε is the normal strain. Isotropic elasticity is assumed, thus two independent stiffness parameters are needed. In this thesis, either the Young's modulus and the Poisson's ratio, ν, or the bulk modulus, K, and the shear modulus, G, are used. These parameters are related through the following equations:

$$G = \frac{E}{2(1+\nu)}, \text{ and} \tag{3.4}$$

$$K = \frac{E}{3(1-2\nu)}. \tag{3.5}$$

The shear modulus relates the shear stress to the shear strain. Hence, G is the gradient in the shear stress versus shear strain curve in the elastic region, which can be seen in Figure 3.4.

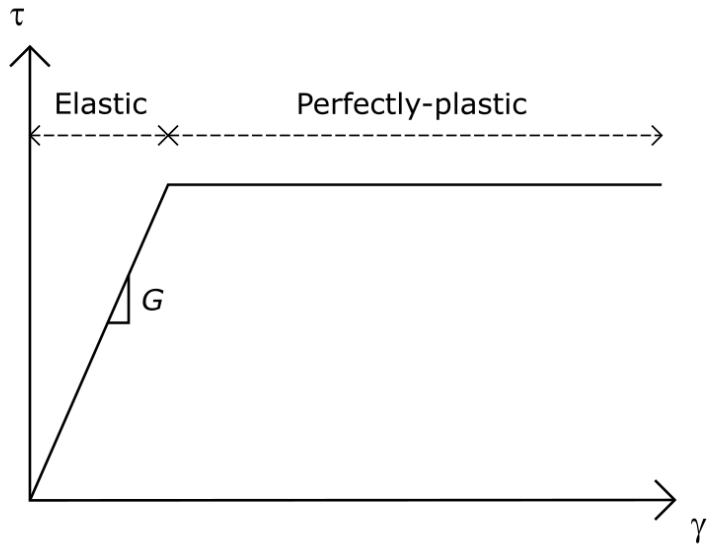

Figure 3.4: Elastic perfectly-plastic behavior in Mohr-Coulomb.

When the failure criterion is reached, the soil will experience plastic deformation and the shear strength will be defined by the failure criterion. Since Mohr-Coulomb is perfectly plastic in the plastic region, the shear stress will remain constant with increasing shear strain. However, for increasing normal stress, the shear stress will also increase for Mohr-Coulomb, but remain constant for Tresca. This can be seen from Figure 3.3.

Based on the theory presented above, the shear strength can be described by:

$$\tau = \begin{cases} G \cdot \gamma & \gamma \leq \gamma_e \\ c + \sigma' \tan(\varphi) & \gamma > \gamma_e,\ dry\ crust \\ s_{u,ref} & \gamma > \gamma_e,\ clay \end{cases} \tag{3.6}$$

where γ_e is the shear strain at maximum shear stress.

3.2.3 Strain Softening

Mohr-Coulomb is a fairly simple material model, and in reality, the soil will experience hardening or softening when loaded above the yield strength. This is particularly relevant for modeling sensitive clay. As presented in section 2.3, the shear strength of the sensitive clay decreases when the shear strain increases. The material model is therefore extended to take this option into account. Figure 3.5 illustrates the chosen shear strength relation.

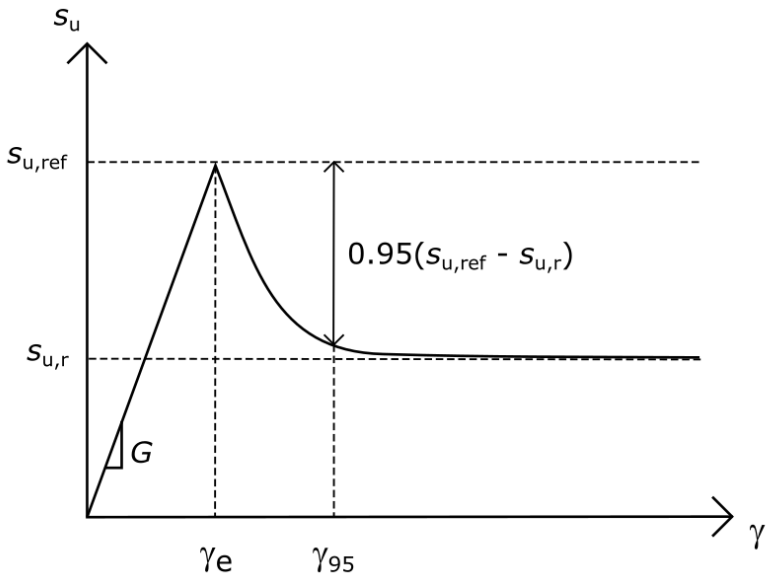

Figure 3.5: Shear strength softening model used in the constitutive material model.

The relation was first proposed by Einav and Randolph (2005) and is defined as follows:

$$s_u(\gamma, S_t) = s_{u,ref}\left(\frac{1}{S_t} + \left(1 - \frac{1}{S_t}\right) e^{\frac{-3\gamma}{\gamma_{95}}}\right), \gamma > \gamma_e \tag{3.7}$$

where γ is the shear strain, γ_{95} is the shear strain at 95% reduction of shear strength. Sensitivity, S_t, is defined as

$$S_t = \frac{s_{u,ref}}{s_{u,r}} \tag{3.8}$$

where $s_{u,ref}$ is the reference undisturbed undrained shear strength and $s_{u,r}$ is the remolded undrained shear strength.

3.3 Input Parameters

The constitutive model for the soil can be summarized with the following shear strength formulation:

$$\tau = \begin{cases} G \cdot \gamma & \gamma \leq \gamma_e \\ c + \sigma' \tan(\varphi) & \gamma > \gamma_e,\ dry\ crust \\ s_{u,ref}\left(\frac{1}{S_t} + \left(1 - \frac{1}{S_t}\right) e^{\frac{-3\gamma}{\gamma_{95}}}\right) & \gamma > \gamma_e,\ clay \end{cases} \tag{3.9}$$

A full list of input parameters is given in Table 3.1 below.

Table 3.1: Input parameters for the soil model

Parameter	**Symbol**
Young's modulus	E
Poisson's ratio	ν
Cohesion/reference undrained shear strength	$c/s_{u,ref}$
Friction angle	φ
Remolded undrained shear strength	$s_{u,r}$
Dilatancy angle	ψ
Shear strain at 95% reduced shear strength	γ_{95}

Chapter 4

Landslide in Gjerdrum

This chapter firstly presents the area where the landslide in Gjerdrum occurred, Secondly, the landslide and its stages are described based on the finding of Ryan et al. (2021).

4.1 Description of the Area

Ask in Gjerdrum is situated in Romerike, northeast of Oslo. The location is shown in Figure 4.1 a. Romerike is known for its marine clay deposits and is characterized by a significant number of quick clay hazard zones. The relevant quick clay hazard zones for the slide can be seen in Figure 4.1 b.

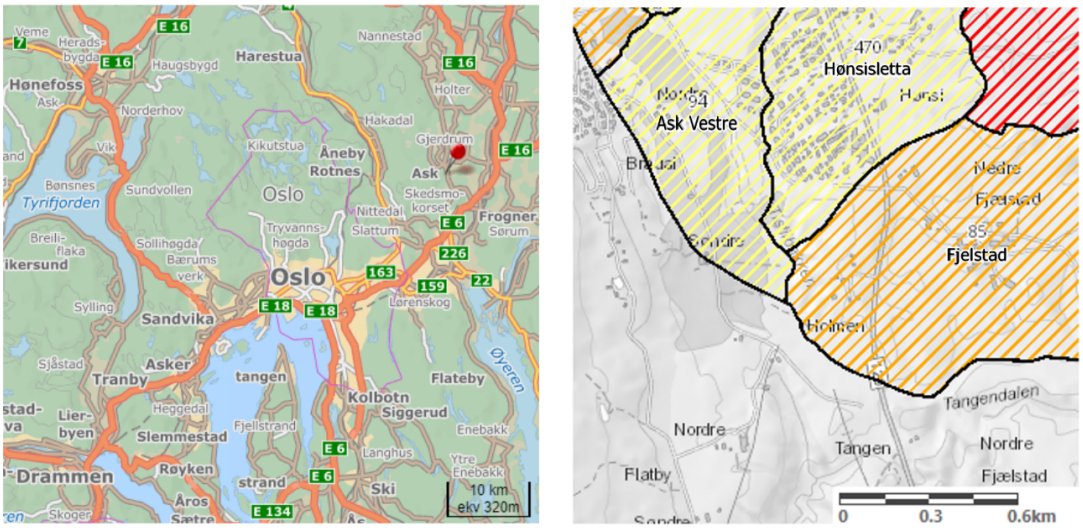

(a) (b)

Figure 4.1: a) Map showing the position of Ask (from *Finn Kart*). b) Quick clay hazard zones in the relevant area (from *NVE Atlas*).

A map of the Quaternary deposits is shown in Figure 4.2. It can be observed that Ask is covered with marine deposits, while there are moraine and thin covers of humus/peat on bedrock toward the west.

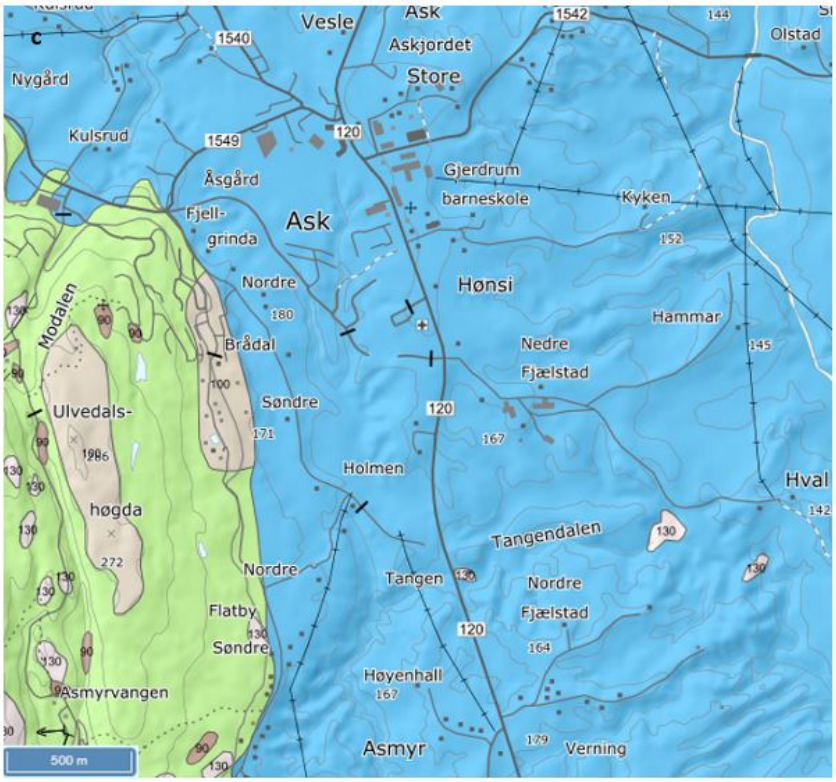

Figure 4.2: Map of Quaternary deposits in Ask. The blue is marine deposits, the green is moraine and the grey is thin covers of humus/peat on bedrock (from *NGU Map of Quarternary deposits*).

The depth to bedrock is a few meters on the plateau in the center of Ask (Penna and Solberg, 2021). A larger soil depth is found north and east of the plateau. The area south of Ask center is hilly with varying depths of soil deposits overlying bedrock.

4.2 The Landslide

The landslide in Gjerdrum, southwest of the center in Ask, occurred the 30th of December 2020 around 4 a.m. Ryan et al. (2021) summarizes that the total slide crater as approximately 120 000 m^2, and the run-out area was 260 000 m^2. The length from the back scarp to the front of the landslide crater was around 630 meters and the run-out had a total length of around 2 kilometers. The detachment area of the slide is located in the quick clay zones Hønsisletta and Fjeldstad, while the run-out followed the boundary of the zone Fjeldstad down to the hazard zone Hval. The run-out also displaced into hazard zone Ask Vestre.

Figure 4.3 shows the area before the landslide, while Figure 4.4 shows the area after the landslide.

Figure 4.3: Aerial photo of the landslide area from 2020, before the slide (from *Norge i bilder*).

Figure 4.4: Aerial photo of the landslide area from 2021, after the slide (from *Norge i bilder*).

4.2.1 Stages

Ryan et al. (2021) has investigated how the slide developed based on the interpretation of aerial photos, videos, physical traces, geotechnical and hydrological investigations, an elevation model of the terrain, and testimonies from witnesses. Ryan et al. (2021) concluded that the slide had a retrogressive behavior which can be described by nine stages, see Figure 4.5. The following description of the landslide is based on the work of Ryan et al. (2021).

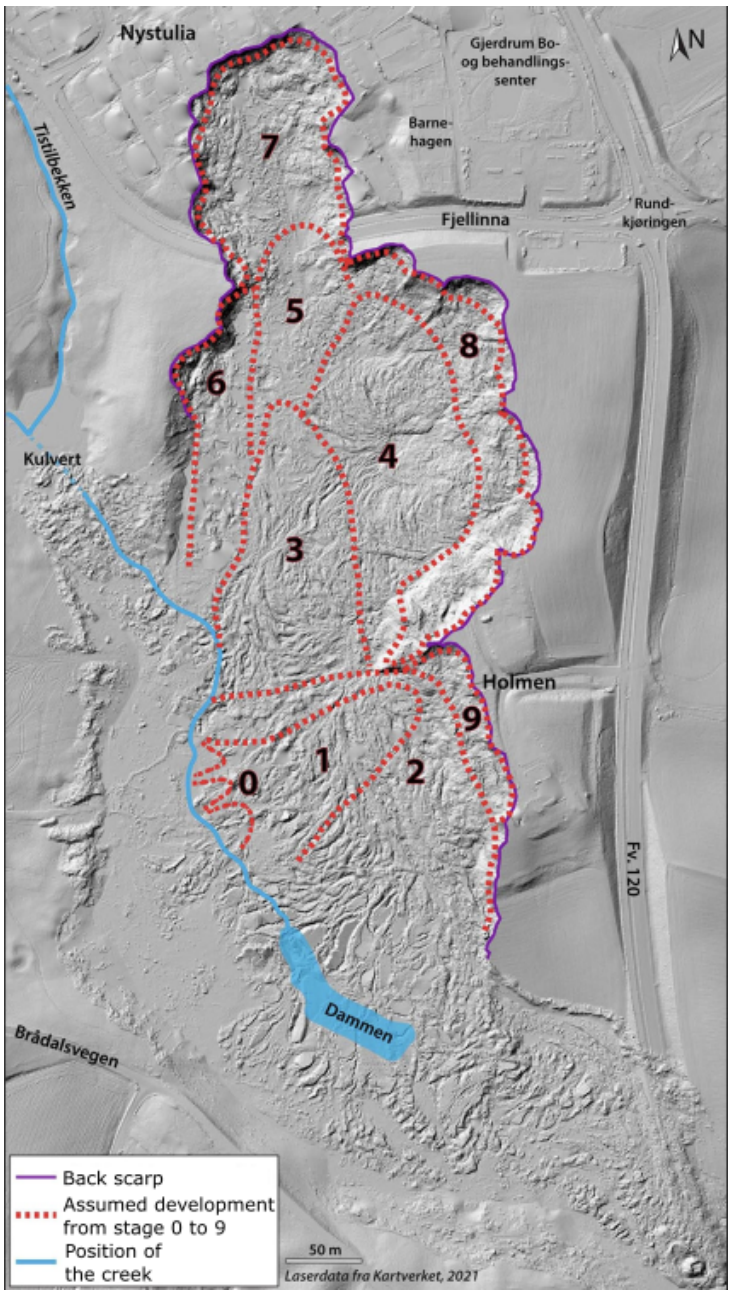

Figure 4.5: Assumed development of the slide (from Ryan et al., 2021).

The slide started by a small local failure close to the creek Tistilbekken east of Holmen. This is denoted step 0 and is the initial slide. Multiple possibilities of this failure are drawn since the placement is uncertain. This or these small failures are believed to cause the slide in step 1. The triggering factor for the initial slide is reportedly erosion of the slope over an extended period, combined with a high pore pressure due to high precipitation in the fall of 2020. Slide 1 propagated up to a barn in Byvegen 3 at Holmen. The remolded masses are believed to have displaced toward the southwest.

After the masses from step 1 ran out from the slide crater, an unstable back scarp was left. This caused a larger part of Holmen to slide out in step 2. The slide expanded both sideways and slightly backward toward the east. The slide debris ran out of the slide crater toward the southwest, then ran south and the debris flow followed the creek Tistilbekken downstream. A smaller part of the debris flow followed the river Tangelva. Building from step 2 was found 2 km downstream of Tistilbekken.

The slide in step 2 left a steep main scarp toward the north and the east. This caused the slides in steps 3 and 4. Step 3 included the forest-covered ravines northwest of Holmen. Partly intact slabs of the dry crust were found 300 - 400 m southwest of the ravines. The slide debris followed the same path toward southeast and the river course of Tistilbekken and Tangelva. Step 4 is believed to slide in one slab right after step 3. This area was cultivated land with a thick dry crust. The dry crust was divided into smaller pieces in the slide and was found 300 to 600 m from the failure plane. The remolded quick clay from below the thick dry crust followed the same path as for step 3.

Step 5 extended the total slide crater toward Fjellinna before step 6 extended the total slide crater to the west. Step 5 is believed to have occurred around 2 minutes after step 2. The slide then propagated toward the north, and the following step 7 destroyed numerous houses in Nystulia. Masses from this step displaced toward the west side of the crater. Some of the masses from steps 6 and 7 traveled up-streams Tistilbekken. The slide extended toward the east due to the steep back scarp. Several small slides happen during and after steps 5 to 7. These are denoted step 8.

Step 9 occurred during the daytime on the 30th of December, and is the last step of the main slide. In the following days and the rest of January 2021, there were several small slides due to steep back scarps.

Chapter 5

Method

This chapter will present the three different methods used for the analyses. Firstly, the method for the 2D sensitivity analysis using the MPM is described. Secondly, the empirical criteria used to determine the retrogression distance based on the terrain and soil layering, are presented. Lastly, the method for the 3D MPM simulations is presented.

The focus of this thesis is to compare different methods to evaluate retrogression and the effects of levels of detail in soil layering and shear strength parameters. The methods are therefore based on existing information and no additional interpretations of ground investigations or laboratory tests are made, nor any stability calculations. Necessary information about the area consists of terrain and bedrock profiles, soil layering, and material properties of the clay and sensitive clay. The terrain, bedrock, and soil layering are obtained from Multiconsult's Leapfrog model (Multiconsult, 2021c; Multiconsult, 2022). Material properties are retrieved from Multiconsult (2021a) and Multiconsult (2021b).

5.1 2D Numerical Method

5.1.1 Profile

The 2D analysis is performed on the slope east of Tistilbekken up to Holmen. This scope has been chosen because the initial slide occurred in this slope. The geometry and soil layering of profile *MC6* from Multiconsult (2021b) are used, see Appendix A. The placement of the soil profile is shown in Figure 5.1. The elevation profile is based on digital maps used for geotechnical reports before 2004 (Multiconsult, 2021b).

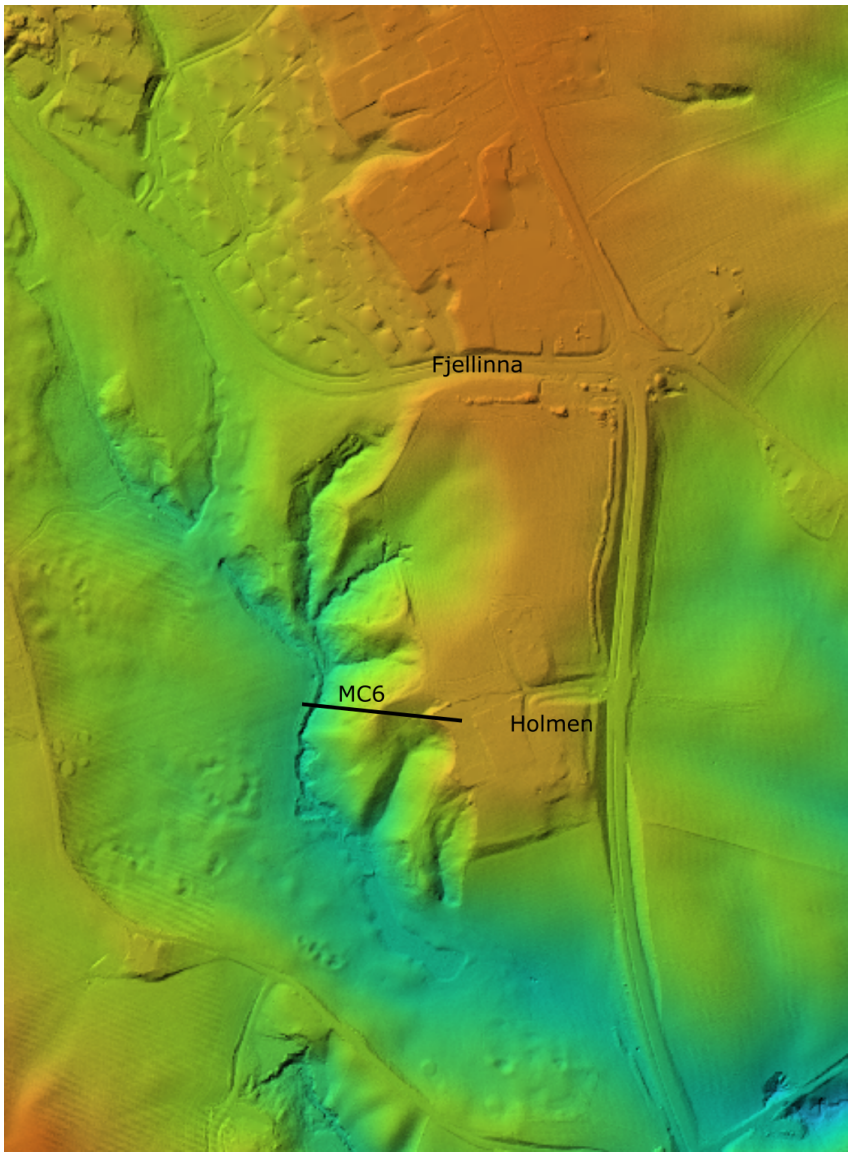

Figure 5.1: Location of the profile *MC6* (from Multiconsult, 2021b).

To perform an MPM simulation, the soil profile was simplified into the profile shown in Figure 5.2. The slope is divided into the dry crust, clay, and sensitive clay. The sensitive clay layer is divided in two parts to assign different sensitivities and strength profiles. Except for the effect of strain softening, the clay and sensitive clay are assumed to have the same properties. One part of the clay layer is omitted in the MPM simulation. Due to an increasing shear strength with depth, the failure will not propagate into this area. Together with the simplification of the profile, omitting this part of the profile has been chosen to reduce the computational cost.

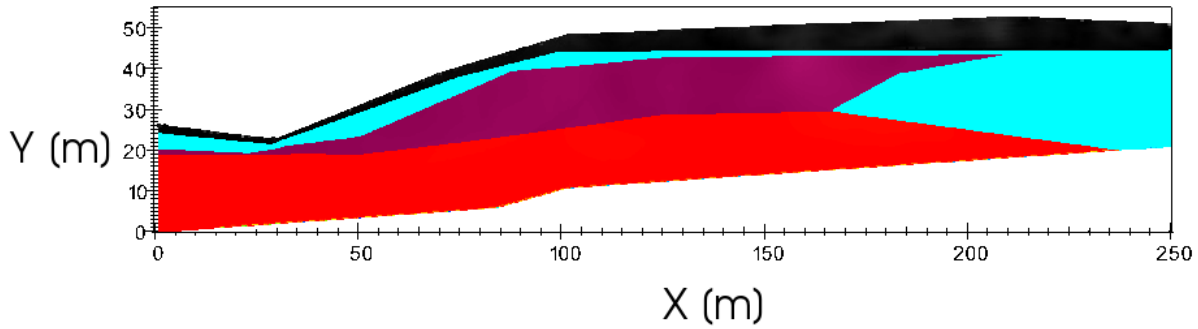

Figure 5.2: Simplified profile with soil layering for the MPM simulation. Dry crust is black, clay is blue, and sensitive clay is purple and red.

The right boundary, at x = 253 m, is fixed by defining zero-velocity. To be able to simulate a flowslide, the masses must be able to flow out of the profile. Thus, the left boundary is open, to allow material points to cross this boundary. The lower boundary is fixed since there is the bedrock beneath the clay layers.

5.1.2 Geotechnical Parameters

The material model described in section 3.2, is used for the simulation. The values for the different layers are based on interpretations of ground investigations and laboratory tests done by Multiconsult and NGI. All investigations were performed after the slide occurred. Some of the values are therefore adjusted to give a reasonable condition of the soil before the slide. Empirical relations are also used to determine appropriate values. The parameters used for the different layers are presented in Table 5.1.

Table 5.1: Soil properties for the 2D simulations.

Parameter	Unit	Dry crust	Clay	Sensitive clay (purple)	Sensitive clay (red)
γ	kN/m^3	19.5	19.5	19.5	19.5
E	MPa	10	$1000s_{u,ref}$	$1000s_{u,ref}$	$1000s_{u,ref}$
ν/ν_u	-	0.3/-	0.3/0.49	0.3/0.49	0.3/0.49
$c/s_{u,ref}$	kPa	0	68	68	68 + 3/m
φ	°	30	0	0	0
$s_{u,r}$	kPa	-	-	0.5	1
γ_{95}	-	-	-	2	2
ψ	°	0	0	0	0

The average soil density is 19.5 kN/m^3 (Multiconsult, 2021a), and is used for all layers.

The shear strength is controlled by c and φ or s_u. The dry crust is set to $c = 0$ and φ= 30°according to Multiconsult (2021b) and the Norwegian Public Roads Administration (2018). $c = 0$ ensures that the dry crust will not have any tensile strength. The undrained shear strength for the clay and sensitive clay is retrieved from the shear strength profiles used for the stability calculation in MC6 Multiconsult (2021b), see Appendix A. The local variation between the profiles is simplified into an average undrained shear strength. For the purple sensitive clay layer, the undrained shear strength is 68 kPa. The red sensitive clay layer has an undrained shear strength of 68 kPa at the top of the layer and increase in depth with a value of 3 kPa per meter. The variation of $s_{u,ref}$ is shown in Figure 5.3.

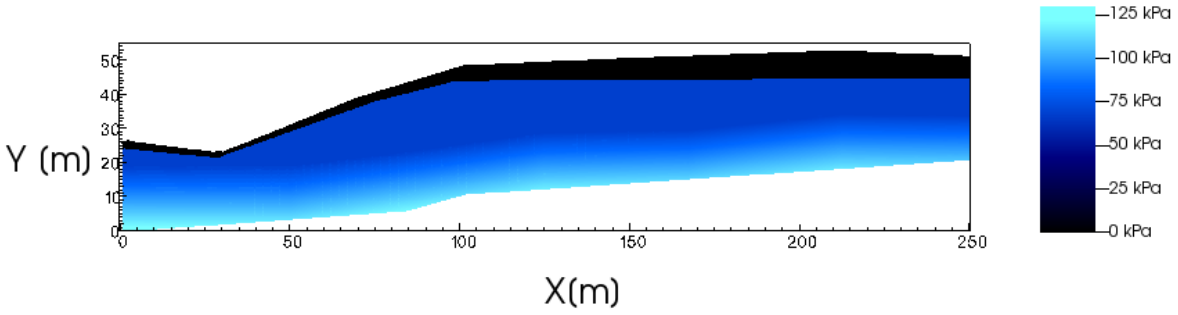

Figure 5.3: Reference undrained shear strength variation in soil profile.

The undrained stiffness for the clay is retrieved from an empirical relation proposed by Duncan and Buchignani (1976). These authors related the ratio of E_u/s_u to the plasticity index, I_p and the over-consolidation ratio, OCR. The plasticity index for the boreholes close to profile MC6, 2020-120 and 2020-121, is between 5 and 15% (Multiconsult, 2021a). The over-consolidation ratio (OCR) for the relevant boreholes is around 1.5 (Multiconsult, 2021b). This results in E_u equal to around 1000 times s_u. The stiffness will therefore increase with depth where the reference shear strength is increasing with depth.

The stiffness for the dry crust is set to 10 MPa. A Poisson's ratio of 0.3 is chosen as a reasonable value for a drained analysis for all layers. The undrained Poisson's ratio for the clay is 0.49 to avoid volume change. A value closer to 0.5 uses too much computational capacity, and 0.49 is assumed sufficient.

The remolded shear strength, $s_{u,r}$, varies greatly with depth and between the boreholes 2020-120 and 2020-121. As described in section 2.4.2, a value of 1 kPa is often used as a threshold for the development of retrogressive sensitive clay landslides. 1 kPa is therefore used for the red sensitive clay layer in this simulation. The boreholes showed a higher sensitivity closer to the terrain and a value of 0.5 was chosen for the purple sensitive clay layer. These values may be too high with regards to the semi-solid behavior of clay with 0.5 kPa $< s_{u,r} <$ 1 kPa shown by Thakur and Degago (2012). However, as the material model does not take into account an increase in shear strength for increasing strain rate during the flow, a slightly higher $s_{u,r}$ might partly compensate for this. Since $s_{u,r}$ is fixed, the sensitivity, S_t, will vary

proportionally to the undrained shear strength. γ_{95} is set to 2.

The dilatancy angle, ψ, is set to 0 for all layers to avoid plastic volume change.

Both drained and undrained parameters for the clay are defined. Except for Poisson's ratio, all drained parameters are set equal to the undrained parameters. The Poisson's ratio influences the vertical stresses for gravity loading and is therefore changed to give a more realistic approach. The strength parameters are kept the same in the drained approach as the undrained approach to avoid mobilization above the failure criterion. The stiffness is not significant for the drained condition and is therefore kept the same for both approaches for simplicity.

5.1.3 Simulations

The simulation is divided into two phases:

1. Initial phase: Establish initial stresses with gravity loading with drained parameters
2. Slide phase: Change the soil properties to undrained parameters and allow strain softening

The first phase uses gravity loading to calculate the initial stresses. To obtain equilibrium faster, numerical damping is used. The initial phase is run for 5 seconds to ensure equilibrium is established. The second phase simulates the slide by changing the parameters to undrained parameters and allow strain softening.

To perform the sensitivity analysis, either γ_{95} or $s_{u,r}$ is varied, while the rest of the material parameters are kept constant. This results in the following simulations:

Table 5.2: 2D sensitivity analysis.

Simulation nr.	$s_{u,r}$ [kPa]		γ_{95} [-]
	Purple	Red	
1	0.5	1	2
2	1	2	2
3	0.25	0.5	2
4	0.5	1	4
5	0.5	1	1

Based on the values for γ_{95} and $s_{u,r}$, the shear strength degradation after peak strength will be as shown in Figure 5.4 for $s_{u,ref}$ equal to 68 kPa.

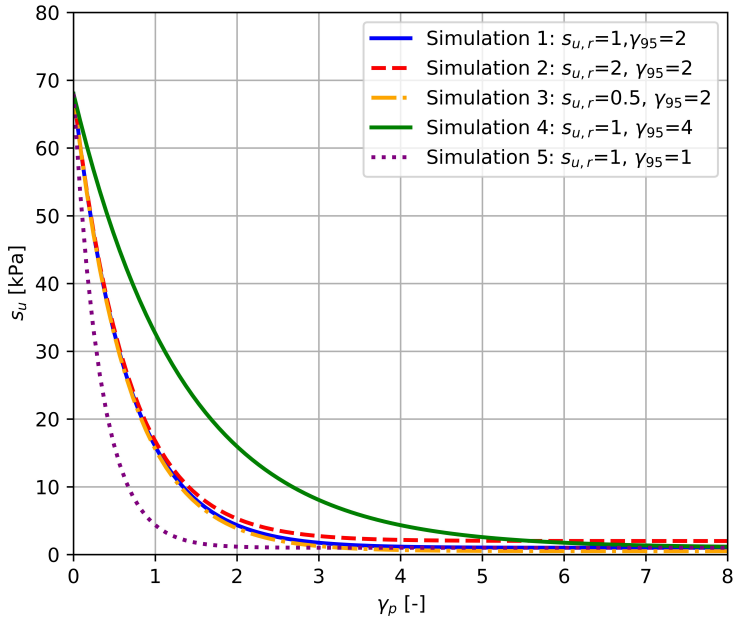

Figure 5.4: Accumulated plastic shear strain versus undrained shear strength for the 2D simulations.

The second phase of the simulation is run for 70 seconds with a time step of 5 seconds. Table 5.3 shows the specifications for the simulations. The simulations were performed on the supercomputer Betzy provided by Sigma2 - the National Infrastructure for High Performance Computing and Data Storage in Norway.

Table 5.3: Specifications for the 2D MPM simulations.

Grid size	0.2 m x 0.2 m
Number of elements	1 040 412
Material points per cell	4

5.2 3D Empirical Methods

The empirical methods are used to estimate the retrogression distance based on the geometry of the slope and the soil layering. It is therefore not necessary to determine any material properties. As the criteria only apply backward or perpendicular to the contour lines for an initial slide, several profiles are drawn to define the retrogression extent for the whole area. The profiles are drawn where the slopes are

assumed the most critical. Some additional profiles in the bottom of the ravines are also used. Figure 5.5 shows a map with all the profiles used in the analyses.

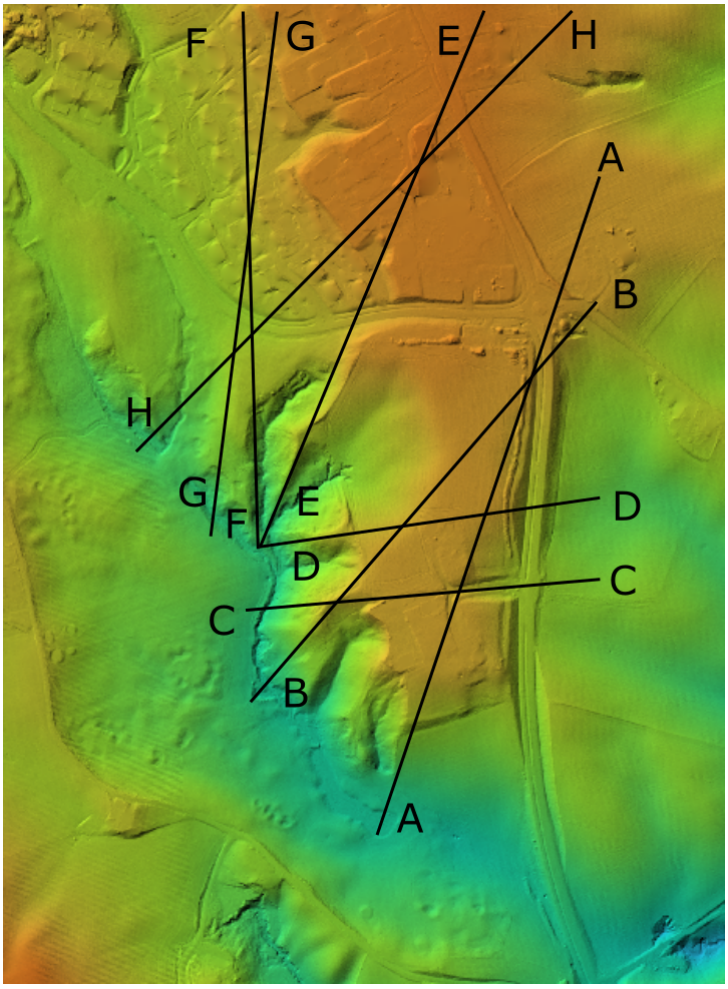

Figure 5.5: Profiles used for the empirical criteria.

The empirical methods are divided into three analyses, with successively more information about the area and soil profile:

1. Terrain
2. Terrain and bedrock
3. Terrain, bedrock and sensitive clay layer

The same soil profiles are used for all three analyses. All information on terrain, soil layering, and bedrock is retrieved from the Leapfrog model made by Multiconsult for NVE. The Leapfrog model from 23.03.2022 (revision 1) is used for the profiles, see Multiconsult (2022) for documentation.

5.2.1 Terrain

The first method evaluates the retrogression distance based on the terrain profile. The chosen criteria is a 1:15 line, drawn from 0.25H below the toe of the slope. This criterion is similar to the national mapping criteria in Norway $L = 15H$, where L is the length of retrogression and H is the height of the slope (Norwegian Water Resources and Energy Directorate, 2019). For plateaus, $L = 15H$ will coincide with a line with an inclination of 1:15 drawn from the toe of the slope. However, if the plateau has a limited extent, $L = 15H$ will overestimate the length of retrogression and give a gentler inclination than 1:15. This is not desired, and a 1:15 line $0.25H$ below the toe of the slope is chosen instead. The criterion is illustrated in Figure 5.6.

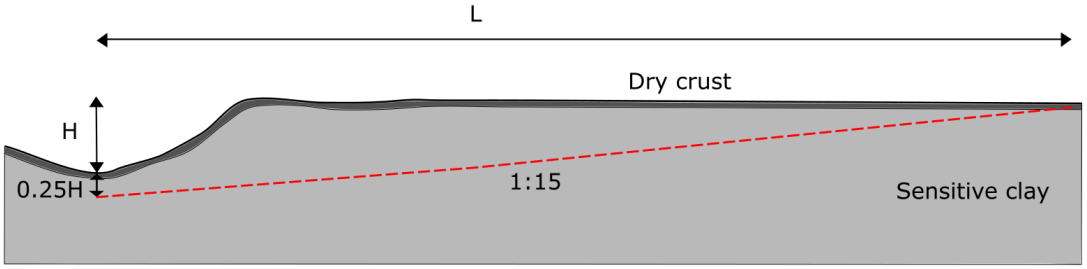

Figure 5.6: Criterion based on terrain.

5.2.2 Terrain and Bedrock

The second method accounts for the terrain profile and the bedrock elevation. The bedrock elevation could either be assumed from geotechnical ground investigations, such as total sounding, or be estimated from seismic investigations. 1:15 lines are plotted from $0.25H$ below the toe of the slope. If the line hits bedrock, a new line with the inclination of 1:3 is drawn from the bedrock up to the terrain. This point in the terrain defines the maximum extent of retrogression. 1:3 or 1:2 is commonly used to define the angle of the back scarp, as described in section 2.4.4. An illustration of this criterion is given in Figure 5.7.

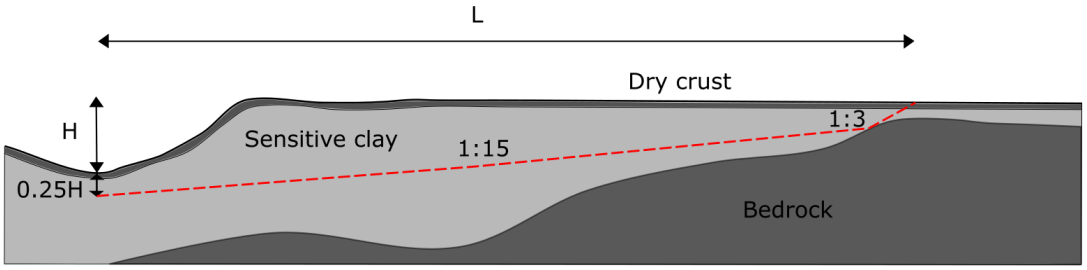

Figure 5.7: Criterion based on terrain and bedrock.

5.2.3 Terrain, Bedrock and Sensitive Clay Layer

For the third method, the terrain profile, the bedrock elevation, and the sensitive clay layer are taken into account, which gives the most restricted retrogression distance. Ground investigations must be interpreted to indicate the placement and extent of the sensitive clay layer. 1:15 lines are plotted from $0.25H$ below the toe of the slope until it hits bedrock or the outer boundary of the sensitive clay layer. Similar to the second method, a new line with the inclination of 1:3 is drawn from this point and up to the terrain to limit the retrogression distance. This corresponds to the simplified NGI-method for the extent of retrogression (Haugen, Tveit, and Heyerdahl, 2017). Figure 5.8 shows the principle of the criterion.

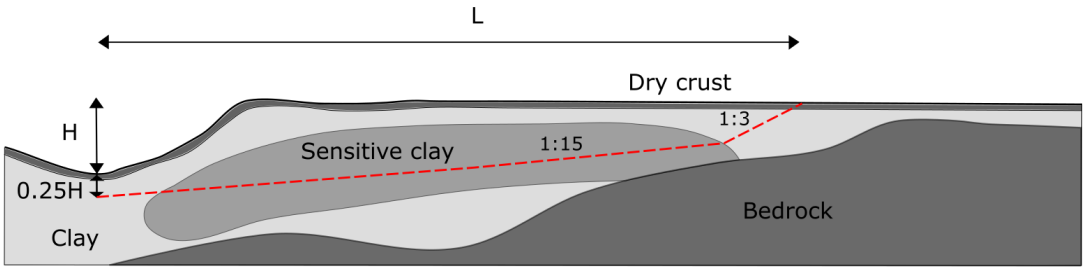

Figure 5.8: Criterion based on terrain, bedrock, and sensitive clay layer.

5.3 3D Numerical Method

5.3.1 Numerical Geometry

The soil layering for the numerical model is based on the Leapfrog model from 01.07.2021 (revision 0). Multiconsult (2021c) provides documentation for this model. The changes between revisions 0 and 1 are minimal. Due to the complexity and the necessary computational capacity, a simplified version of the soil layering was used. Therefore, only the bedrock and sensitive clay is considered, while the rest is assumed as clay.

The MPM model is made according to the principles by Fernández, Amaral Vargas, and Quadros Velloso (2020). To make the numerical geometry each soil layer must be defined. A layer is defined by two surfaces, that are constructed by several coordinates (x, y, z). All material points between two surfaces are set to one type of soil material. To define all of the layers it was necessary with six surfaces, hence z_0 to z_5. In points where not all layers were present, the z for these surfaces was omitted, see Figure 5.9. For the outer boundaries of each layer, the z-value of the turning point was used for both the upper and lower surface to close the layer.

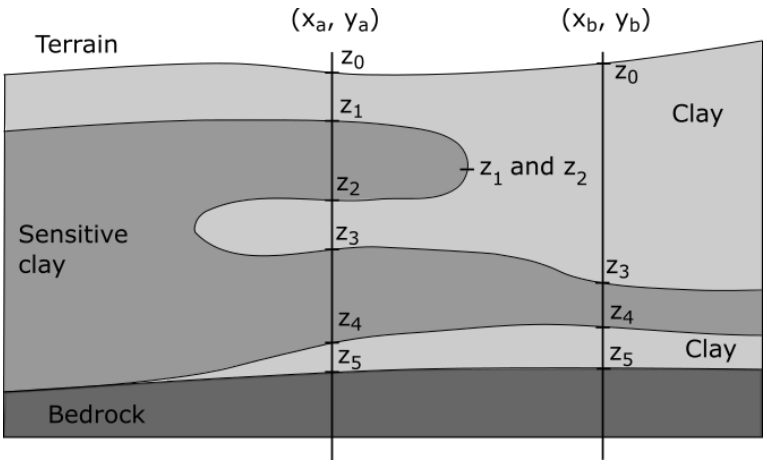

Figure 5.9: Illustration of how layers are made for the MPM model.

The Leapfrog model uses the digital terrain model (DTM) *NDH Akershus 2pkt 2015* from Kartverket (2015) to define the terrain. The same DTM is therefore used to define the terrain (surface z_0) for the simulation. Figure 5.10 shows the terrain elevation used.

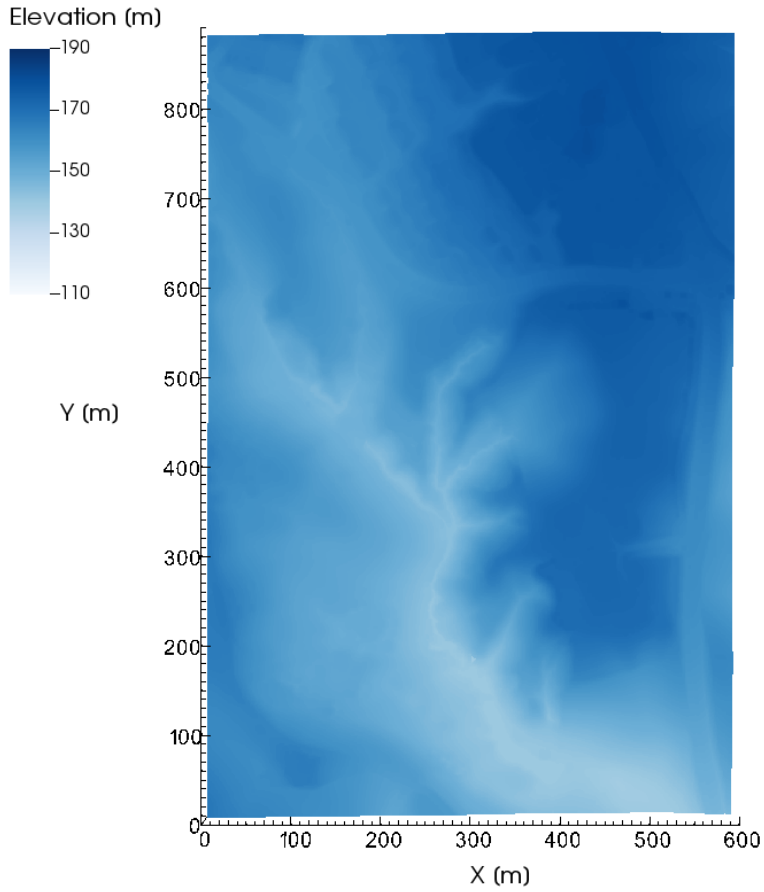

Figure 5.10: Terrain elevation used for the 3D simulations.

The bedrock layer is retrieved directly from the Leapfrog model. The Leapfrog mesh of the bedrock is coarse, and linear interpolation is therefore used to obtain a resolution of 1 m. This gives the bedrock elevation shown in Figure 5.11. The bedrock is extended upwards to the terrain along each side to avoid the clay from collapsing due to lack of side-support.

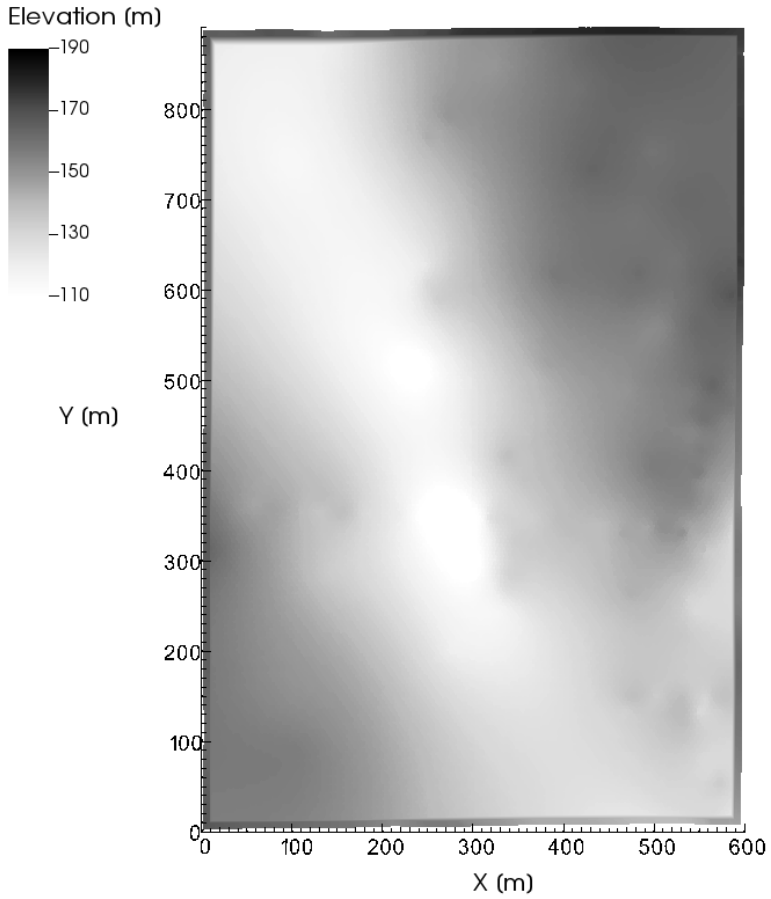

Figure 5.11: Bedrock elevation used for the 3D simulations.

The sensitive clay layer in the Leapfrog model is highly detailed. The mesh is therefore too complex to be used directly for the numerical geometry for the sensitive clay. To extract coordinates from the mesh to define surfaces, a regular grid of points is needed. This ensures that all points (x, y) have several z-values and therefore simplifies the process to define which surface each z-value belongs to. To create the regular grid, each vertex is moved, with a maximum of 5 meters. This ensures that there are points every 10 meters in both x- and y-direction within the layer. All vertices were moved to the closest grid point. Figure 5.12 shows the sensitive clay layer before and after the modification. Areas where the sensitive clay layer was thinner than 1 m, are omitted because the grid size of 1 m does not allow layers thinner than this.

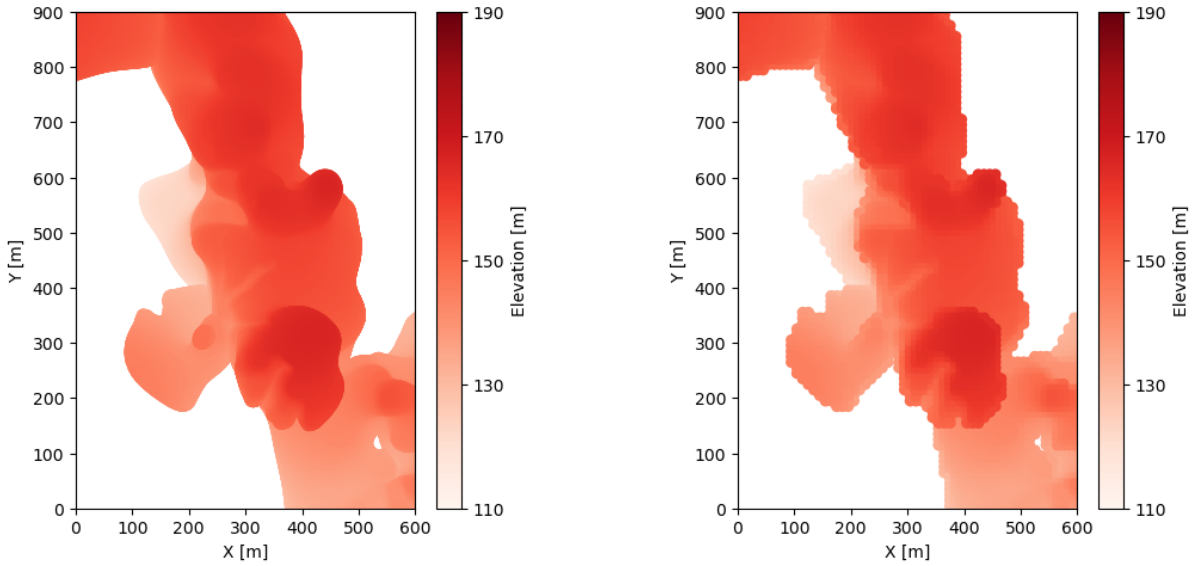

(a) (b)

Figure 5.12: Numerical geometry of sensitive clay layer a) before modification, directly from the Leapfrog model and b) after modification to a regular grid.

The numerical geometry of the sensitive clay layer used in the MPM model is shown in Figure 5.13. Due to how each surface was defined and the interpolation in the MPM, there are some differences between Figure 5.12b and Figure 5.13.

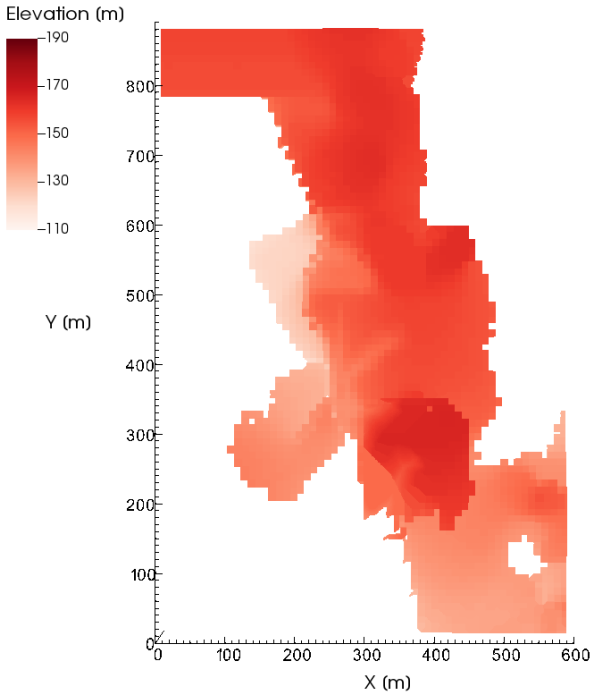

Figure 5.13: Final numerical geometry of the sensitive clay layer.

5.3.2 Geotechnical Parameters

The material model described in section 3.2 is used for the 3D simulations. Table 5.4 summarizes the chosen parameters for the different layers.

Table 5.4: Soil properties for the 3D simulations.

Parameter	Unit	Clay	Sensitive clay
γ	kN/m^3	19.5	19.5
K	MPa	102	102
G	MPa	72	72
$s_{u,ref}$	kPa	Spatially varying	Spatially varying
φ	°	0	0
$s_{u,r}$	kPa	-	1
$S_{t,1}/S_{t,2}$	-	1/2	-
γ_{95}	-	0.2	0.2
ψ	°	0	0

The friction angle is set to 0 to have an undrained condition. The values of K and G are chosen to minimize the computational capacity needed for the simulation. The remolded shear strength is set to 1 kPa, as in the 2D analysis. The sensitivity of the clay layer is set to either 1, meaning no shear strength degradation, or 2 which gives the clay semi-brittle behavior. The two different sensitivities are chosen to investigate whether the latter gives a more realistic approach to the Gjerdrum slide because clay rarely has a perfectly plastic behavior after failure.

γ_{95} is scaled according to the scale of the grid, such that $\gamma_{95} = 1$ for the 2D simulation corresponds to $\gamma_{95} = 0.2$ for the 3D analysis. The dilatancy angle is set to 0 to avoid plastic volume change.

The undrained shear strength has a spatial variability. Available shear strength profiles from Multiconsult (2021a) are used to determine the shear strength. The position of the boreholes is shown in Figure 5.14.

Each material point in the MPM model must be assigned an undrained shear strength. To obtain the undrained shear strength in every point, the RBFInterpolator function in the scipy library was used to perform a linear radial basis interpolation between the boreholes. This interpolation function takes the nearest boreholes to the material point into account and scales the different boreholes based on the distances from the material point to the boreholes. To use a more accurate method is not reasonable, as the input data has high uncertainty.

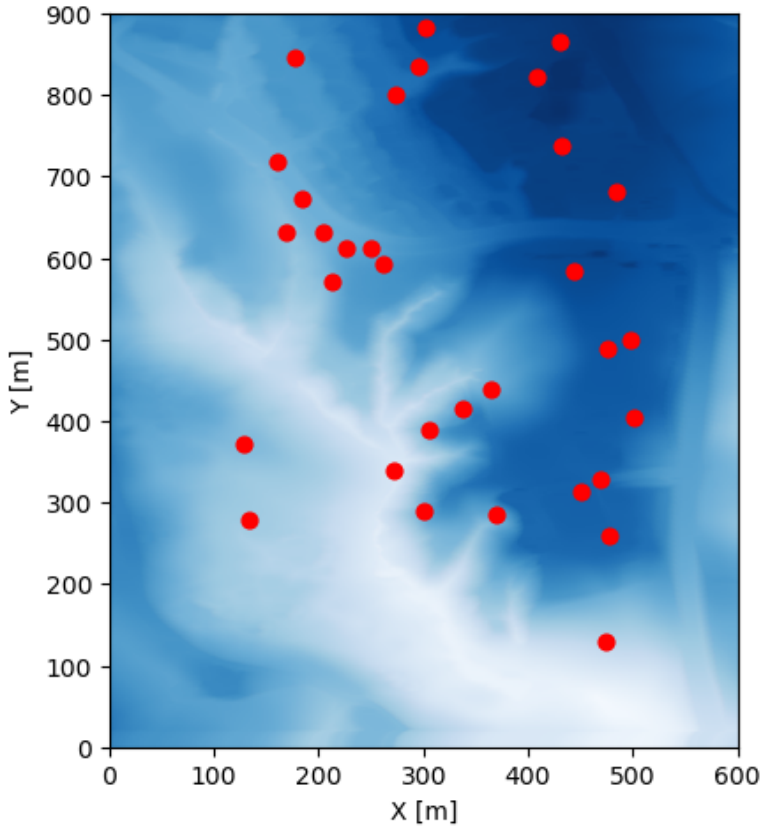

Figure 5.14: Position of boreholes used to define the undrained shear strength for the 3D simulations.

The interpolation results in the spatial variability of the undrained shear strength shown in Figure 5.15 and Figure 5.16. Both layers show an increasing shear strength with depth. The strength is high toward the east. Furthermore, the strength is higher in the bottom of the ravines and along Tistilbekken. Figure 5.15 shows that a low value is obtained for the nearest corner of the clay layer. This is due to few boreholes in this area, and a trend of decreasing shear strength with increasing elevation. There are also several other areas with particularly low shear strength. Appendix B shows additional figures of the undrained shear strength from other angles.

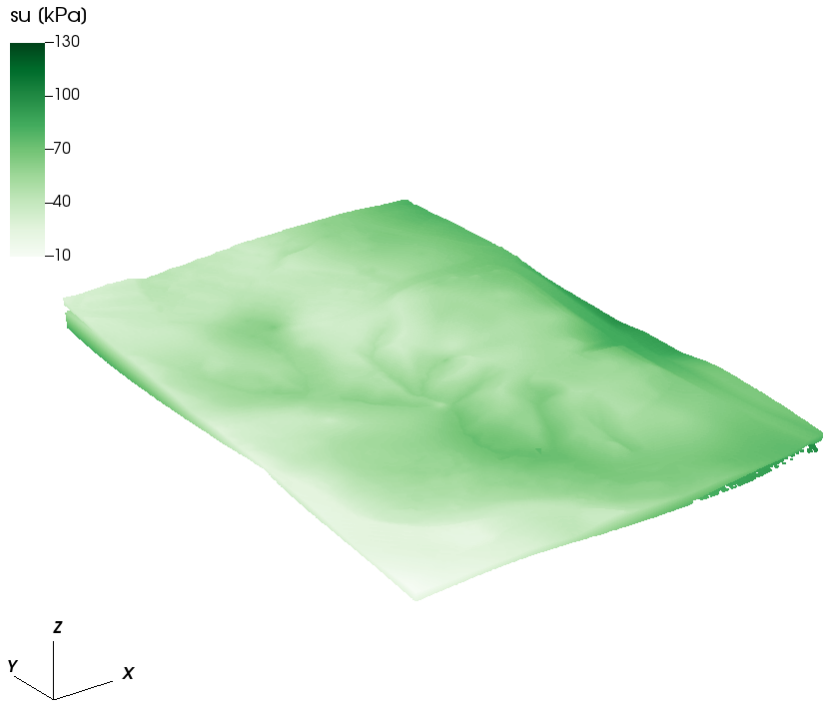

Figure 5.15: Spatial variability of the reference undrained shear strength of the clay layer for the 3D simulations.

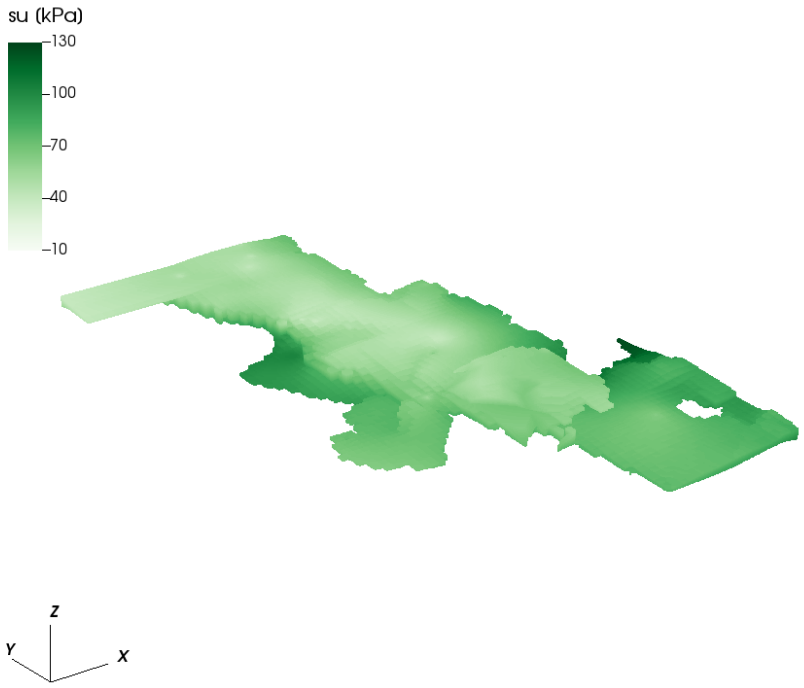

Figure 5.16: Spatial variability of the reference undrained shear strength of the sensitive clay layer for the 3D simulations.

5.3.3 Simulations

Three different simulations are run for the 3D analysis. The first simulation only accounts for terrain and bedrock and assumes all material between as sensitive clay. The second and third simulation also takes the sensitive clay layer into account. All non-specified material between bedrock and terrain is defined as clay. The second simulation uses a sensitivity of 1 for the clay, while the third simulation uses a sensitivity of 2.

All three simulations are run with a time step of 10 seconds. Table 5.5 shows the specifications for the simulations. The simulations were performed on the supercomputer Betzy provided by Sigma2 - the National Infrastructure for High Performance Computing and Data Storage in Norway.

Table 5.5: Specifications for the 3D MPM simulations.

Grid size	1 m x 1 m
Number of elements	45 924 000
Material points per cell	8

Chapter 6

Results

This chapter presents relevant results from the 2D numerical analyses, as well as the 3D empirical and numerical analyses.

6.1 2D Numerical Analyses

Simulation 1 is treated in depth to show the results from the simulations. Both shear strain and velocity are presented for specific time steps. To present the difference in retrogression distance between the simulations, the final time step is shown for all simulations. Additional results can be found in Appendix C, which shows shear strain and velocity for every time step from all the simulations.

The shear strain contours show the development of failure surfaces, see Figure 6.1. After 10 seconds, a large single rotational failure has developed and the slide masses have begun to move away from the failure surface. After 20 seconds, two additional rotational failure surfaces have developed. The slide has become retrogressive. The masses from the second failure have already moved away from the back scarp and the soil from the third failure is visible above the bottom of the last failure surface. The debris from the first failure has moved further to the left boundary and has experienced increased shear strain. At 30 seconds, a fourth and fifth failure surface has developed. The shear zone of the fifth failure is visibly thicker than the previous shear zones and has a gentler inclination. The only slide debris left from the first failure in the profile is the two large blocks of blue soil material in the left of the figure. These blocks partly prevent slide debris from the consecutive failures to move away from the back scarp. After 40 seconds, a sixth failure surface starts to develop with a shear strain of around 0.25. More of the slide debris have moved out of the left boundary and only a small amount from the first failure remains within the profile. The remaining debris has also moved toward the left. When time is equal to 70 seconds the sixth failure surface has not developed any further, and the retrogression has stopped. More

of the slide debris has moved out of the left boundary and the remaining debris in the slide crater has an approximately horizontal surface.

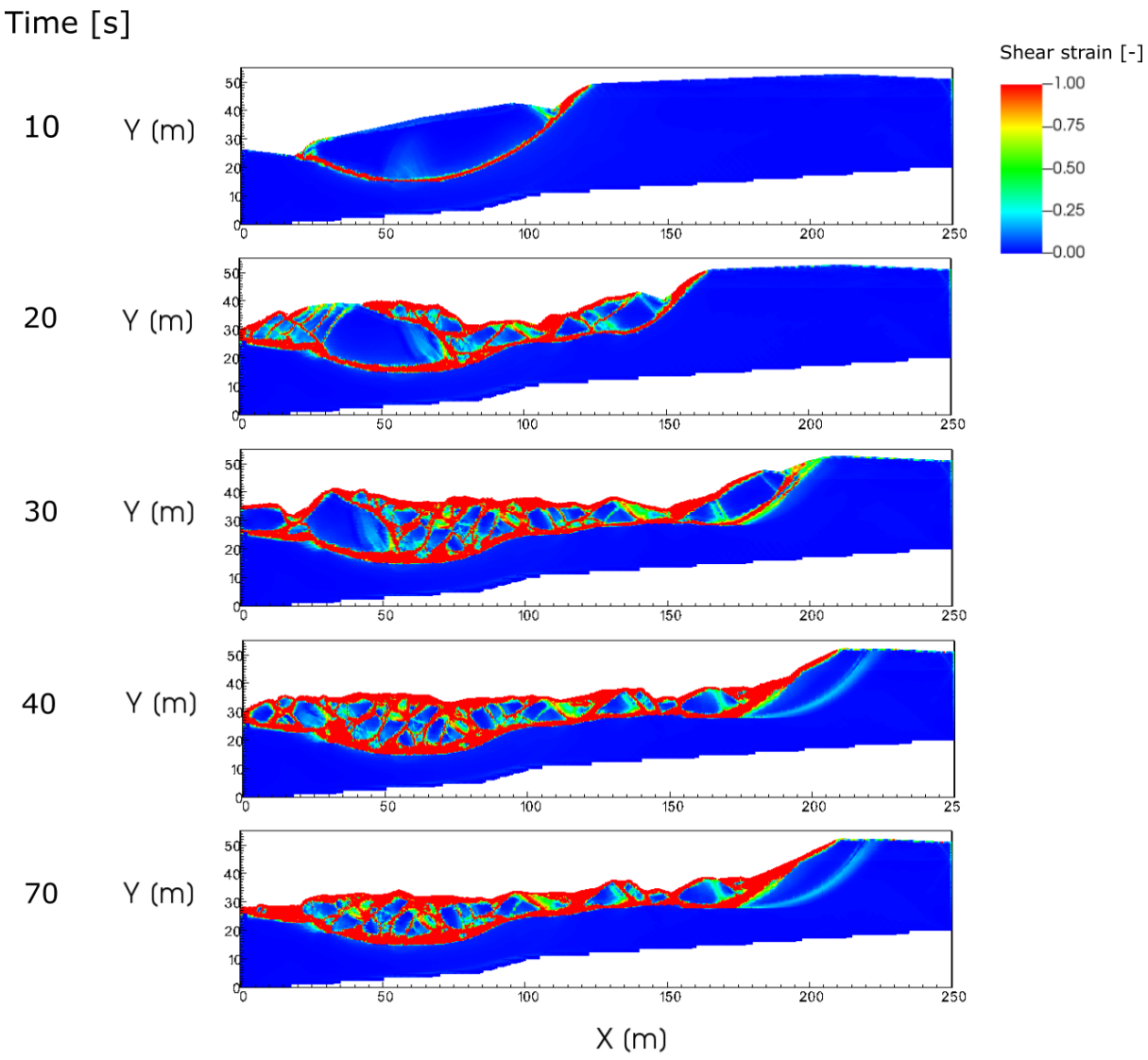

Figure 6.1: Shear strain for chosen time steps for simulation 1. All shear strain larger than 1 is displayed as red.

The velocity of the soil block from the first failure after 10 seconds, shown in Figure 6.2, is higher at the bottom of the soil block near the failure surface. At 20 seconds, the third slide mechanism has a high velocity. The material from the second slide is placed above and to the right of the displaced material from the first slide and has a velocity of around 3.5 m/s. The material closest to the left boundary has a high velocity, while the rest of the material from the initial slide has a lower velocity. The light blue block with a velocity of around 2 m/s corresponds with the intact soil block shown in Figure 6.1.

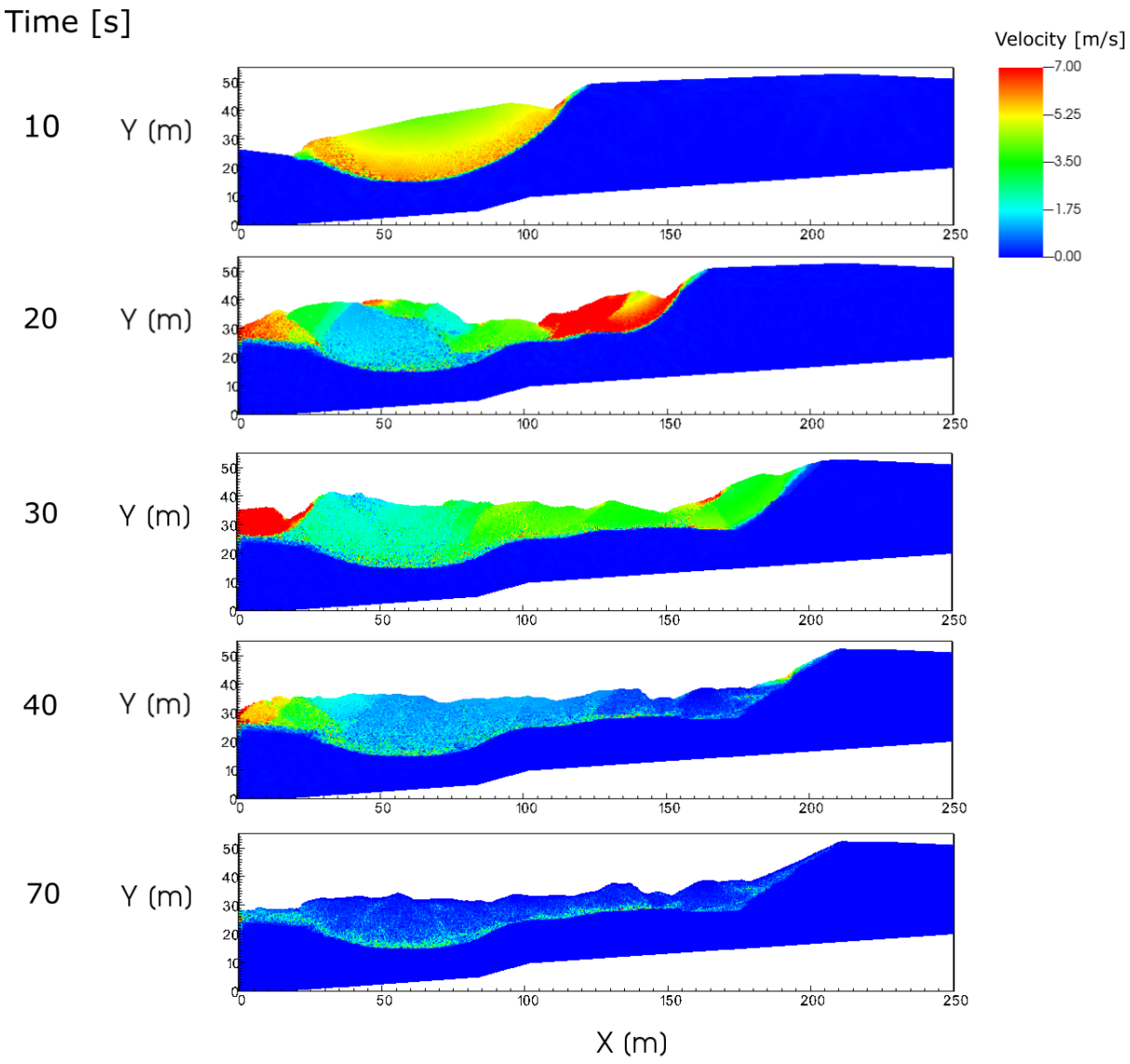

Figure 6.2: Velocity for chosen time steps for simulation 1. All velocity higher than 7 m/s is displayed as red.

After 30 seconds, the slide debris has a more homogeneous velocity, except for one soil block close to the left boundary. No additional failure surfaces develop after 40 seconds and the displaced material has a significantly lower velocity. There is little to no movement at 70 seconds. The top of the slide debris has zero velocity, while the material closer to the bottom of the slide crater has a velocity of around 1.75 m/s.

Simulation 1 shows a retrogression distance of 180 m, see Figure 6.3. Simulation 2 in Figure 6.4 gives the same retrogression distance of 180 m as simulation 1. There is slightly more accumulated material above the original terrain close to the left boundary. The final shear band has a lower shear strain than

in simulation 1.

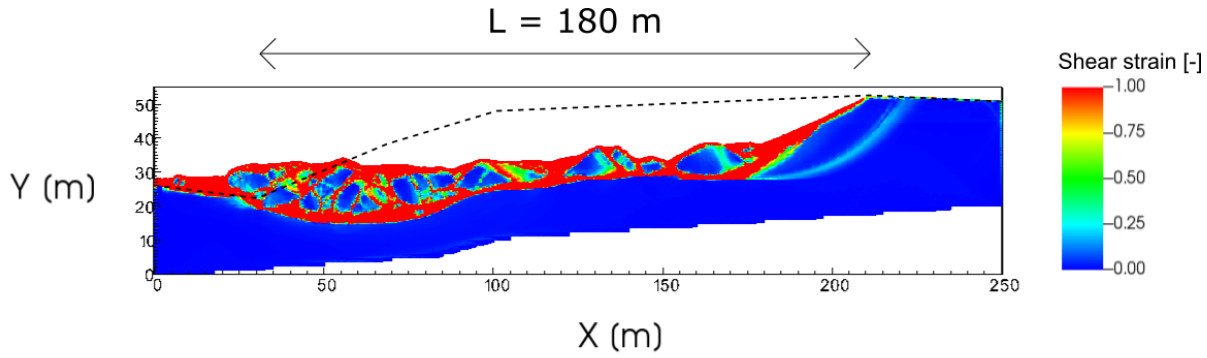

Figure 6.3: Retrogression distance of simulation 1. All shear strain larger than 1 is displayed as red.

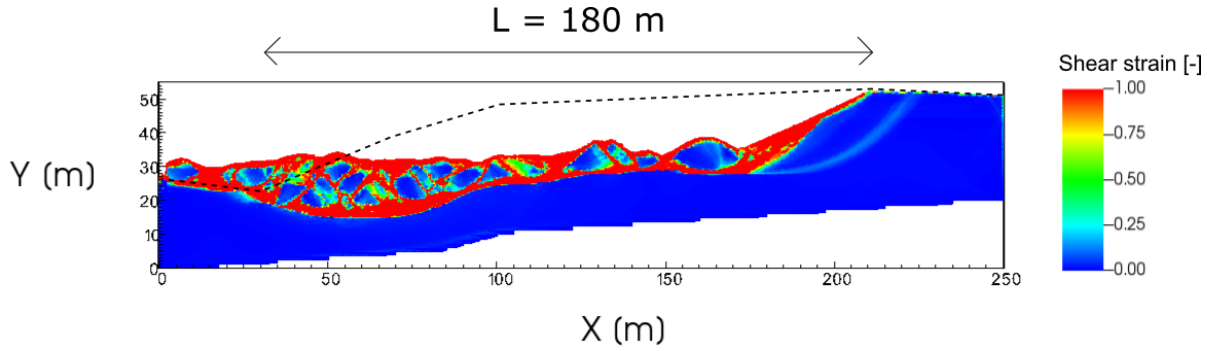

Figure 6.4: Retrogression distance of simulation 2. All shear strain larger than 1 is displayed as red.

Simulation 3 in Figure 6.5 shows the same retrogression distance of 180 m as the previous two simulations. However, the displaced material has moved less than in simulations 1 and 2.

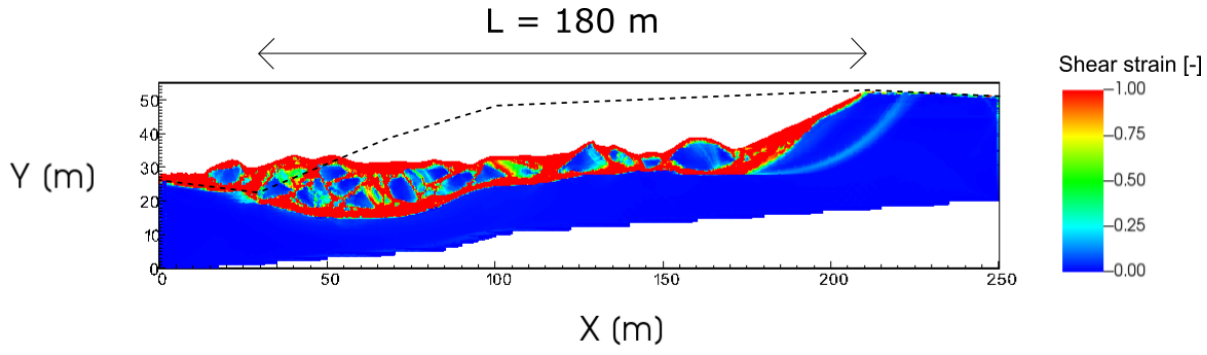

Figure 6.5: Retrogression distance of simulation 3. All shear strain larger than 1 is displayed as red.

Figure 6.6 shows a retrogression distance of 185 m for simulation 4. The crest of the back scarp is less defined than for simulations 1 to 3. In addition, the final shear band is wider and has a larger shear strain than in the previous simulations. The shear failure propagates deeper into the clay near the toe of the slope, and a larger amount of material is remolded.

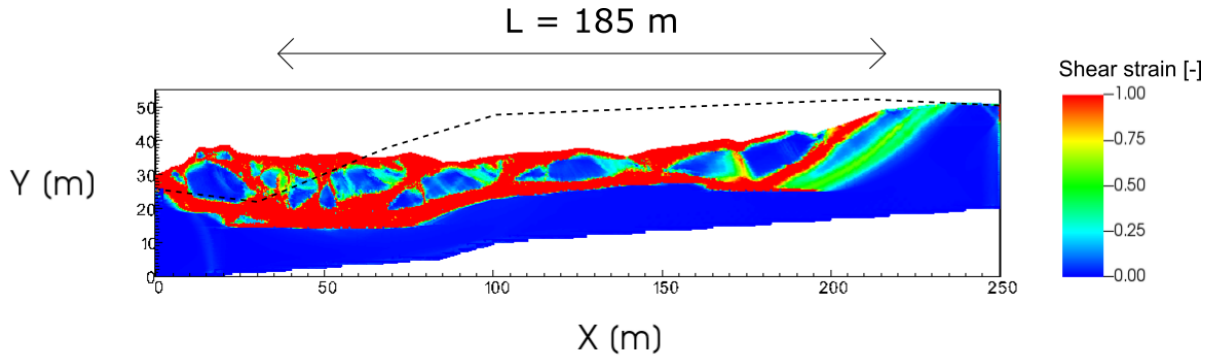

Figure 6.6: Retrogression distance of simulation 4. All shear strain larger than 1 is displayed as red.

Simulation 5 in Figure 6.7 shows a retrogression distance of 205 m. This is the highest retrogression distance obtained in the simulations. Similar to simulation 4, the shear failure near the toe of the slope is deeper than for simulations 1 to 3. The final shear band has a larger shear strain than in simulations 1 to 4. The displaced material has moved further away from the back scarp than in simulation 4, and less material is left in the slide crater. Both simulation 4 and 5 have larger areas that experience shear strain of 1 or larger.

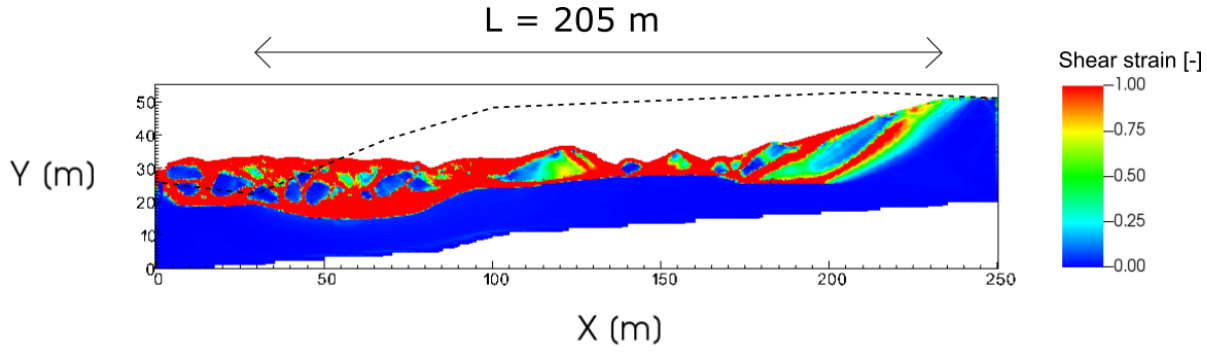

Figure 6.7: Retrogression distance of simulation 5. All shear strain larger than 1 is displayed as red.

The retrogression distance for all five simulations is presented in Table 6.1. To sum up, variation in γ_{95} affects the retrogression distance, while variation in $s_{u,r}$ has no effect on the retrogression distance.

Table 6.1: Retrogression distances for variation of γ_{95} and $s_{u,r}$.

Parameter	Value	Retrogression distance [m]
γ_{95} [-]	1	205
	2	180
	4	185
$s_{u,r}$ [kPa]	0.25	180
	0.50	180
	1.00	180

To compare the retrogression of the simulation to the retrogression of the slide, Figure 6.8 and Figure 6.9 show both the simulation result and the terrain after the slide. Simulations 1 and 5 are chosen because they represent the lower and upper limit.

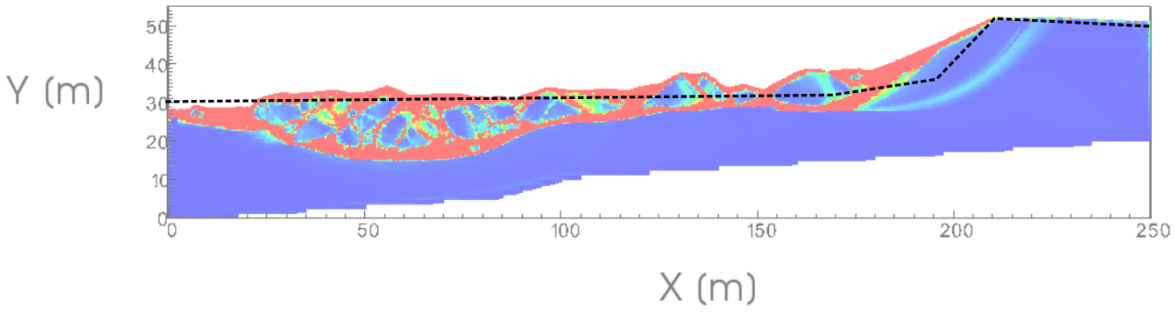

Figure 6.8: Terrain after simulation 1. The terrain after the Gjerdrum slide is shown with a black dashed line.

Simulation 1 shows a good correlation for the crest of the back scarp, while simulation 5 gives a slightly longer retrogression distance compared to the Gjerdrum landslide. Both simulations result in a gentler back scarp than for the slide, which has a back scarp around 47°.

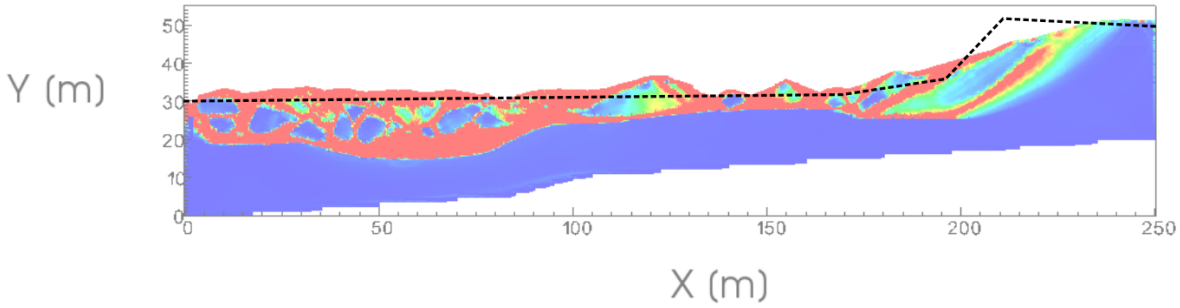

Figure 6.9: Terrain after simulation 5. The terrain after the Gjerdrum slide is shown with a black dashed line.

All simulations show a retrogressive behavior, with several rotational failures, see illustration in Figure 6.10 for the development of failure surfaces for simulation 1. Each failure surface appears to be fully developed before any significant movement occurs. Apart from the elevation of the terrain after the slide, little information is known about how the initial slide developed in the Gjerdrum slide.

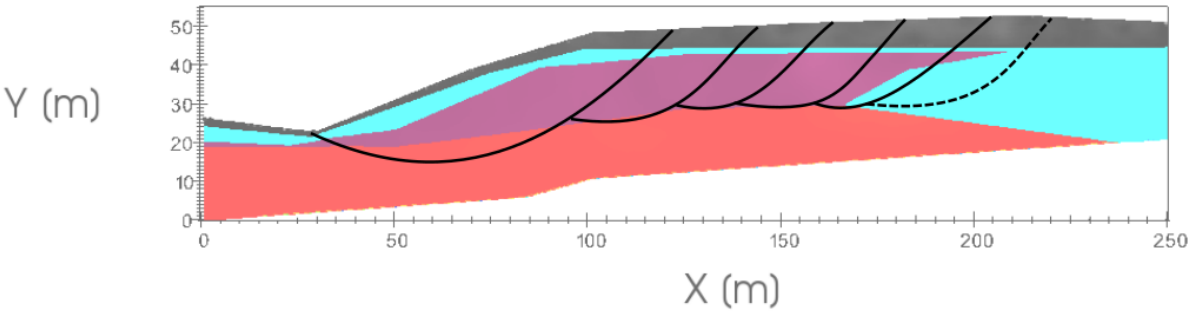

Figure 6.10: Retrogressive development of simulation 1 shown with the soil layering. The dashed line represents a shear band that did not fully develop.

Figure 6.10 shows that the propagation stops approximately where the sensitive clay layer stops.

6.2 3D Empirical Analyses

The retrogression areas are drawn based on the retrogression distances obtained from the empirical criteria. In some areas that had profiles close together, the different retrogression distances conflicted. In these cases, the retrogression distance which gave the largest area was chosen to have a conservative approach. Appendix D shows the retrogression distances and criteria for all the profiles.

The potential retrogression area is the largest for the criterion that only takes the terrain into account, see Figure 6.11. This gives an area that extends east of the road and north of the *Gjerdrum bo- og*

behandlingssenter. An area significantly larger than the Gjerdrum slide is defined as the potential retrogression extent.

The criterion that accounts for the bedrock in addition to the terrain, gives a slightly smaller area than the previous criterion. In some areas, the retrogression distance for the first and second criteria coincide. The north boundary is marginally closer to the slide crater, and the east boundary partly follows the road. This gives an area substantially larger than the Gjerdrum slide as potential retrogression extent.

The third criterion, which accounts for the terrain, the bedrock, and the sensitive clay layer, gives a potential retrogression extent closer to the extent of the slide crater. Toward the northwest and partly toward the east, the criterion coincides with the slide crater in Gjerdrum. In the northeast and near Holmen, the criterion defines a larger area than the slide crater. The difference between the second and the third criterion is bigger than the difference between the first and the second criterion.

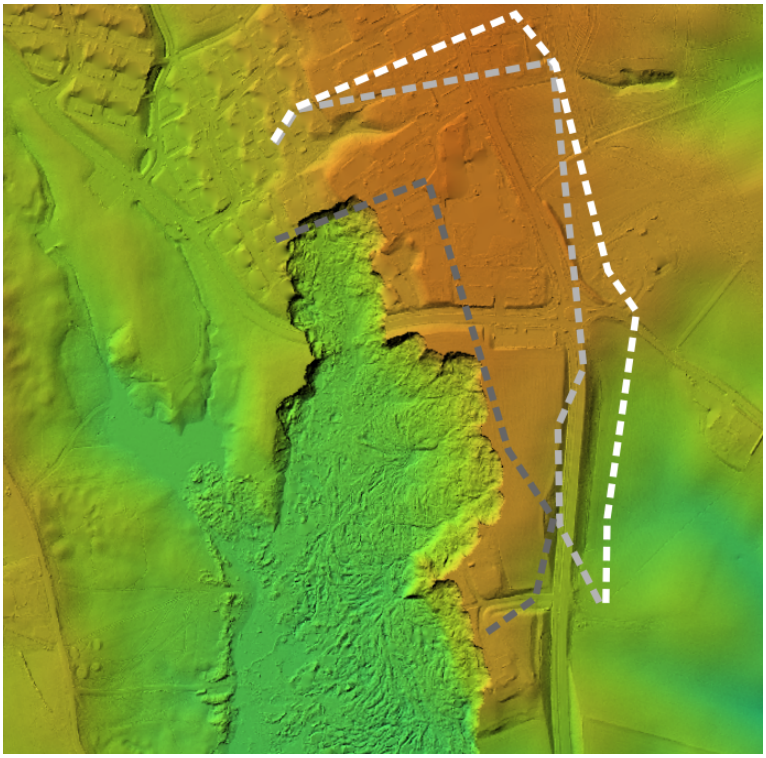

Figure 6.11: Extent of retrogression based on the empirical criteria. White is based on terrain, light grey is based on terrain and bedrock and dark grey is based on terrain, bedrock, and sensitive clay layer.

6.3 3D Numerical Analyses

6.3.1 Terrain and Bedrock

Figure 6.12 shows that failure has occurred in the slope west of Holmen after 10 seconds. The masses within the slide crater are partly remolded, but there are still large blocks of intact clay. Figure 6.13 shows that the slide masses on the top of the plateau at Holmen have a high velocity. The slide debris along the west and the south boundary of the slide crater also has a high velocity. After 20 seconds, the slide has propagated further in all directions. It appears that a soil block is moving downwards from Holmen, as this area shows an extremely high velocity. The slide debris has also displaced toward the south. After 70 seconds, the slide has extended north of Holmen and is moving into Nystulia. At this moment, the center of the slide debris has the highest velocity. It can be seen from Figure 6.13 that there is a lower velocity in a small area in the middle of the high-velocity center. This area coincides with the bottom of one of the ravines. The slide reaches the northern boundary after 130 seconds. The propagation to the east stops when the slide reaches the road. The propagation to the west stops when the terrain elevation starts to increase. The slide debris has moved out of the slide crater and show large mobility. Furthermore, the slide appears to be retrogressive.

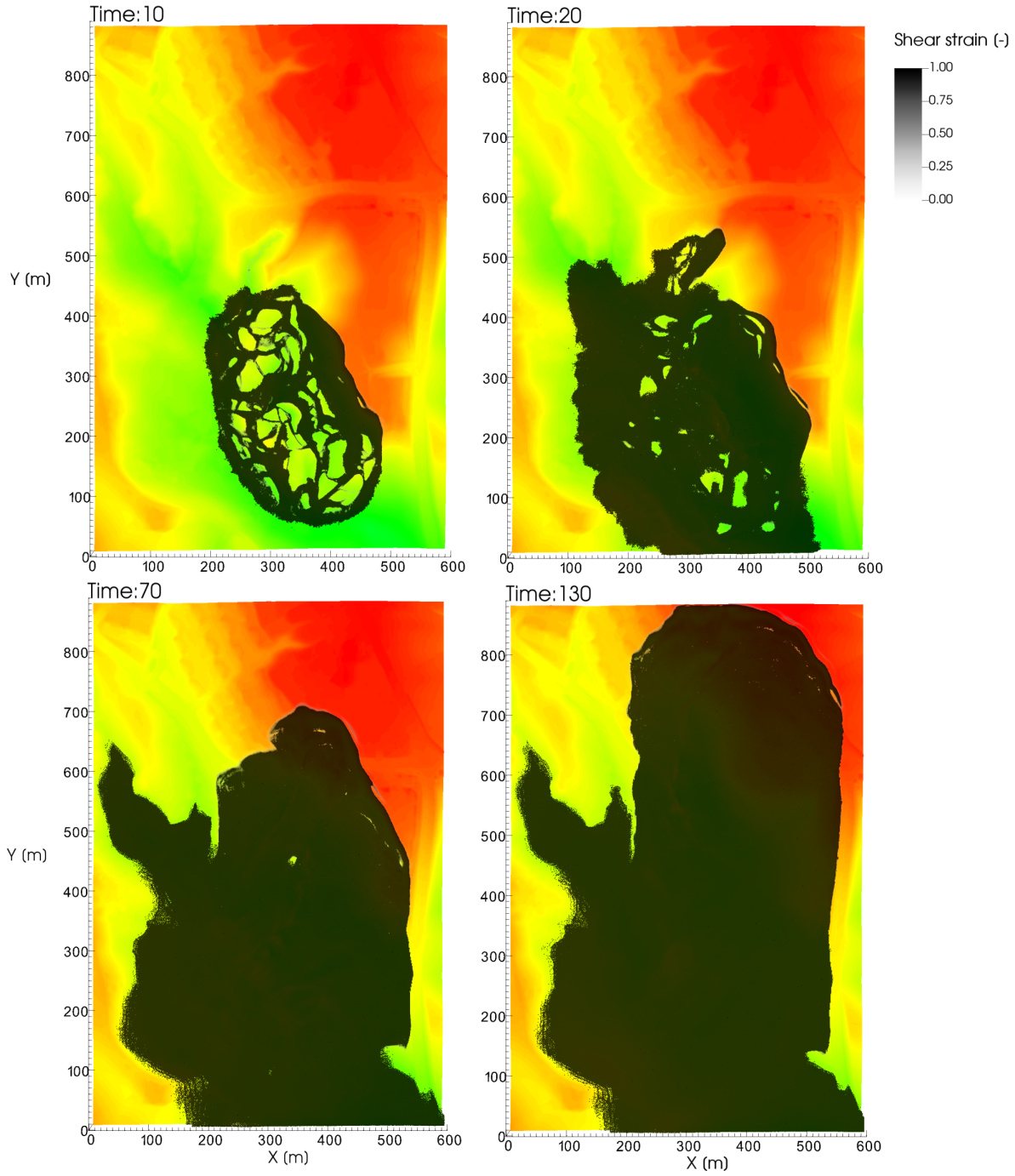

Figure 6.12: Shear strain for simulation 1 for time step 10 s, 20 s, 70 s and 130 s. All shear strain larger than 1 is displayed as black.

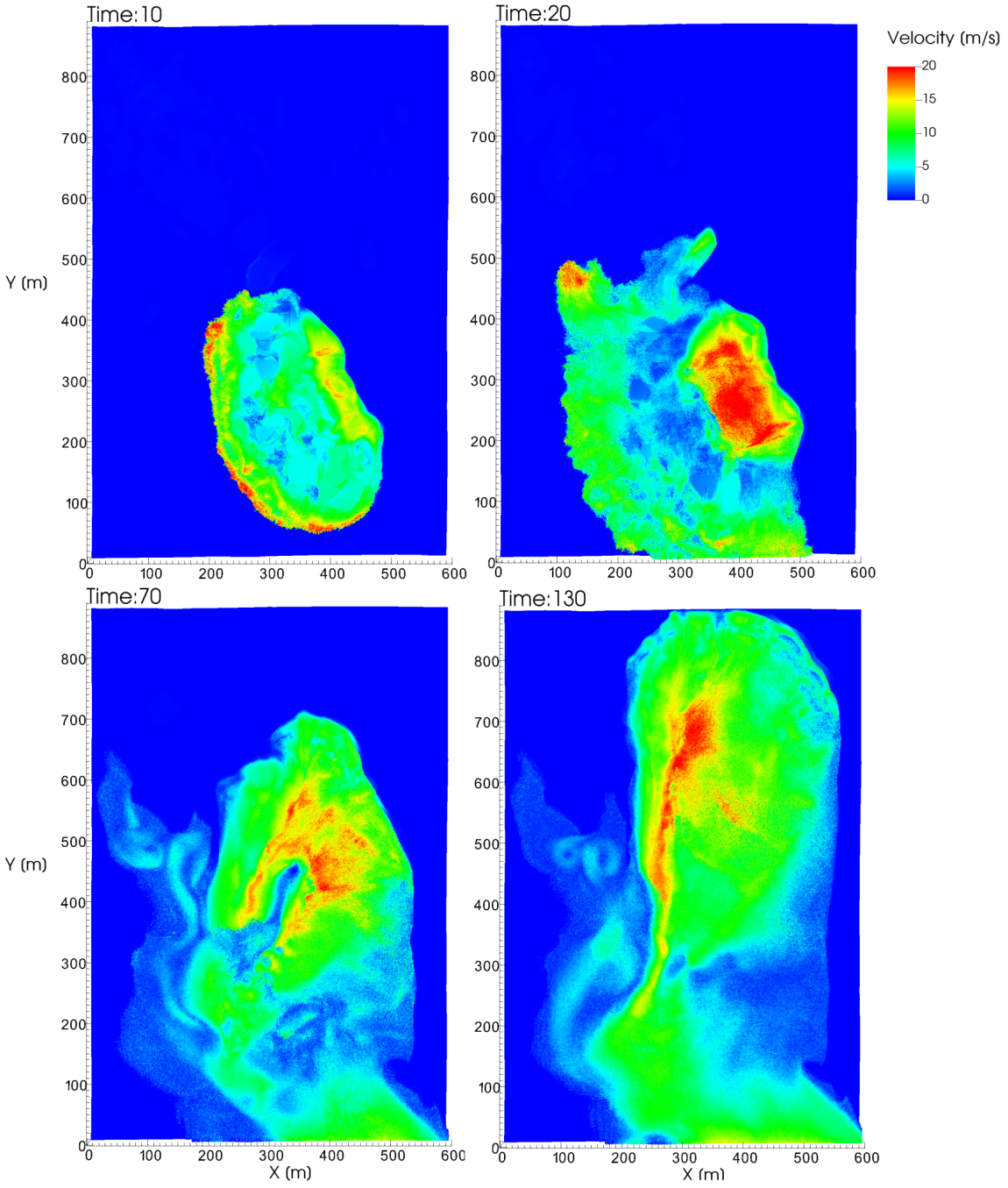

Figure 6.13: Velocity for simulation 1 for time step 10 s, 20 s, 70 s and 130 s. All velocity higher than 20 m/s is displayed as red.

All areas that have moved at least one meter, or have been covered with slide debris are included in the extent of the slide. Compared to the slide at Gjerdrum, the slide in the simulation covers a larger area, see Figure 6.14.

Figure 6.14: Extent of slide in simulation. Background map with outline of detachment area (red) and run-out area (purple) from Ryan et al. (2021).

6.3.2 Terrain, Bedrock, Elastic Perfectly-Plastic Clay Layer, and Sensitive Clay Layer

Figure 6.15 shows that a large failure has occurred after 10 seconds. The slide starts in the slope west of Holmen and it appears to propagate along the ravines toward the northwest. Figure 6.16 also shows a velocity of around 5 m/s in these areas. A higher velocity is found for a small area in the northwest part of the slide. After 20 seconds, the slide has been slightly extended. Toward the east, the failure has propagated further up on the plateau at Holmen. Some of the slide debris appears to move south, as a non-zero velocity is obtained in this area. From Figure 6.16 it can be seen that the small area in the northwest part of the slide still has the highest velocity. An increase in shear strain can also be found here. After 30 seconds, the shear strain is propagating outwards from the small area northwest in the slide area, but a limited extension of the slide can be seen. After 110 seconds, the slide still has not developed remarkably, and the whole area has a low velocity. However, failure has propagated into one of the ravines below Fjellinna. The slide masses do not move out of the crater, as there is no displacement of the intact masses of clay after 20 seconds. The slide does not appear to be retrogressive.

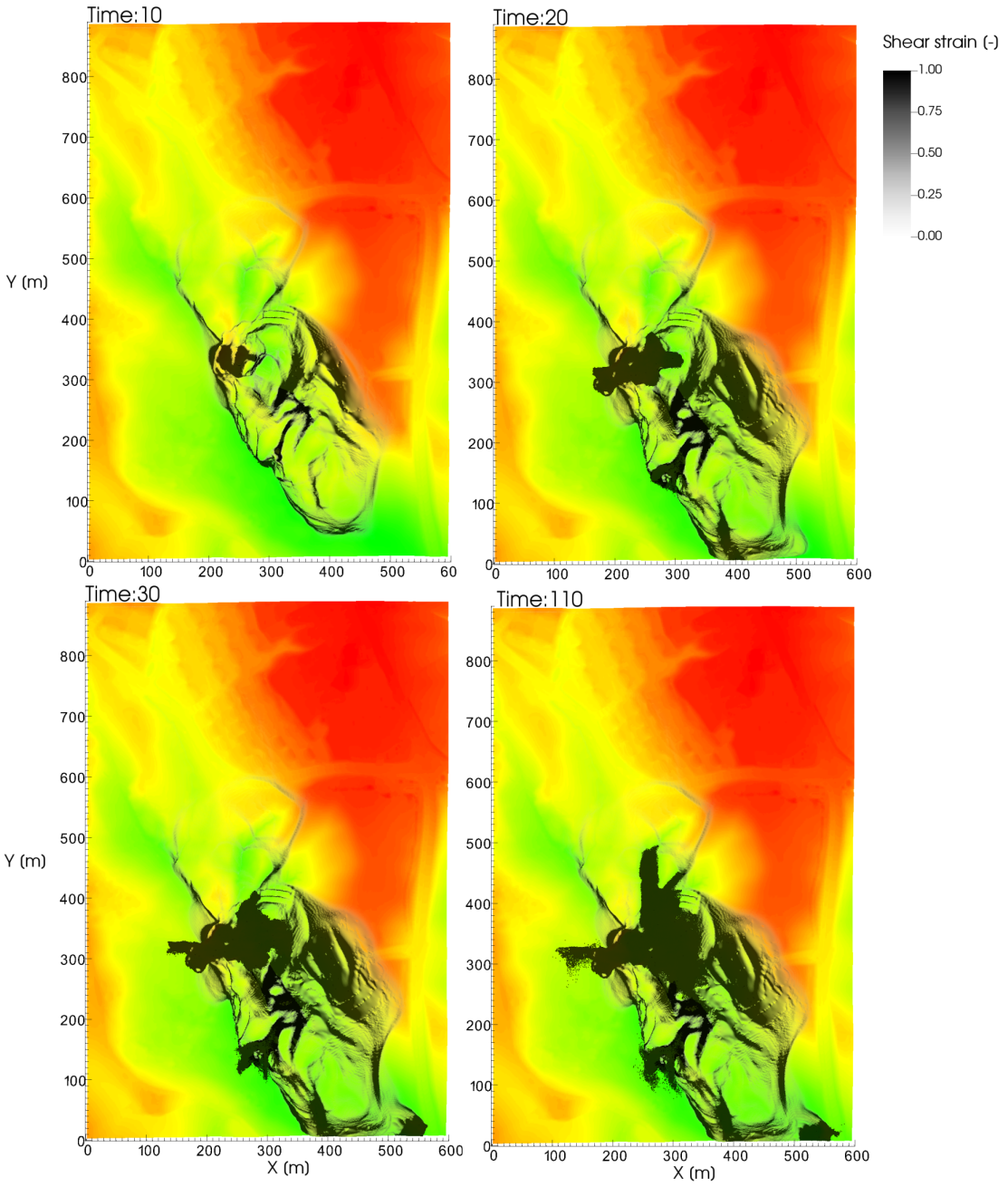

Figure 6.15: Shear strain for simulation 2 for time step 10 s, 20 s, 30 s and 110 s. All shear strain larger than 1 is displayed as black.

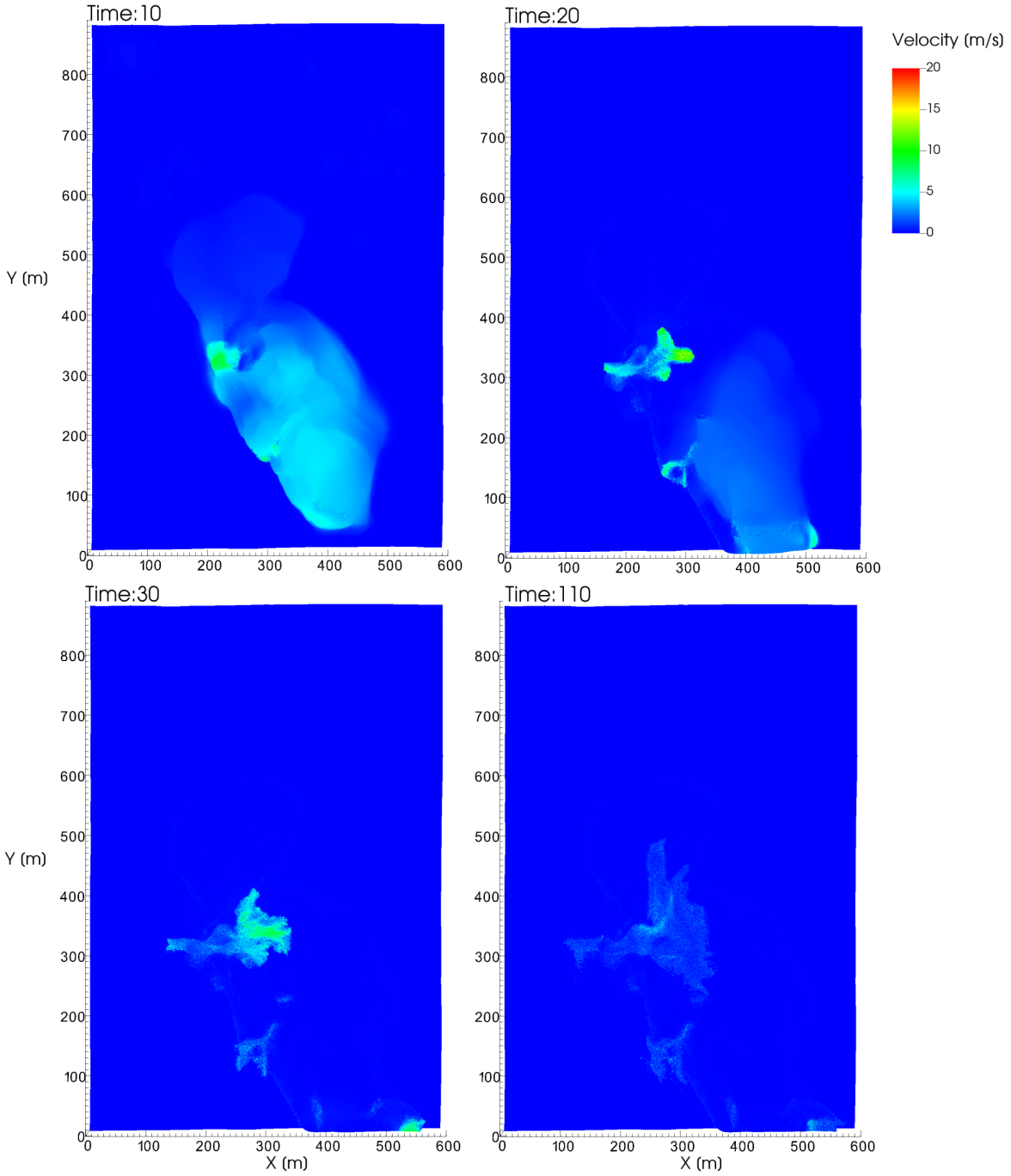

Figure 6.16: Velocity for simulation 2 for time step 10 s, 20 s, 30 s and 110 s. All velocity higher than 20 m/s is displayed as red.

Figure 6.17 shows the extent of the slide in the simulation. Compared to the slide in Gjerdrum, the failure in the simulation propagated further toward Holmen. The slide in the simulation also followed the ravines toward the northwest instead of developing toward the north and northeast.

Figure 6.17: Extent of slide in simulation 2. Background map with outline of detachment area (red) and run-out area (purple) from Ryan et al. (2021).

The slide in the simulation partly follows the sensitive clay layer, which can be seen in Figure 6.18. Figure 6.18 shows the slide extent with the sensitive clay layer.

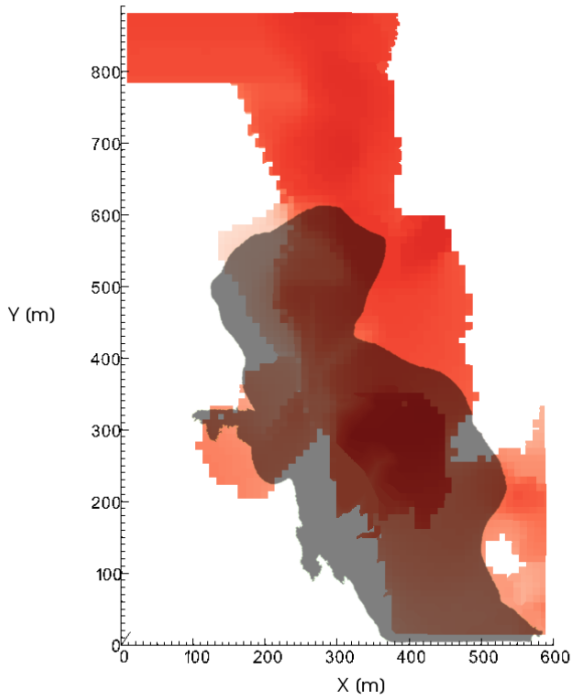

Figure 6.18: Extent of the slide in simulation 2 (grey) with the sensitive clay layer (red).

6.3.3 Terrain, Bedrock, Semi-Brittle Clay Layer, and Sensitive Clay Layer

Figure 6.19 shows that a significant failure has happened after 10 seconds. The failure extends from the slope west of Holmen, along the ravines toward the northwest, and ends west of Nystulia. The southern part of the slide area has a high velocity. After 20 seconds, some of the slide masses have been displaced to the south, which can be seen by a high velocity in this area in Figure 6.20. The slide has also been extended toward the east at Holmen. The highest velocity after 20 seconds can be found in the middle of the slide, which appears to develop toward the west. There is little difference in shear strain between 20 and 30 seconds. However, the velocity shows that the middle of the slide is still developing. After 110 seconds, there is minimal velocity, and there is no significant change in shear strain between 30 and 110 seconds. Similar to the second simulation, there is a minimal amount of slide debris that flows out of the crater. This can be seen by the placement of the intact blocks of clay. The slide does not appear to be retrogressive.

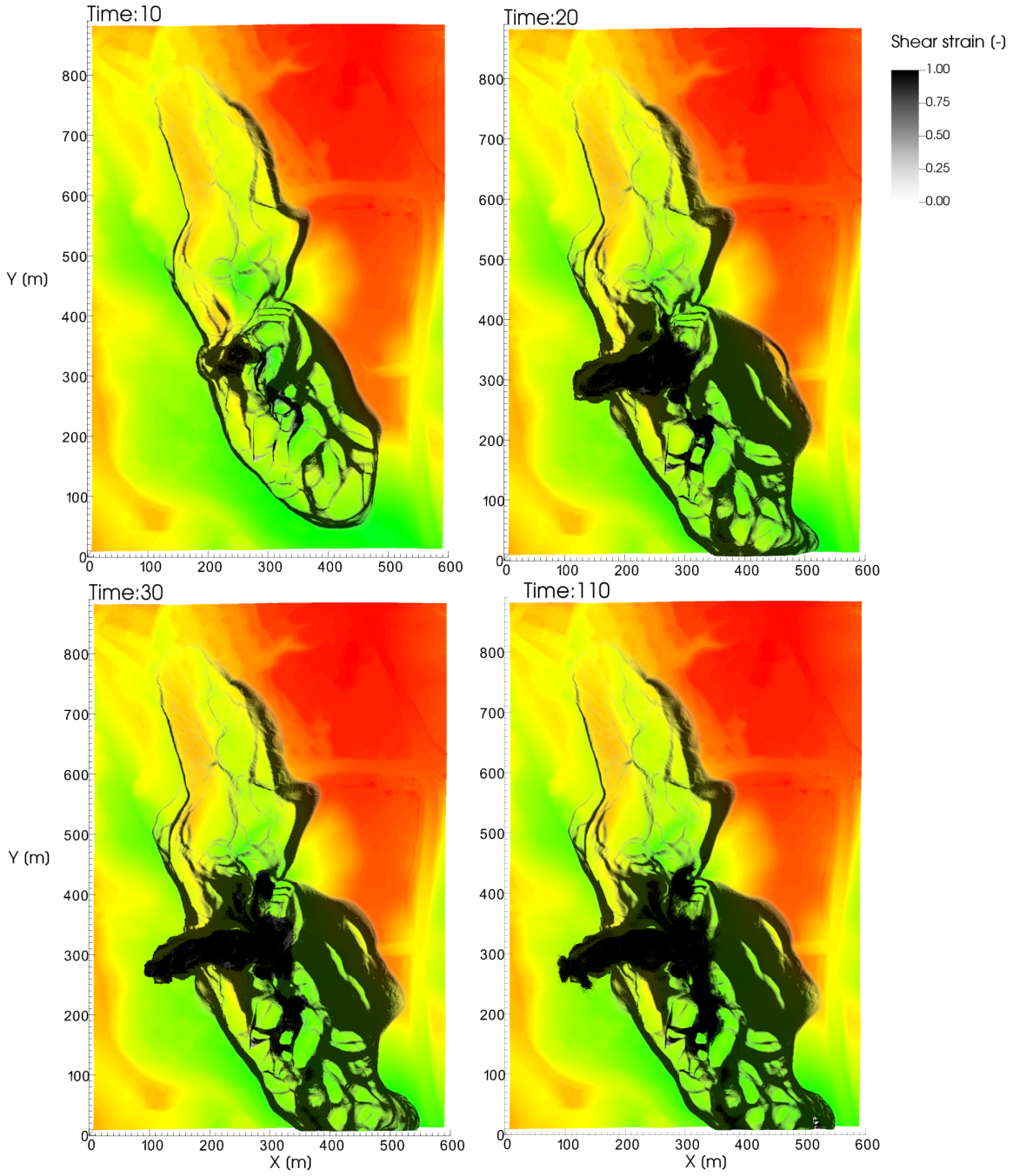

Figure 6.19: Shear strain for simulation 3 for time step 10 s, 20 s, 30 s and 110 s. All shear strain larger than 1 is displayed as black.

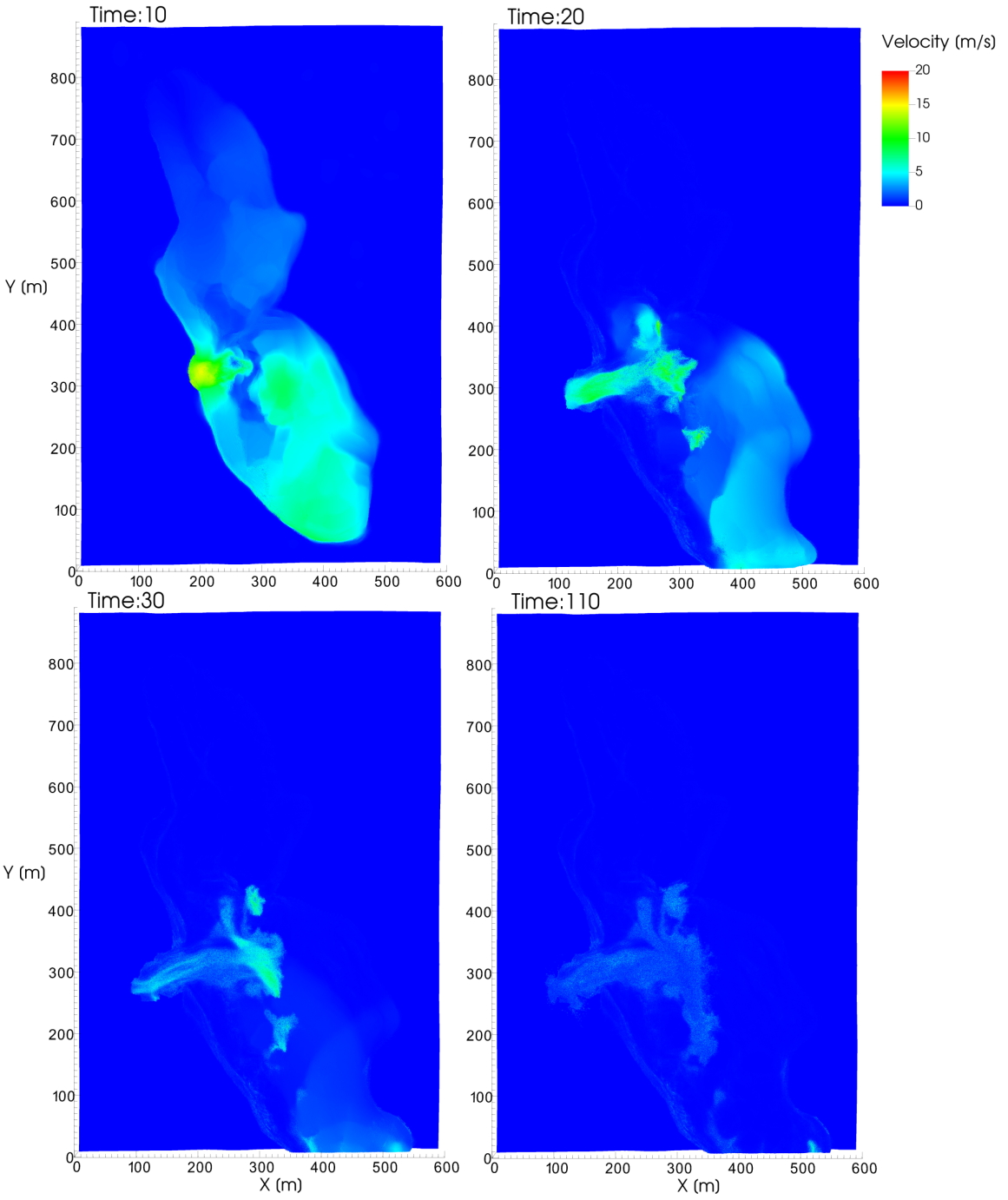

Figure 6.20: Velocity for simulation 3 for time step 10 s, 20 s, 30 s and 110 s. All velocity higher than 20 m/s is displayed as red.

Figure 6.21 shows that the simulated slide developed further toward Holmen than the Gjerdrum slide. The simulation also has a failure that propagates further toward the west. Toward the north did the shear bands stop further north than the detachment area of the Gjerdrum slide.

Figure 6.21: Extent of slide in simulation 3. Background map with outline of detachment area (red) and run-out area (purple) from Ryan et al. (2021).

Figure 6.22 shows the slide in relation to the extent of sensitive clay.

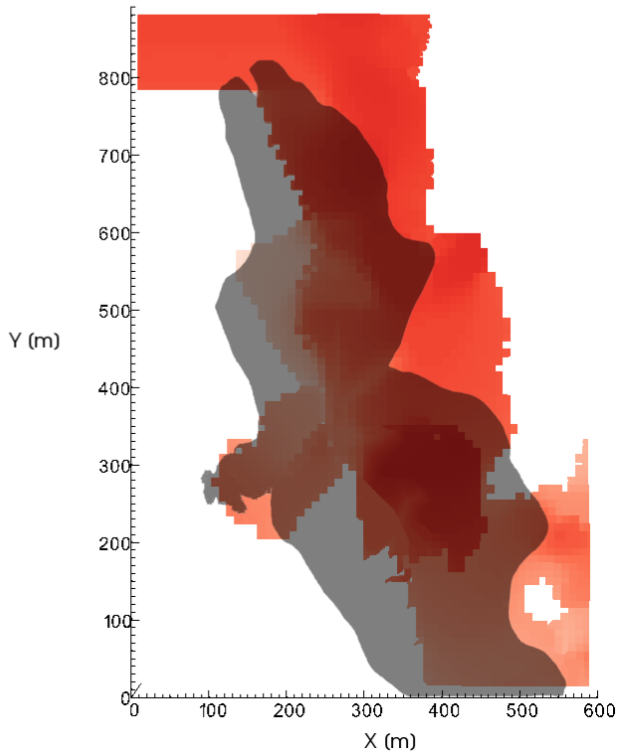

Figure 6.22: Extent of the slide in simulation 3 (grey) with the sensitive clay layer (red).

Chapter 7

Discussion

This chapter will discuss the findings and results from chapter 6. The results are compared with the information about the Gjerdrum landslide from Ryan et al. (2021) and relevant theory.

7.1 2D Analyses

7.1.1 Comparison Between the MPM Simulations and the Gjerdrum Slide

The differences in retrogression distance and accumulated material between the 2D simulations and the Gjerdrum slide may have several causes. One key point is the inability to represent the 3D effects in a 2D slope. Furthermore, neither nearby terrain, bedrock nor the extent of sensitive clay is considered. These aspects might affect the development of the slide, both the failure surface and the length of the slide. The slide masses from the first step of the landslide are believed to have displaced southwest (Ryan et al., 2021), which corresponds to out of the plane of the 2D profile. This is partly compensated for by the open left boundary, but will not give a fully correct representation of the accumulated masses in the crater. In addition, slide debris from further north in the detachment area of the Gjerdrum slide is believed to be deposited in the area of the 2D profile.

Simplification in geometry and interpretation of soil parameters will also affect the results. An example is the increase in undrained shear strength which forces the failure surfaces to follow the boundary between the two sensitive clay layers. Furthermore, the soil parameters are simplified to an average value over the whole profile instead of allowing local variation. The simulation is also controlled by the chosen constitutive material model and may, among other things, cause the difference between the angle of the back scarp in the simulation and the slide.

7.1.2 Sensitivity Analysis

The sensitivity analysis shows that different $s_{u,r}$ has a negligible impact on the retrogression length. Furthermore, the difference in accumulated and displaced material for different values of $s_{u,r}$ is not significant. The mobility of the displaced material can be related to the remolding energy. Because the shear strength degradation happens equally fast for all three simulations, the remolding energy is approximately the same. This will lead to the same amount of remaining energy to displace the masses, which correlates well with similar accumulation and displacement of masses.

In reality, it would be expected that clay with low $s_{u,r}$ gives a more liquid remolded clay which flows easier than a stiffer clay, as shown by Thakur et al. (2013). It is therefore expected that simulation 3 would have less accumulated material than simulations 1 and 2. One reason why the simulations did not give these results can be that $s_{u,r}$ equal to 0.5 kPa is not low enough to behave as a liquid such as indicated by Thakur and Degago (2012). In addition, not all the material in the slide remolds and the slide masses consist of several blocks of intact clay. The mobility of the slide masses is therefore lower than if all the clay was remolded. Thus, the clay blocks may be limiting the effect of variation in $s_{u,r}$.

Another factor that controls the mobility of the slide masses, is the geometry of the slope. As there is a small slope opposite the slope at Holmen, the material cannot flow easily out of the slide crater. This slope limits the possibility of the slide debris from the initial slide to deplete the slide crater, and it acts as a barrier for the subsequent slides. The accumulated masses will then be stabilizing for the back scarp. However, the accumulated masses do not seem to stabilize enough to stop the further retrogressive development of the slide. The geometry effect from the opposite slope and the debris barrier might limit the effect $s_{u,r}$ has on the flow as the material cannot flow freely out of the slide crater.

Simulations 1, 4, and 5, which had different values of γ_{95}, obtained different retrogression distances. With γ_{95} equal to 1, there is a considerable increase in the retrogression distance compared to the other simulations, and the slide also develops faster than for higher values of γ_{95}. A lower γ_{95} gives a faster decrease of the undrained shear strength. Thus, the local point that has experienced failure will redistribute stresses to the nearby points quickly, and the progressive failure mechanism will develop rapidly. This appears to lead to a higher velocity of the debris, see Appendix C. A high velocity will make the debris flow faster away from the slide crater which may explain why there is less accumulated material. It does not, however, give a clear explanation for the gentler inclination of the back scarp and longer retrogression distance. It should also be noted that the large retrogression distance is mainly due to the crest of the back scarp, and how the retrogression distance is defined.

Based on the relation between the remolding energy and the displacement of slide masses, it is natural to assume that γ_{95} equal to 2 would show a higher retrogression distance than γ_{95} equal to 4. However, this is not the case, and either simulation 1 or 4 is presumably incorrect. Further analysis with several different values of γ_{95} might be able to evaluate the presumption that a higher γ_{95} leads to a smaller retrogression distance. It should be noted that the retrogression distances from the five simulations do

not deviate exceptionally from one another.

When γ_{95} is equal to 4, a larger amount of energy to remold the clay is required. Thus the remaining energy left to displace the material is significantly lower, which correlates well with most accumulated material for simulation 4. Even though the masses are displaced slightly differently, the amount of accumulated material when $\gamma_{95} = 1$ does not deviate much from when $\gamma_{95} = 2$. This can be explained by the larger increase in remolding energy from γ_{95} equal to 2 to 4, than from 1 to 2.

The extent of quick clay appears to be the determining factor for the retrogression distance. For all five simulations, the retrogression stops when there is no more sensitive clay, regardless of $s_{u,r}$ and γ_{95}. For the studied slope profile *MC6*, it seems that the sensitivity parameters influence the shear failures, mobility of the debris, and velocity in the slide. However, the sensitivity parameters do not significantly affect when the retrogression stops. In particular, $s_{u,r}$ may be completely irrelevant for the retrogression as long as there is an initial failure.

7.1.3 Numerical Effects

No upper bound for the velocity was used for the simulations, and there were observed high velocities for several material points close to the left boundary. When material points are close to the boundary they might get an increase in velocity since there is no material on the other side of the boundary to limit the velocity and displacement. This numerical effect may lead to abnormal high velocity in these areas, which may further affect the flow of the material. If the velocity had an upper limit, it is reasonable to believe there would be more accumulated material in the slide crater.

The grid size and the number of material points also influence the simulations. Smaller grid size and a larger number of material points will lead to smaller errors (Tran and Sołowski, 2019). One reason is that the size of the grid will affect the shear band development. When the shear band develops, it cannot have a thickness smaller than the grid size. Thus, the shear bands in the simulations may be larger than in reality when the progressive failure starts to develop. The rapidity of the slide may therefore increase and affect the slide development.

7.2 3D Analyses

7.2.1 Comparison Between the MPM Simulations and the Gjerdrum Slide

Due to the discrete time steps and the output from the simulation, it is not possible to evaluate whether the specific steps assumed by Ryan et al. (2021) are present in the simulations. However, it is possible to compare tendencies of development-patterns and the extent of the failure for the different time steps.

In the first simulation where all material between the bedrock and the terrain is considered sensitive clay, the simulation follows a similar pattern to the steps in the Gjerdrum slide. The failure that has occurred

after 10 seconds is located in the same area as the initial slide in Gjerdrum, but the slide area in the simulation appears to have a larger extent in the north-south direction. This extent appears similar to the slide extent after step 2 in the Gjerdrum slide. The extent toward the east at Holmen for time step equal to 20 seconds corresponds well with the final extent in this area in the Gjerdrum slide. On the other hand, the run-out after 30 seconds, which has moved upstream Tistilbekken and toward the west, corresponds well with the final extent of the slide debris. The propagation toward the north indicates a direction of development similar to the Gjerdrum slide. After 70 seconds, the slide has propagated beyond the road at Fjellinna and into Nystulia. The location where the simulation propagates into Nystulia corresponds quite well with the Gjerdrum slide. However, the simulation keeps propagating both toward the north, east, and west until it reaches the northern boundary of the numerical geometry. The final extent of the slide in the simulation is therefore significantly larger than the extent of the Gjerdrum slide. Nonetheless, the simulation gives a conservative approach to the retrogression of the Gjerdrum landslide.

When the extent of the sensitive clay layer is included, the simulations develop along the ravines but do not further propagate to the east or into Nystulia. This differs from how the Gjerdrum slide developed according to Ryan et al. (2021). However, the initial failure occurs at Holmen where the initial slide is believed to have happened. The extent of the simulations in this area after 10 seconds is similar to the extent of the first simulation. The simulations do not propagate significantly further and therefore show a fairly good approximation to the Gjerdrum slide toward the east at Holmen. However, because the simulations do not develop any further, the final extent is governed by the failure after 10 or 20 seconds. This does not correspond particularly well with the Gjerdrum slide which had a larger detachment area. There can also be observed a local failure in the middle of the slide area for these simulations, which develops toward the west. This does not correspond to how the slide is believed to have occurred according to Ryan et al. (2021).

The three following sections discusses how different factors control the failure in the simulation and the effect of these.

7.2.2 Effect of Bedrock, Soil Layering, and Terrain

In the first 3D simulation, all material between terrain and bedrock is sensitive clay. Therefore, this simulation gives a good impression of how the bedrock and terrain influence slide development. Figure 6.12 shows that there is an increased elevation in the area where the slide debris stops toward the west and the southwest. The terrain appears to limit the run-out and slide debris in these areas. The slide propagates toward the north from Holmen and follows the plateau to Nystulia. The propagation continues until the northern boundary in the numerical geometry. It does not appear as the bedrock elevation and thin soil layer in this area are enough to stop further propagation. This could indicate that other factors played a more important role in where the final back scarp ended up for the Gjerdrum slide.

For the simulations that take the sensitive clay layer into account, the extent of the slide appears limited by the sensitive clay layer. The shear bands first develop in the sensitive clay layer at Holmen. Moreover, the failure is spreading along some of the terrain formations, such as the ravine ridges, instead of further toward the northeast in the sensitive clay layer. The bottom of the largest ravine north of Holmen does not experience any shear strain, even though there is failure south, west and north of this area. Thus, the failure does not propagate into the plateau in this area, even though there is a large extent of sensitive clay east of the ravine. This shows that the terrain is an equally important factor for the development of the slide as the extent of the sensitive clay layer. However, there are also clear indications of how the sensitive clay layer controls the failure. In both simulations, the extent of the slide is limited by the discontinuity in the sensitive clay layer in the southeast part of the layer. This can be seen from Figure 6.18 and Figure 6.22. The discontinuity is significantly larger than it appears to be in the Leapfrog model, Figure 5.12a. Furthermore, this discontinuity appears to explain why the slide does not propagate further east in this area. The two simulations also have a local failure in the middle of the slide, which has a high velocity compared to the rest of the slide area. This local failure appears to follow the sensitive clay layer toward the west.

7.2.3 Mobility of the Slide Debris

The simulation where all material between bedrock and terrain is sensitive clay appears to have higher mobility than the two other simulations. This is expected as a larger amount of the material can remold and then flow out of the slide crater. The second and third simulations show low mobility of the slide masses. This could be due to the large blocks of intact clay that are left in the slide crater. For the debris to flow out of the slide crater, there must be enough remolded clay so that the overlaying stiff blocks can be transported away. The amount and size of the intact blocks compared with the amount of remolded clay, appears to be too high to achieve high mobility. Thus, the non-sensitive clay layer appears to be dominating.

The semi-brittle behavior of the clay shows little effect on the mobility of the masses compared to the perfectly-plastic behavior of the clay layer. This corresponds well with the study by Thakur et al. (2014), which shows that sensitive clay with $s_{u,r}$ larger than 0.5 kPa has a semi-solid behavior when remolded. When the lowest $s_{u,ref}$ is 11 kPa, the lowest $s_{u,r}$ in the clay layer is 5.5 kPa when S_t is 2. Hence, based on the described study the clay will not act as a liquid after failure, but as stiff soil. It is plausible that an increase in sensitivity for the clay layer with semi-brittle behavior will affect the flow of the slide debris. However, the sensitivity threshold value to obtain a fluid material in the simulation is not investigated.

As both simulations with a sensitive clay layer had a $s_{u,r}$ of 1 kPa and γ_{95} equal to 0.2, it is not possible to validate whether a lower $s_{u,r}$ and γ_{95} would give higher mobility of the slide masses. However, the 2D simulations showed that γ_{95} had a larger impact on the slide development than $s_{u,r}$. As discussed earlier, the extent of the 2D slide appears to be controlled by the sensitive clay layer rather than the shear strength parameters. Nonetheless, it is reasonable to believe that if either $s_{u,r}$ or γ_{95} is lower,

a higher amount of the sensitive clay will get remolded which could lead to higher mobility. Yet, the amount of clay above the sensitive clay layer and its behavior could be the leading factor for the overall mobility.

The flow of the slide debris and the amount of accumulated masses in the slide crater greatly affect the development of the slide in the simulation. For the second and third 3D simulations, the simulation mostly propagates sideways after the initial failure. The initial failures do not develop into retrogressive slides. The absence of further propagation to the north and into Nystulia is probably due to the low mobility of the slide masses, as the first simulation does not show a similar pattern.

7.2.4 Effect of Shear Strength Parameters

The influence of the reference undrained shear strength is an interesting aspect. Due to the simplified approach with a linear radial basis interpolation, the shear strength is illogically low in some areas. Therefore, it was a risk that the failure would propagate into one of these areas, such as the lower-left corner. However, the failure does not propagate into this area in any of the simulations. In the first simulation, the slide debris stops where the elevation increases toward the lower-left corner. Therefore, the terrain appears to control the propagation for that specific area. In other areas, such as along the road from Holmen to the roundabout and further toward the north, east of Nystulia, the reference shear strength is significantly higher. As the terrain along the road inclines downwards toward the east, and Nystulia lays on a plateau, the reference shear strength is the controlling factor of the slide in these areas, because the terrain inclination implies further failure propagation to the east. In the two simulations with a defined sensitive clay layer, there is no clear visible effect in the failure propagation from the reference shear strength.

The change from an elastic perfectly-plastic clay layer to a semi-brittle clay layer gives an increase in the extent of the shear bands toward the north. After 10 seconds, the simulation with a semi-brittle clay has propagated 200 meters longer than the other simulation. The softening in the clay layer, in addition to the softening in the sensitive clay layer, allows the shear bands to develop to a larger extent. However, due to the lack of mobility of the masses within the slide area, the sensitivity of the clay layer does not affect the further development of the slide.

7.2.5 Comparison Between the MPM Simulations and the Empirical Criteria

The simulation that accounts for the bedrock and terrain, gives a similar extent toward the east as the empirical criterion that accounts for the bedrock and terrain. Toward the north, the empirical criterion has a retrogression potential slightly north of the *Gjerdrum bo- og behandlingssenter*. On the other hand, the MPM simulation propagated all the way to the boundary of the numerical geometry. There are no indicators that the simulation would have stopped developing further north if the boundary was not present. The empirical criterion is therefore considered to be more suitable to define the retrogression

extent. However, both the numerical and empirical method which accounts for bedrock and terrain, overestimate the extent of the slide and are conservative approaches.

The criterion and simulations which account for bedrock, terrain, and the sensitive clay layer, show a similar extent at Holmen. The retrogression is slightly further east at Holmen than in the Gjerdrum slide for both the numerical and empirical methods. However, for the other areas in the study area, the two methods give quite different results. The empirical criterion corresponds well with the Gjerdrum slide and gives a retrogression that is nearly identical to the retrogression of the slide. On the other hand, the MPM simulations do not give a retrogression extent that covers the whole detachment area of the Gjerdrum slide.

Both the numerical and empirical methods have a soil layering based on the Leapfrog model and therefore have a similar soil layering. When only bedrock and terrain are taken into account, the soil layering used for the two methods is nearly identical. Thus, the main difference between these two methods is that the numerical method accounts for material parameters. For the other simulations and empirical criterion, there is a difference in the sensitive clay layer. This is due to the necessary simplification of the sensitive clay layer to make the numerical geometry for the MPM model. This may explain some differences between the numerical and empirical results. However, it does not explain why the failure did not propagate further toward the east in the area north of Holmen in the MPM simulations.

7.2.6 Necessary Resources for the MPM Simulations and the Empirical Criteria

In general, the empirical methods require fewer ground investigations than the MPM simulations. To use the empirical criterion which only accounts for terrain, a DTM can be used directly. This requires a minimum amount of resources. To evaluate the retrogression distance based on the other two empirical criteria, it is sufficient to establish the soil layering for each of the profiles examined. As concerns Gjerdrum, the terrain criterion did not differ that much from the criterion which also accounts for bedrock. Whereas the empirical criterion with the sensitive clay layer gave a much smaller area than the two previous criteria, which corresponded well with the slide extent in the Gjerdrum slide. Therefore, it appears as the additional resources to define a soil layering are worth the cost. However, the differences in retrogression distance for the different criteria may vary based on the soil layering and terrain in the specific area in question.

On the other hand, the MPM simulations require a complete 3D soil layering. To reduce the uncertainty of the soil layering, an extensive ground investigation program must be performed. In addition to the 3D soil layering, the MPM simulations require material parameters for every material point. If these parameters are lacking from ground investigations and laboratory tests, they must be determined empirically. In total, the necessary input parameters for an MPM simulation require extensive knowledge about the soil layering and the material parameters of the soil. If only the bedrock and terrain are used

for the numerical geometry in the simulation, the placement of the sensitive clay layer and its numerical geometry do not need to be defined. This will reduce the resources used to determine the layer and the computational cost of the simulation. However, all MPM simulations require a high computational capacity. In total is the MPM simulations more demanding and require more resources than the empirical criteria.

Chapter 8

Conclusions and Recommendations for Further Work

8.1 Conclusions

The sensitivity parameters had an impact on the retrogression distance in the 2D analyses. The 2D simulations showed that the retrogression distance was constant when $s_{u,r}$ was varied. However, variation in γ_{95} gave different retrogression distances. The lowest γ_{95} gave the highest retrogression distance, which was expected. On the other hand, γ_{95} equal to 4 gave a higher retrogression distance than γ_{95} equal to 2. This was not as expected, but there was found no clear cause. One of the simulations is therefore assumed to be incorrect. It should be noted that the retrogression distance mainly appears controlled by the extent of the sensitive clay layer.

The 3D MPM simulations and the retrogression distances from the empirical criteria have been compared to the Gjerdrum slide. The empirical criterion that took into account the bedrock, terrain, and sensitive clay layer, gave the best approximation of the retrogression extent. The empirical criterion that took into account the bedrock and the terrain gave significantly larger retrogression distances. Furthermore, the criterion that only took the terrain into account gave the largest retrogression extent.

The simulation that takes the bedrock and terrain into account gave a similar result as the corresponding empirical criterion. Compared to the Gjerdrum slide, the slide in the simulation followed a similar development-pattern. On the other hand, the failure did not stop propagating toward the north until it reached the boundary of the numerical model. The failure also propagated further to the east and the west than the slide. The extent of the simulated slide appeared to be governed by both the terrain and the shear strength of the soil. In general, this simulation could be used as a conservative approach for the retrogression extent.

It was not obtained a good approach to the Gjerdrum slide for the two simulations that took the sensitive clay layer into account. The simulations had an initial failure in the slope west of Holmen, where the initial slide is believed to have occurred. However, the shear bands further developed along the ravines, without propagating into Nystulia. The slide length in the direction north-south for the simulation with a semi-brittle clay was 200 meters longer than the slide length for the simulation with an elastic perfectly-plastic clay. The reason for this was that the shear bands were able to propagate into the clay layer when the clay had a semi-brittle behavior. However, the mobility of the slide masses for the two simulations was low, and the masses did not flow out of the crater to create successive slides. The change in sensitivity for the clay layer had a minor impact on the slide development. Both the terrain and the geometry of the sensitive clay layer seemed to be important factors to determine where the failure occurred.

The different levels of detail in soil layering gave different results for both the MPM simulations and the empirical criteria. For the MPM simulations, the least detailed soil layering gave the best results. For the empirical criteria, the most detailed soil layering gave the best results. Taking into consideration the necessary resources to perform an MPM simulation, the empirical criteria appear to be the most favorable way to determine the retrogression extent for the Gjerdrum slide.

8.2 Recommendations for Further Work

More thorough investigations should be made regarding the effect of sensitivity parameters. Due to the uncertainty of the effect of γ_{95}, several different values should be tested to examine if there exists a threshold value for developing a retrogressive slide. Furthermore, it should be investigated if the retrogression distances are reduced for an increased γ_{95}. In addition, it would be interesting to examine if a similar effect due to variation of $s_{u,r}$ and γ_{95} apply to other 2D profiles.

For the 3D MPM simulations, a better fit between the fully detailed soil layering and the Gjerdrum slide should be aspired. A further variation of the sensitivity parameters for both the sensitive clay layer and the clay layer should be examined. Additionally, it is desired to improve the conformity of the geometry of the numerical sensitive clay layer used in the simulations and the sensitive clay layer from the Leapfrog model. This is especially applicable to the discontinuity in the southeast corner of the layer, and the middle area, where there is a large divergence between the slide extent in the simulations with the sensitive clay layer and the Gjerdrum slide. Lastly, it would be desirable to investigate whether the empirical criteria give a better fit than the 3d MPM simulations for other areas than the area in Gjerdrum investigated in this thesis.

Bibliography

Aas, G. (1979) Kvikkleireskred. *Skredfare og arealplanlegging : vurdering av faregrad og sikringstiltak. 24-26. april, Lofthus*. Oslo: NIF.

Aunaas, K. et al. (2016) *NIFS-rapport 14/2016 Metode for vurdering av løsne- og utløpsområder for områdeskred*.

Bardenhagen, S. G. and Kober, E. M. (2004) The generalized interpolation material point method. *Computer Modeling in Engineering and Sciences*, 5(6), pp. 477–496.

Bjerrum, L. (1954) Geotechnical Properties of Norwegian Marine Clays. *Géotechnique*, 4(2), pp. 49–69.

Brackbill, J. U., Kothe, D. B., and Ruppel, H. M. (1988) Flip: A low-dissipation, particle-in-cell method for fluid flow. *Computer Physics Communications*, 48(1), pp. 25–38.

Brackbill, J. U. and Ruppel, H. M. (1986) FLIP: A method for adaptively zoned, particle-in-cell calculations of fluid flows in two dimensions. *Journal of Computational Physics*, 65(2), pp. 314–343.

Cruden, D. and Varnes, D. (1996) Landslide Types and Processes. *Special Report - National Research Council, Transportation Research Board*, 247, pp. 36–57.

De Vaucorbeil, A., Nguyen, V. P., Sinaie, S., and Wu, J. Y. (2020) Material point method after 25 years: Theory, implementation, and applications. *Advances in Applied Mechanics*, 53, pp. 185–398.

Duncan, J. M. and Buchignani, A. L. (1976) *An Engineering Manual for Settlement Studies*. Department of Civil Engineering, University of California.

Einav, I. and Randolph, M. F. (2005) Combining upper bound and strain path methods for evaluating penetration resistance. *International Journal for Numerical Methods in Engineering*, 63, pp. 1991–2016.

Fernández, F., Amaral Vargas, E. do, and Quadros Velloso, R. (2020) A 3D discretization procedure for the material point method (MPM). *Computational Particle Mechanics*, 7(4), pp. 725–733.

Finn.no (2022) Finn Kart. Available at: `https://kart.finn.no/` (Accessed: Feb. 17, 2022).

Geertsema, M., Cruden, D. M., and Schwab, J. W. (2006) A large rapid landslide in sensitive glaciomarine sediments at Mink Creek, northwestern British Columbia, Canada. *Engineering Geology*, 83(1-3), pp. 36–63.

Geertsema, M. and L'Heureux, J. S. (2014) Controls on the dimensions of landslides in sensitive clays. *Advances in Natural and Technological Hazards Research*, 36, pp. 105–117.

Gregersen, O. (2008) *Program for økt sikkerhet mot leirskred - Metode for kartlegging og klassifisering avfaresoner, kvikkleire.*

Gregersen, O. (1981) The quick clay landslide in Rissa, Norway. *Soil mechanics and foundation engineering. Proc 10th international conference, Stockholm, June 1981.* Vol. 3. A.A. Balkema, pp. 421–426.

Harlow, F. (1964) The Particle-in-Cell Computing Method for Fluid Dynamics. *Methods in Computational Physics*, 3, pp. 319–343.

Haugen, E. D., Tveit, M., and Heyerdahl, H. (2017) Mapping Quick Clay Hazard Zones: Comparison of Methods for the Estimation of the Retrogression Distance. *Advances in Natural and Technological Hazards Research*, 46, pp. 311–321.

Hungr, O., Leroueil, S., and Picarelli, L. (2014) The Varnes classification of landslide types, an update. *Landslides*, 11(2), pp. 167–194.

Karlsrud, K., Aas, G., and Gregersen, O. (1984) Can we predict landslide hazards in soft sensitive clays? Summary of Norwegian practice and experiences. *4th International Symposium on Landslides.* Toronto: University of Toronto Press, pp. 107–130.

Kartverket (2015) NDH Akershus 2pkt 2015. Available at: `https://hoydedata.no/LaserInnsyn/` (Accessed: Feb. 24, 2022).

Kartverket, NIBIO, and Statens Vegvesen (2022) Norge i bilder. Available at: `https://norgeibilder.no/` (Accessed: Feb. 17, 2022).

L'Heureux, J. S. (2012) A study of the retrogressive behaviour and mobility of Norwegian quick clay landslides. *Landslides and Engineered Slopes: Protecting Society through Improved Understanding.Proceedings of the 11th International and 2nd North American Symposium on Landslides and Engineered Slopes, 2012.* CRC Press/Balkema, pp. 981–987.

Li, X., Wu, Y., He, S., and Su, L. (2016) Application of the material point method to simulate the post-failure runout processes of the Wangjiayan landslide. *Engineering Geology*, 212, pp. 1–9.

Llano-Serna, M. A., Farias, M. M., and Pedroso, D. M. (2016) An assessment of the material point method for modelling large scale run-out processes in landslides. *Landslides*, 13(5), pp. 1057–1066.

Locat, A., Demers, D., Locat, P., and Geertsema, M. (2017) Sensitive clay landslides in Canada. *Proceeding of the 70th Canadian Geotechnical Conference, Ottawa, 2017.*

Locat, A., Leroueil, S., Bernander, S., Demers, D., Jostad, H. P., and Ouehb, L. (2011) Progressive failures in eastern Canadian and Scandinavian sensitive clays. *Canadian geotechnical journal*, 48(11), pp. 1696–1712.

Locat, A., Leroueil, S., and Jostad, H. (2014) Failure Mechanism of Spreads in Sensitive Clays. *Advances in Natural and Technological Hazards Research*. Vol. 36, pp. 279–290.

Mitchell, J. K. and Soga, K. (2005) *Fundamentals of Soil Behaviour*. 3rd ed. Hoboken, New Jersey: John Wiley and Sons.

Mitchell, R. J. and Markell, A. R. (1974) Flowsliding in sensitive soils. *Canadian Geotechnical Journal*, 11(1), pp. 11–31.

Multiconsult (2021a) *10226192-01-RIG-BER-001_rev00 Teknisk beregningrapport – Parametere*. Multiconsult.

Multiconsult (2021b) *10226192-01-RIG-BER-002 Teknisk beregningsrapport - Stabilitetsberegninger*. Multiconsult.

Multiconsult (2021c) *Kvikkleireskred Ask Gjerdrum 3D-modell. Leapfrog-modell per 01.07.2021. Følgenotat grunnforholdsmodell*. Multiconsult.

Multiconsult (2022) *Kvikkleireskred Ask Gjerdrum 3D-modell. Leapfrog-modell per 23.03.2022. Følgenotat grunnforholdsmodell*. Multiconsult.

Norwegian Geological Survey (2022) NGU Map of Quarternary deposits. Available at: `http://geo.ngu.no/kart/losmasse_mobil/` (Accessed: Feb. 17, 2022).

Norwegian Geotechnical Society (2011) *Veilding for symboler og definisjoner i geoteknikk—identifisering og klassifisering av jord. NGF-notification Nr. 2, 2nd revision*. Oslo, Norway.

Norwegian Public Roads Administration (2018) *Håndbok V220 Geoteknikk i vegbygging*.

Norwegian Water Resources and Energy Directorate (2019) *NVE Guidelines 2019/01. Sikkerhet mot kvikkleireskred: vurdering av områdestabilitet ved arealplanlegging og utbygging i områder med kvikkleire og andre jordarter med sprøbruddegenskaper*. Norwegian Water Resources and Energy Directorate.

Norwegian Water Resources and Energy Directorate (2022) NVE Atlas. Available at: `https://atlas.nve.no/Html5Viewer/index.html?viewer=nveatlas#` (Accessed: Feb. 17, 2022).

Penna, I. and Solberg, I. (2021) *Landscape changes and bedrock reconstruction in Gjerdrum area. Methodological approach and main results*. NGU-rapport 2021.023.

Quinn, P. E., Diederichs, M. S., Rowe, R. K., and Hutchinson, D. J. (2007) An Exploration of the Mechanics of Retrogressive Landslides in Sensitive Clay. *Ottawa Geotech.* Pp. 721–727.

Quinn, P. E., Diederichs, M. S., Rowe, R. K., and Hutchinson, D. J. (2011) A new model for large landslides in sensitive clay using a fracture mechanics approach. *Canadian Geotechnical Journal*, 48(8), pp. 1151–1162.

Rankka, K., Andersson-Sköld, Y., Hultén, C., Larsson, R., Leroux, V., and Dahlin, T. (2004) *Quick clay in Sweden*. Linköping.

Ryan, I. et al. (2021) *Årsaker til kvikkleireskredet i Gjerdrum 2020*. Norwegian Ministry of Petroleum and Energy.

Sadeghirad, A., Brannon, R. M., and Burghardt, J. (2011) A convected particle domain interpolation technique to extend applicability of the material point method for problems involving massive deformations. *International Journal for Numerical Methods in Engineering*, 86, pp. 1435–1456.

Skempton, A. W. (1964) Long-Term Stability of Clay Slopes. *Géotechnique*, 14(2), pp. 77–102.

Steffen, M., Wallstedt, P., Guilkey, J., Kirby, R., and Berzins, M. (2008) Examination and analysis of implementation choices within the Material Point Method (MPM). *Computer Modeling in Engineering and Sciences*, 31, pp. 107–127.

Sulsky, D., Chen, Z., and Schreyer, H. L. (1994) A particle method for history-dependent materials. *Computer Methods in Applied Mechanics and Engineering*, 118(1-2), pp. 179–196.

Sulsky, D., Zhou, S. J., and Schreyer, H. L. (1995) Application of a particle-in-cell method to solid mechanics. *Computer Physics Communications*, 87(1-2), pp. 236–252.

Sulsky, D. and Gong, M. (2016) Improving the Material-Point Method. *Innovative Numerical Approaches for Multi-Field and Multi-Scale Problems*. 1st ed. Springer Cham, pp. 217–240.

Sulsky, D. and Schreyer, H. L. (1996) Axisymmetric form of the material point method with applications to upsetting and Taylor impact problems. *Computer Methods in Applied Mechanics and Engineering*, 139(1-4), pp. 409–429.

Tavenas, F., Flon, P., Leroueil, S., and Lebuis, J. (1983) Remolding energy and risk of retrogression in sensitive clays. *Symposium on Slopes on Soft Clays, Linkoping, 1983*. Vol. 17, pp. 205–262.

Thakur, V. and Degago, S. A. (2012) Quickness of sensitive clays. *Geotechnique Letters*, 2(3), pp. 87–95.

Thakur, V., Degago, S. A., Oset, F., Dolva, B. K., and Aabøe, R. (2013) A new approach to assess the potential for flow slide in sensitive clays. *18th International Conference on Soil Mechanics and Geotechnical Engineering: Challenges and Innovations in Geotechnics, Paris, 2013*, 3, pp. 2265–2268.

Thakur, V. et al. (2014) Characterization of post-failure movements of landslides in soft sensitive clays. *Advances in Natural and Technological Hazards Research*, 36, pp. 91–103.

Torrance, J. K. (1999) Physical, chemical and mineralogical influences on the rheology of remoulded low-activity sensitive marine clay. *Applied Clay Science*, 14(4), pp. 199–223.

Tran, Q. A. and Sołowski, W. (2019) Generalized Interpolation Material Point Method modelling of large deformation problems including strain-rate effects – Application to penetration and progressive failure problems. *Computers and Geotechnics*, 106, pp. 249–265.

Varnes, D. (1978) Slope Movement Types and Processes. *Special Report - National Research Council, Transportation Research Board*, 176, pp. 11–33.

Wang, B., Vardon, P. J., and Hicks, M. A. (2016) Investigation of retrogressive and progressive slope failure mechanisms using the material point method. *Computers and Geotechnics*, 78, pp. 88–98.

Xu, X., Jin, F., Sun, Q., Soga, K., and Zhou, G. G. (2018) Three-dimensional material point method modeling of runout behavior of the Hongshiyan landslide. *Canadian Geotechnical Journal*, 56(6), pp. 1318–1337.

Zhang, X., Chen, Z., and Liu, Y. (2017) The Material Point Method. *The Material Point Method*. Academic Press, pp. 37–101.

Appendix A

MC6 Profile

MC6 profile from Multiconsult (2021b) which is used as basis for the 2D MPM simulations.

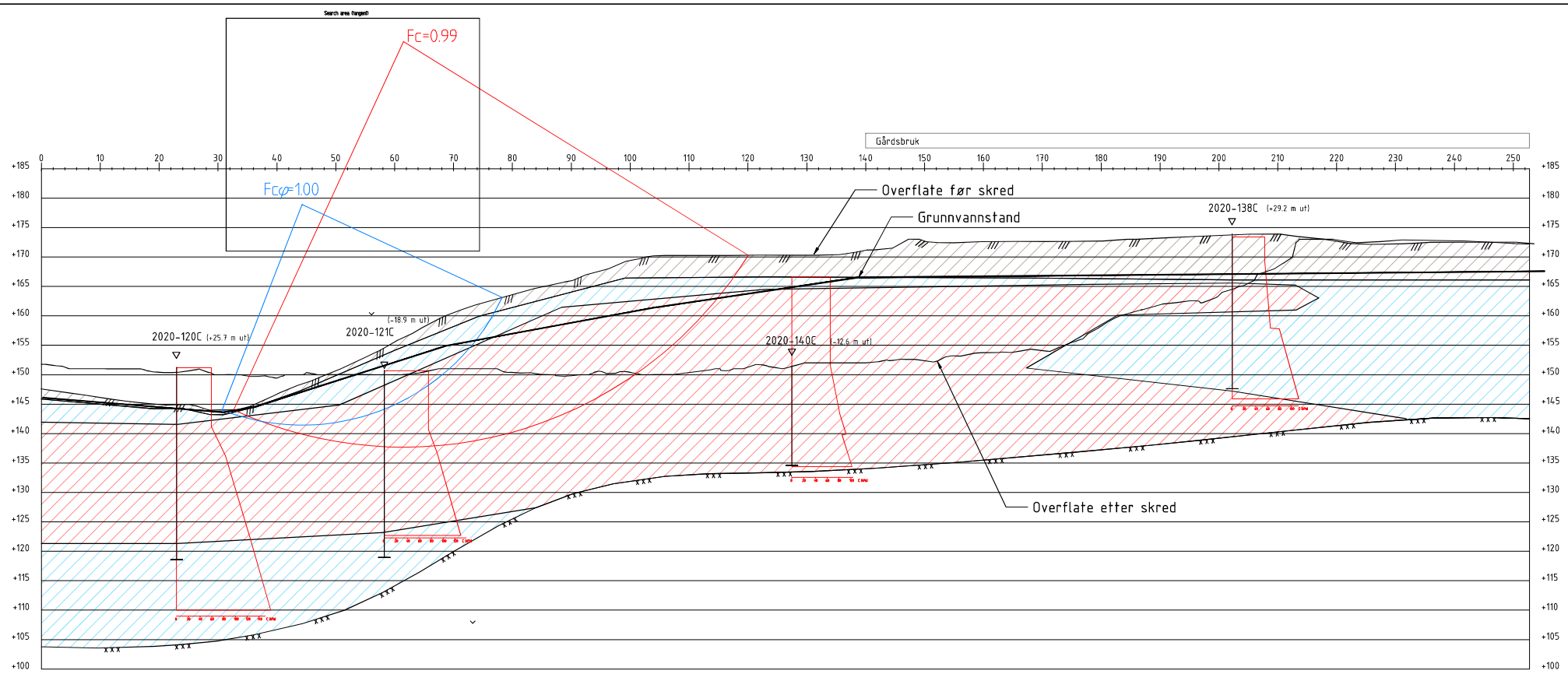

Profil MC 6
1 : 500

Topplag
Leire
Sprøbruddmateriale

Material	Un.Weigth	Sub.Weigth	Fi	C'	C	Aa	Ad	Ap
Topplag	19.50	9.5	30.0	0.0				
Leire	19.50	9.5	28.0	1.0	C-prof	1.00	0.90	0.75
Sprøbruddmateriale	19.50	9.5	28.0	1.0	C-prof	1.00	0.90	0.75

Rev.	Beskrivelse	Dato	Tegn.	Kontr.	Godkj.

Multiconsult
www.multiconsult.no

Olje- og energidepartementet
Ask - Gjerdrum geoteknisk utredning av stabilitet
Profil MC 6 - Stabilitetsberegninger

Status	Fag	Originalt format	Dato
Utsendt	RIG	A3L	2021-06-22
Konstr./Tegnet	Kontrollert	Godkjent	Målestokk
SIE	TGJ	ANG	1:500

Oppdragsnr.	Tegningsnr.	Rev.
10226192-01	RIG-TEG-805	00

Appendix B

Undrained Shear Strength Variation for the 3D MPM Simulations

Additional figures of the spatial variability of the reference undrained shear strength for the clay and sensitive clay layer.

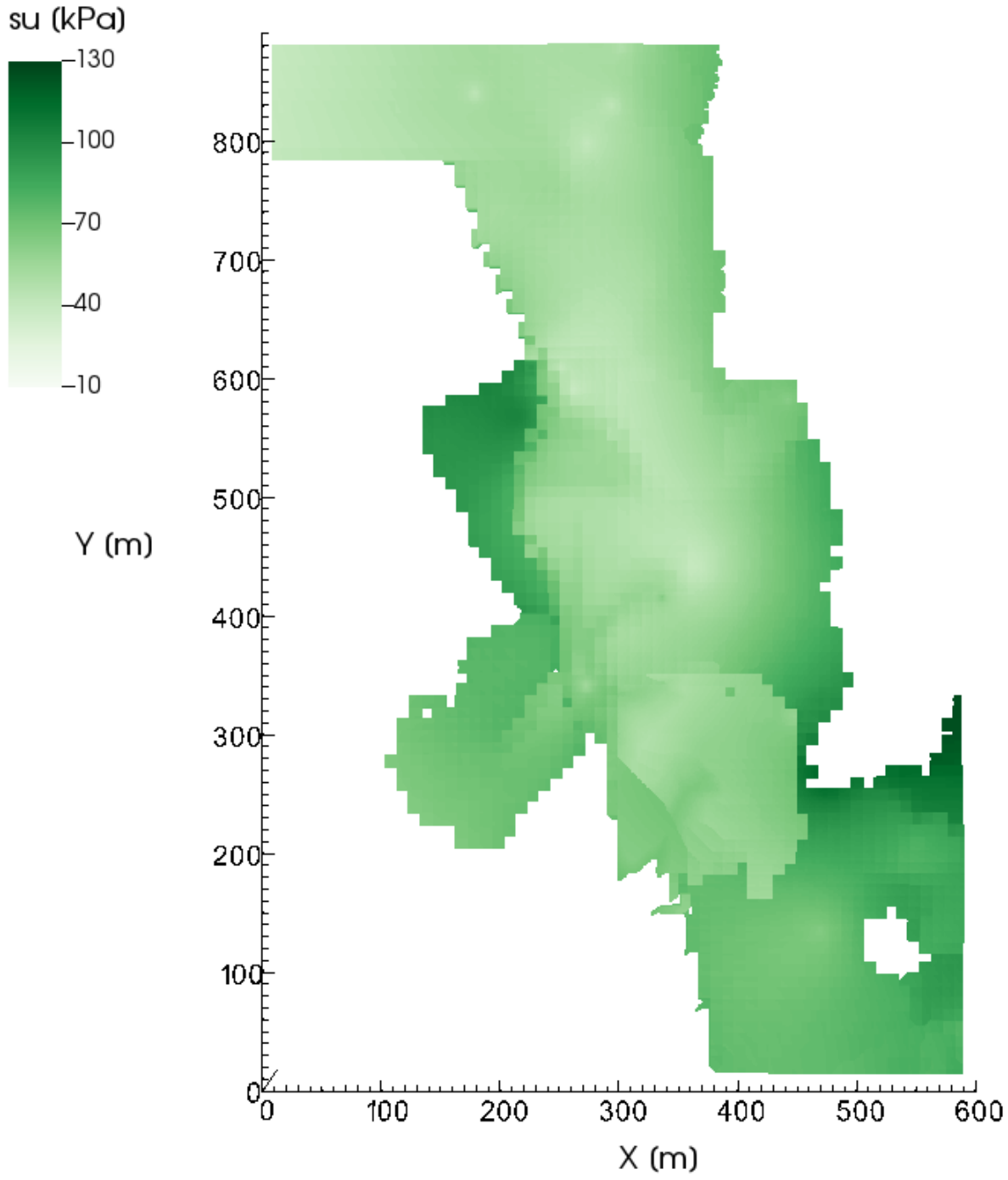
su (kPa)
130
100
70
40
10
Y (m)
800
700
600
500
400
300
200
100
0
0
100
200
300
400
500
600
X (m)

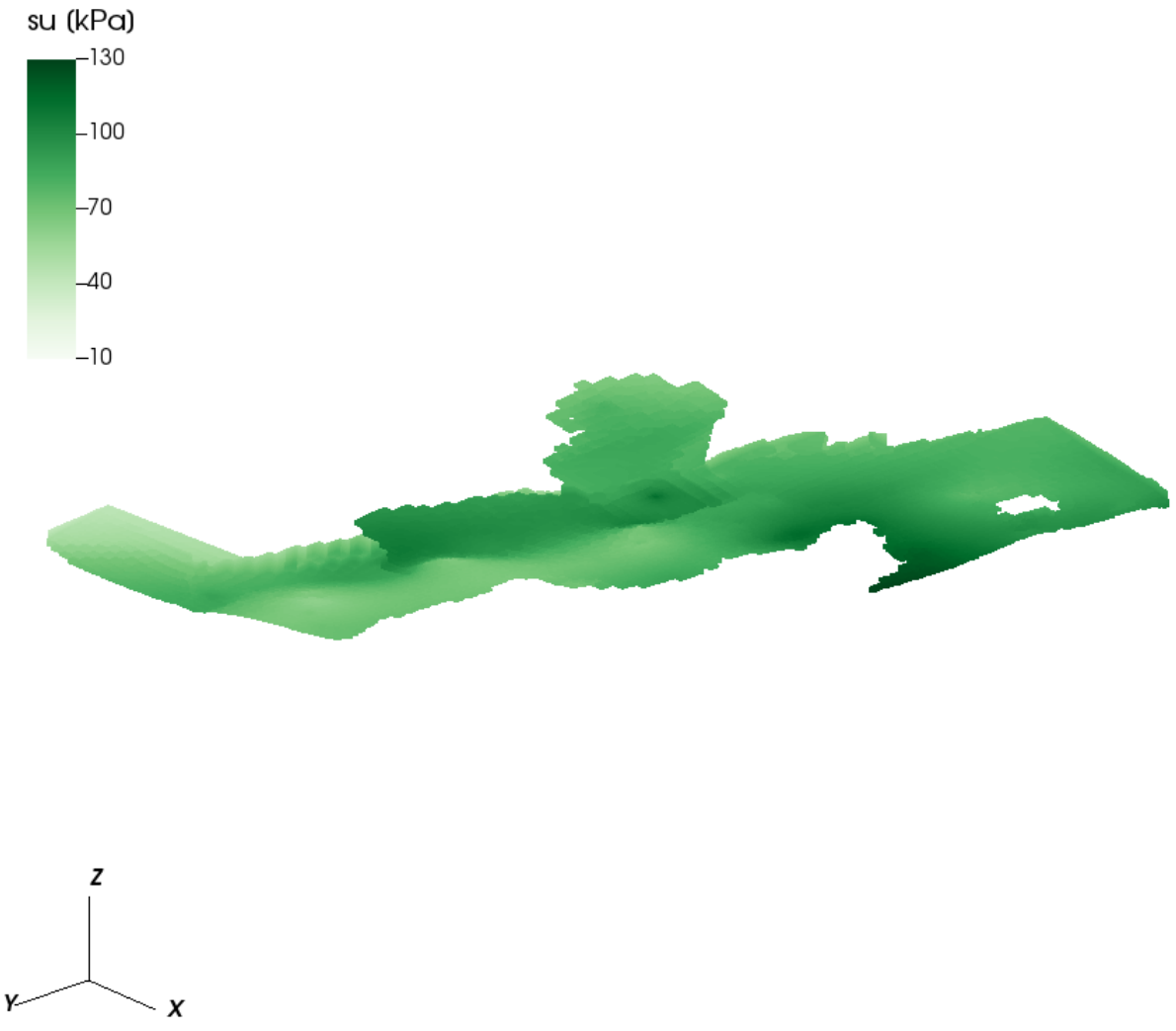
su (kPa)
130
100
70
40
10
Z
Y
X

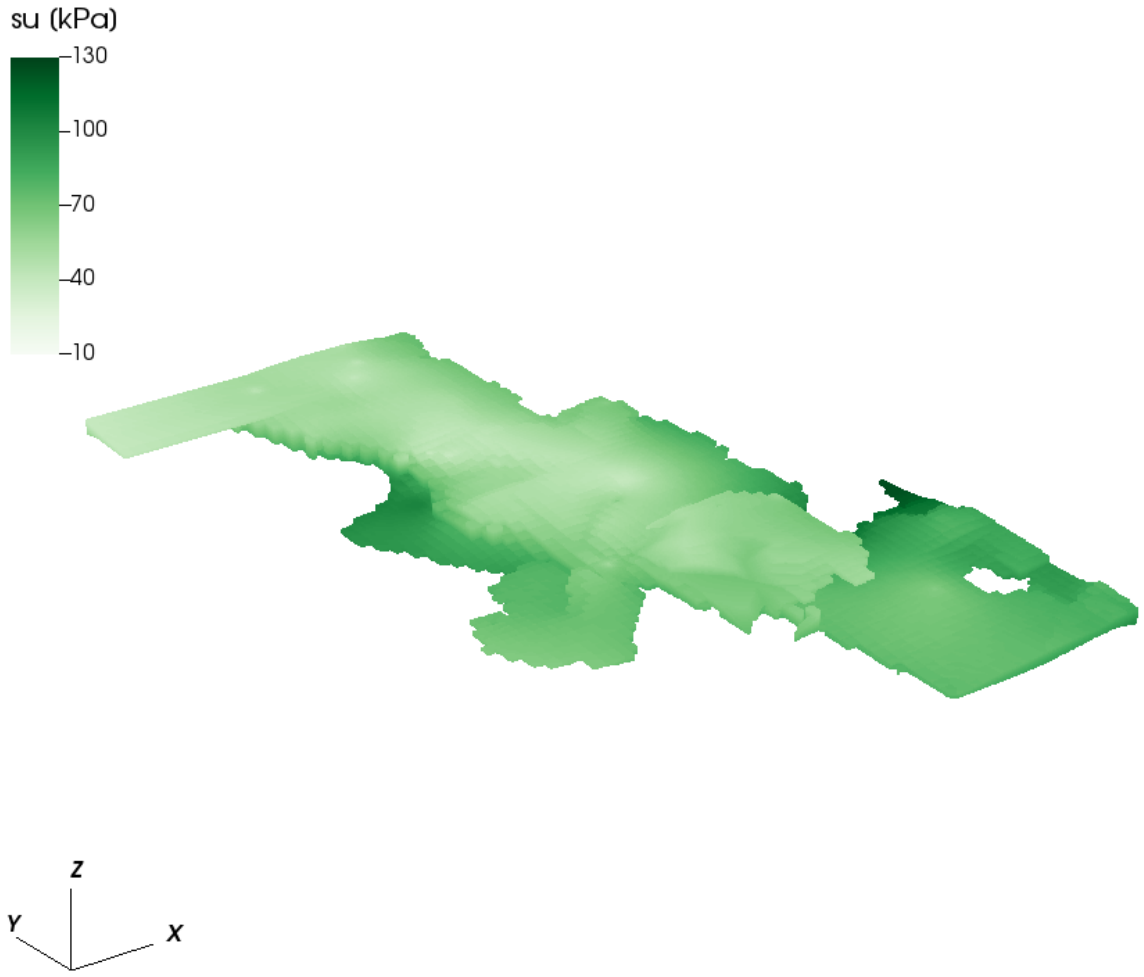
su (kPa)
130
100
70
40
10
Z
Y
X

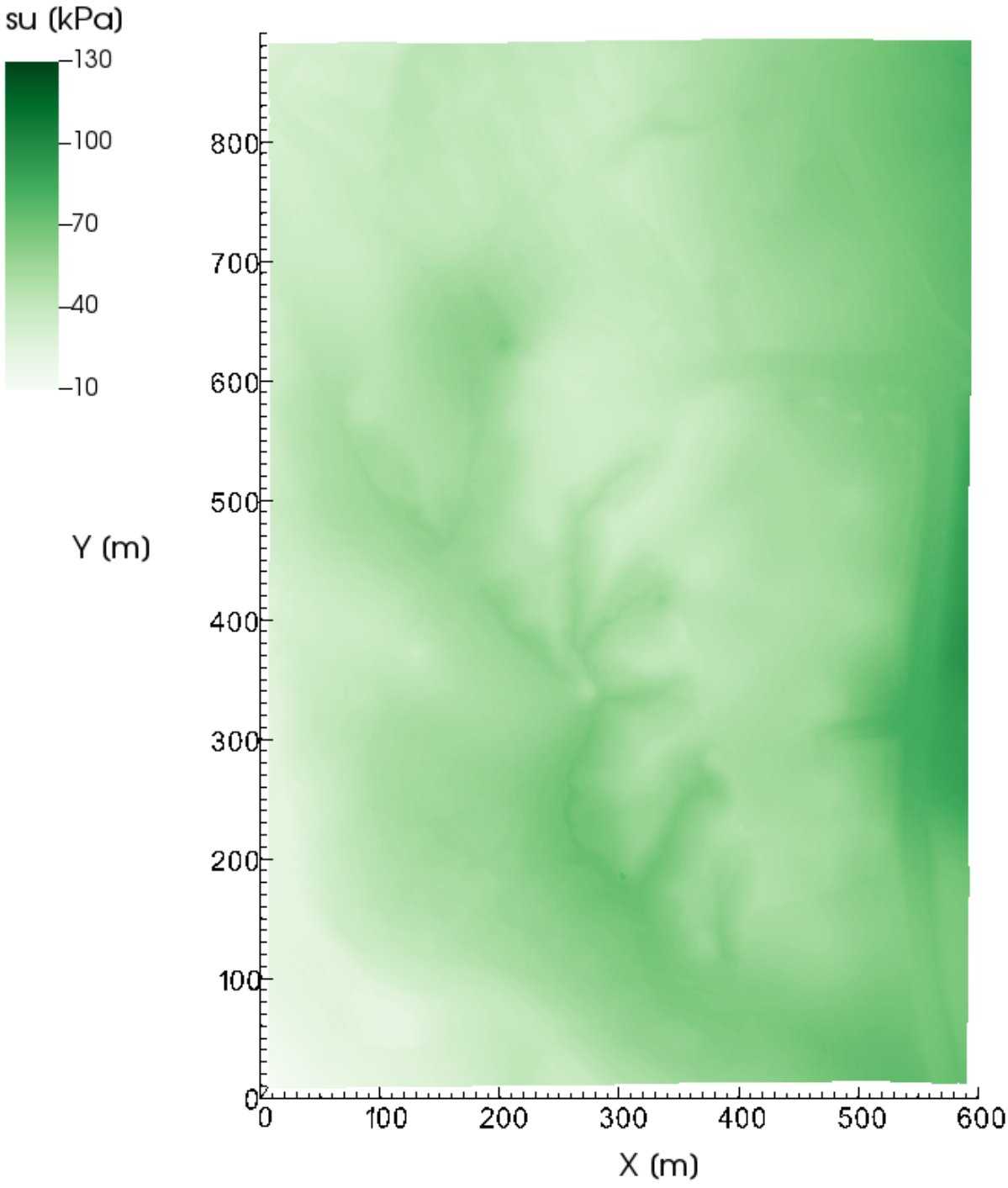
su (kPa)
130
100
70
40
10
Y (m)
800
700
600
500
400
300
200
100
0
0
100
200
300
400
500
600
X (m)

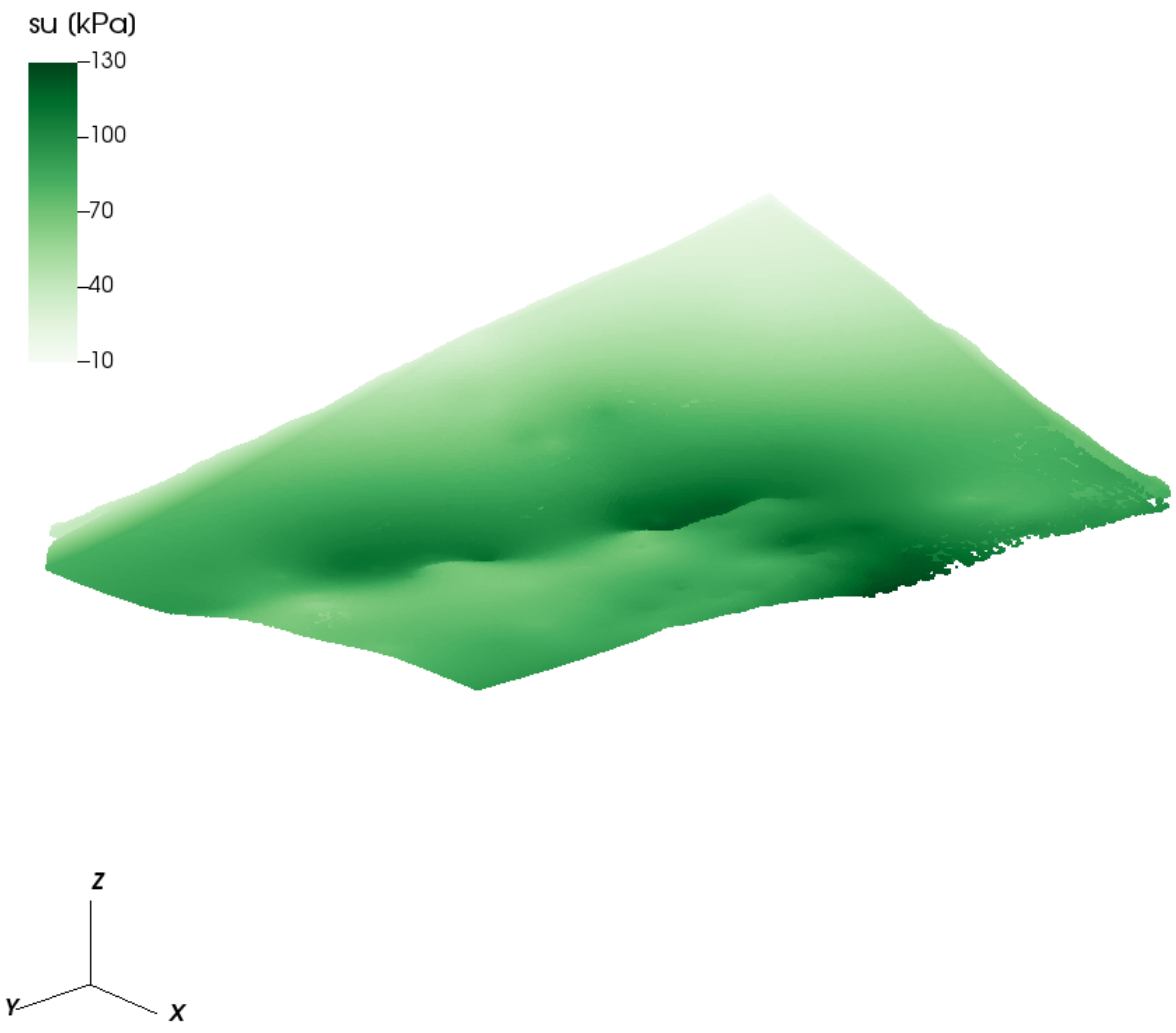
su (kPa)
130
100
70
40
10
Z
Y
X

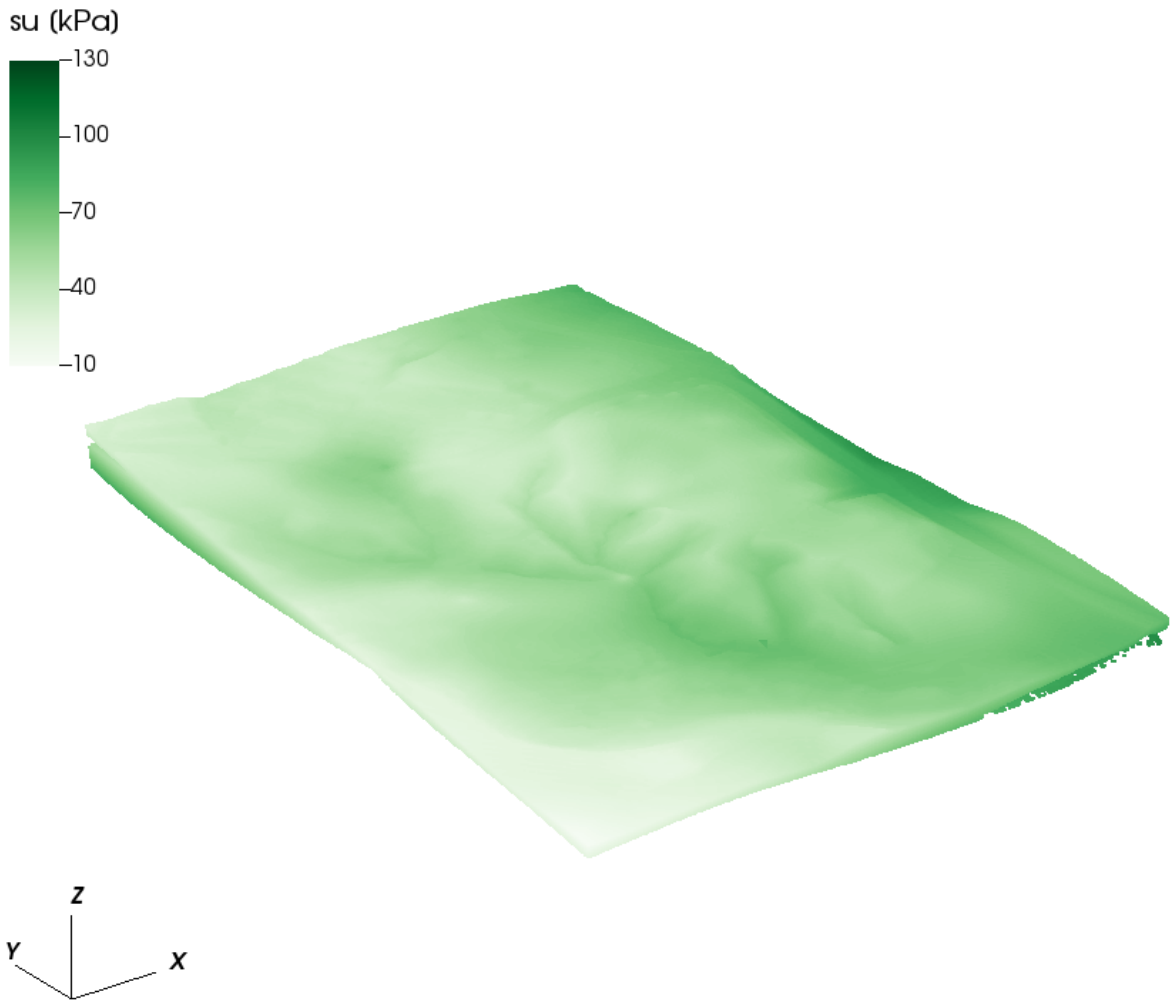
su (kPa)
130
100
70
40
10
Z
Y
X

Appendix C

2D MPM Results

Shear strain and velocity for every time step for the five simulations. All shear strain larger than 1 is displayed as red. All velocity higher than 7 m/s is displaced as red.

Simulation 1

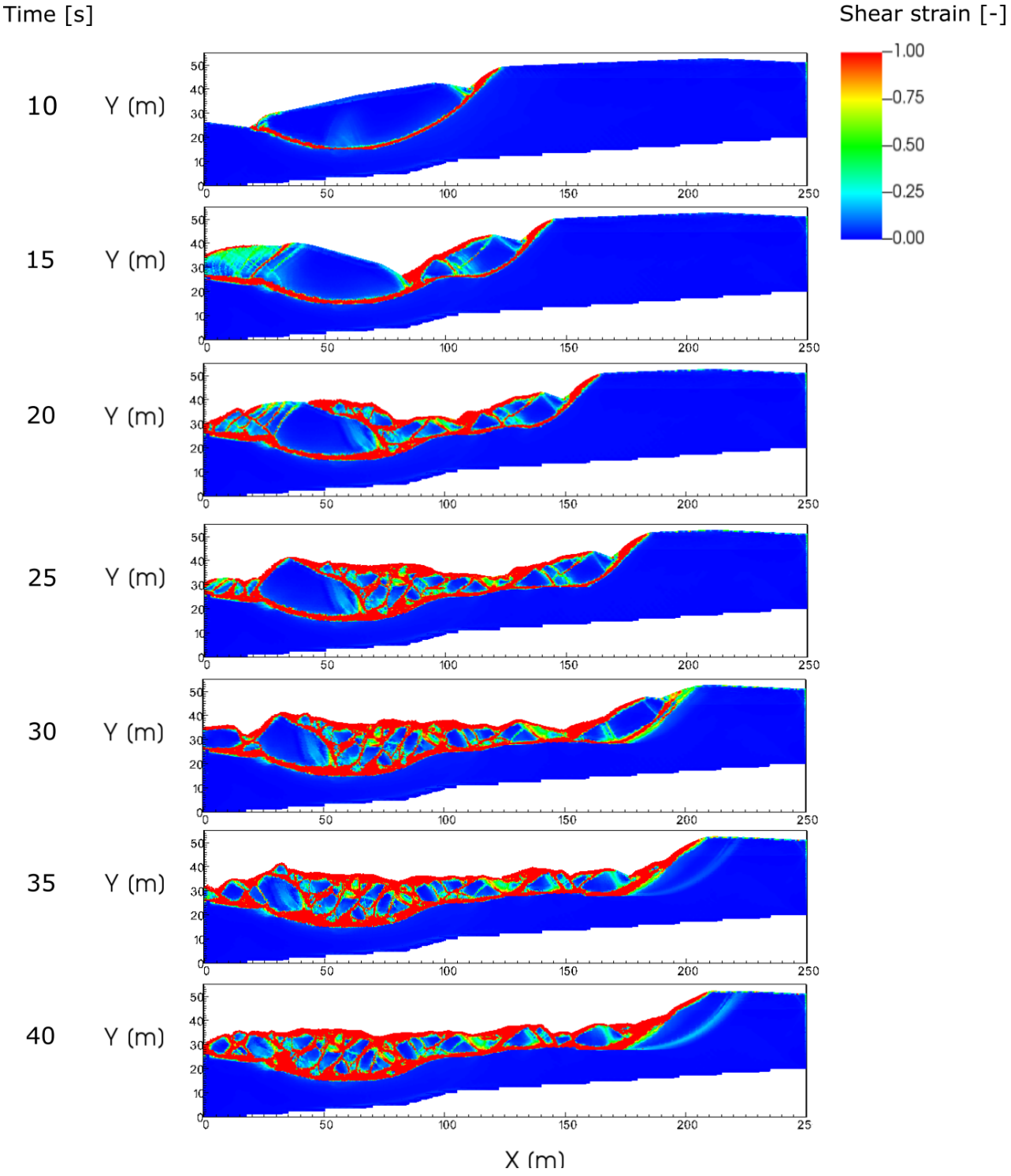

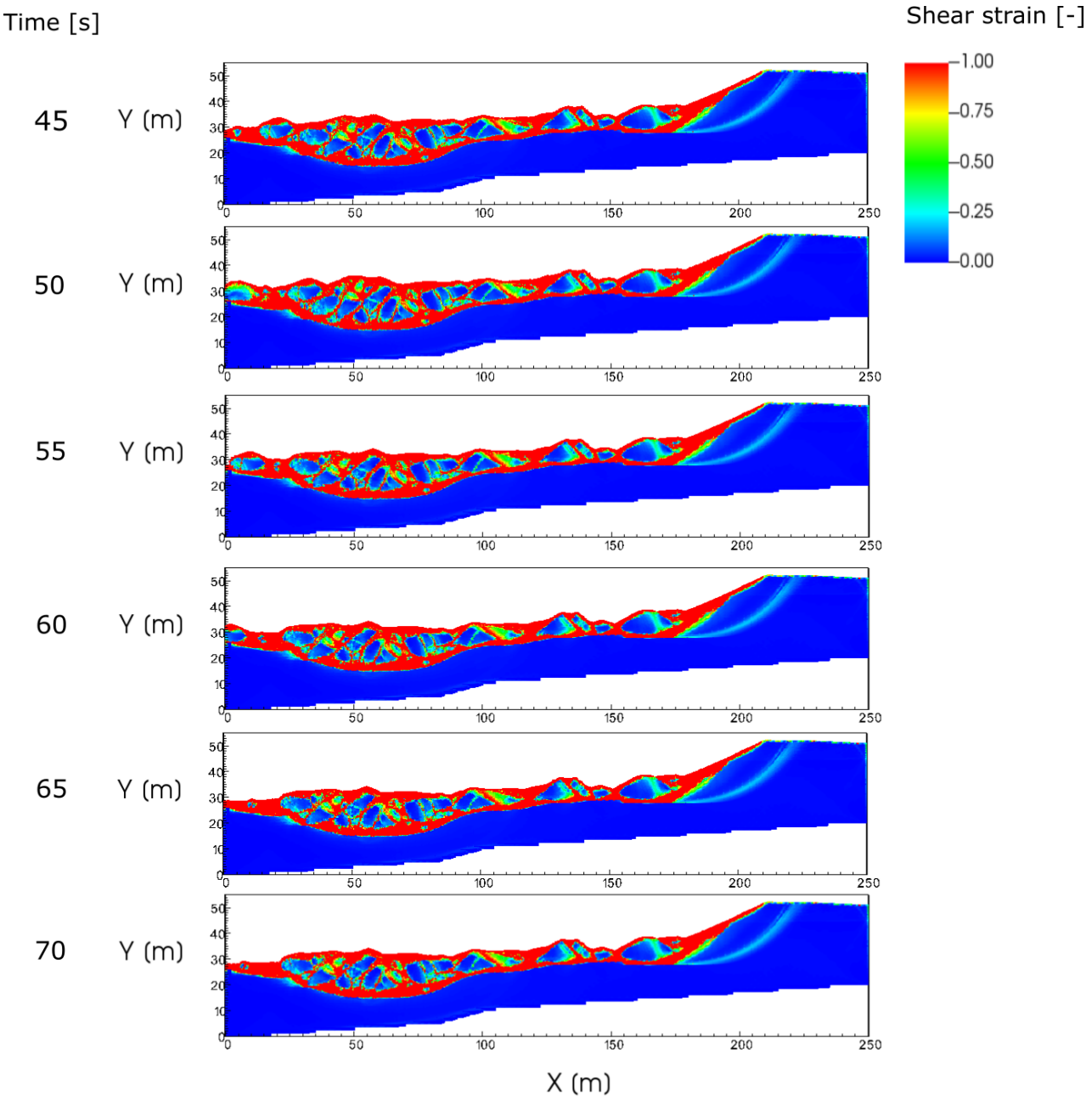
Time [s]
Shear strain [-]
1.00
0.75
0.50
0.25
0.00
45
50
55
60
65
70
Y (m)
X (m)
0
50
100
150
200
250
10
20
30
40

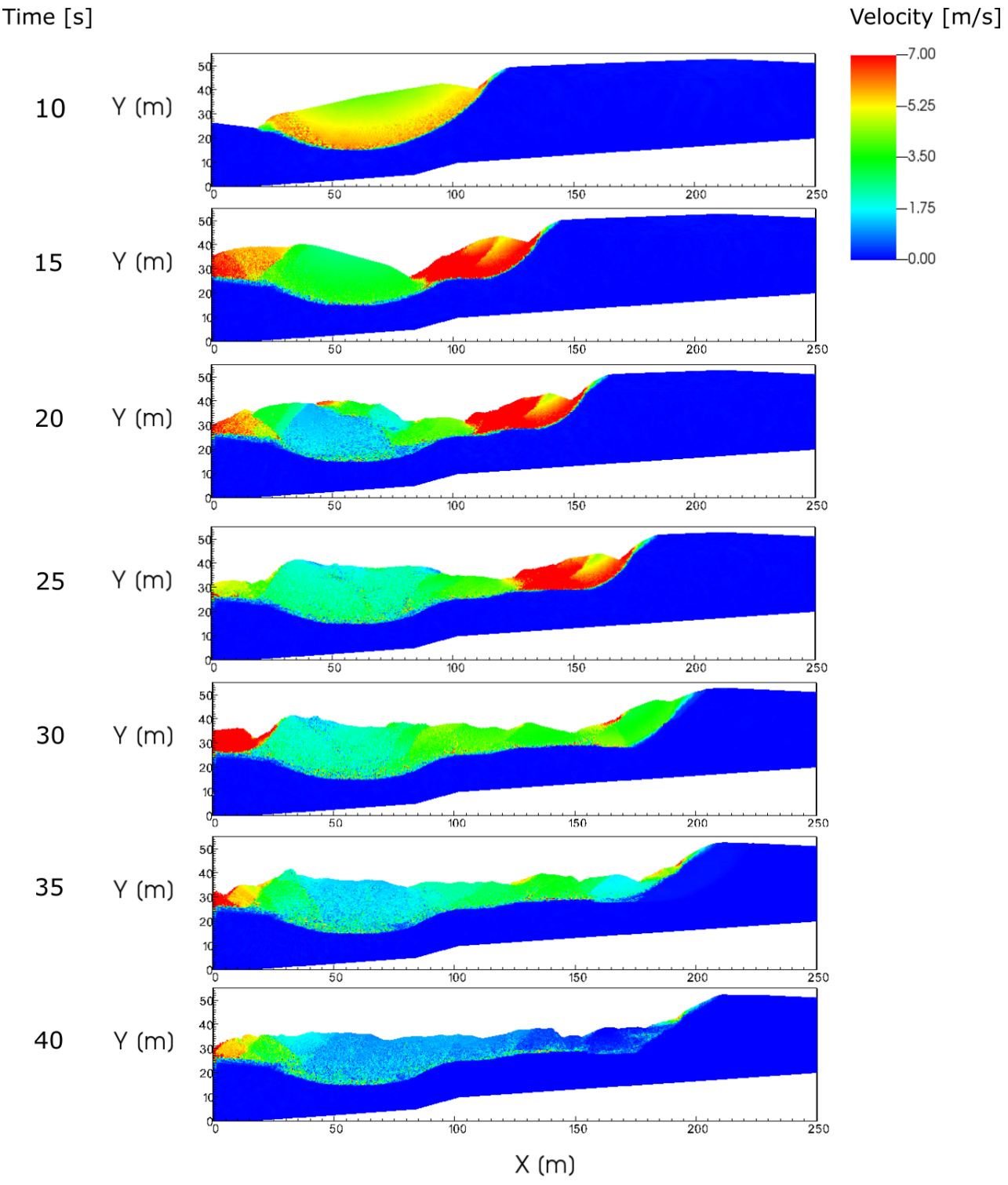
Time [s]
Velocity [m/s]
7.00
5.25
3.50
1.75
0.00
10
15
20
25
30
35
40
Y (m)
X (m)
0
50
100
150
200
250
10
20
30
40
50

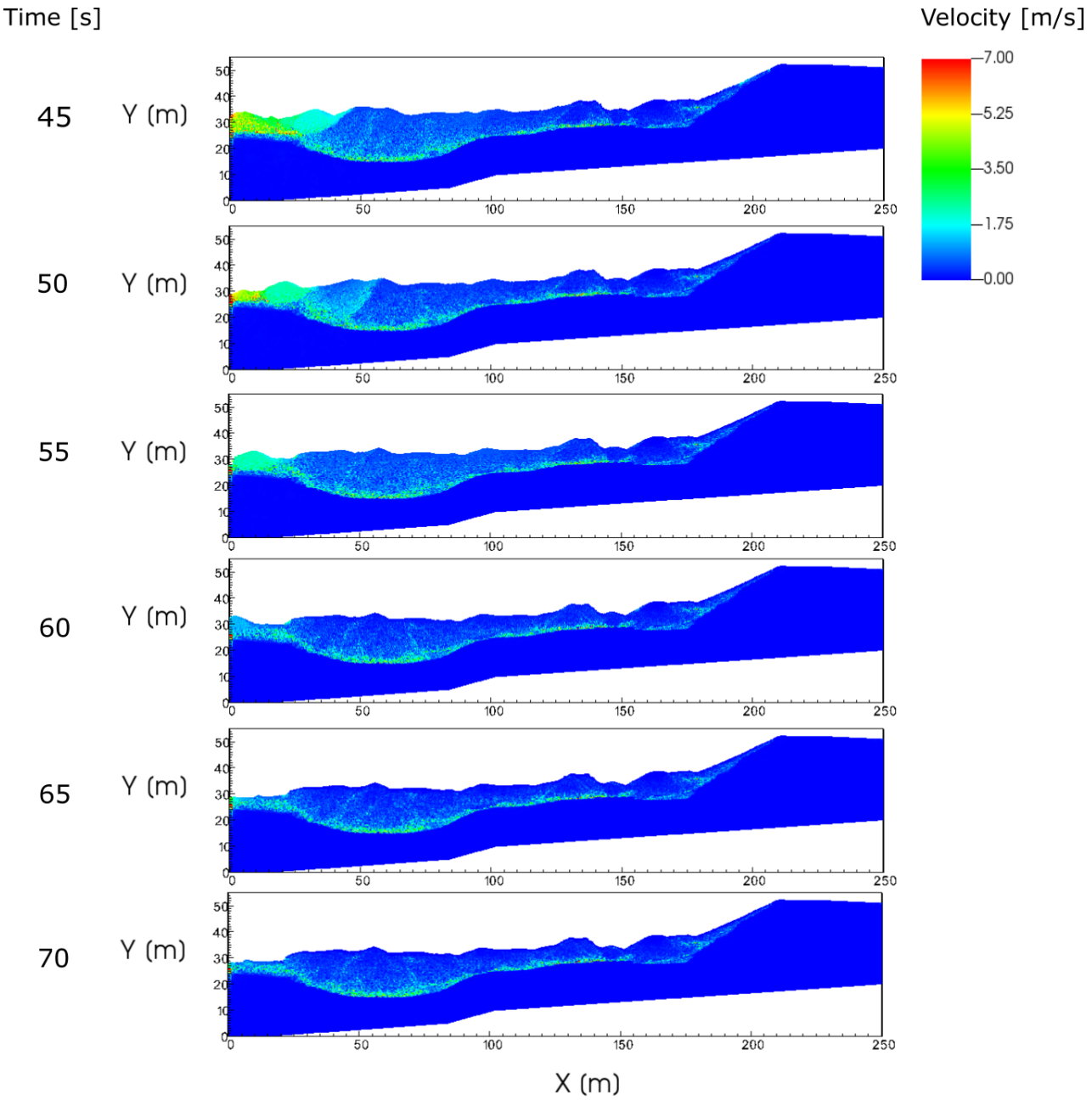
Time [s]
Velocity [m/s]
7.00
5.25
3.50
1.75
0.00
45
50
55
60
65
70
Y (m)
X (m)
0
50
100
150
200
250
10
20
30
40

Simulation 2

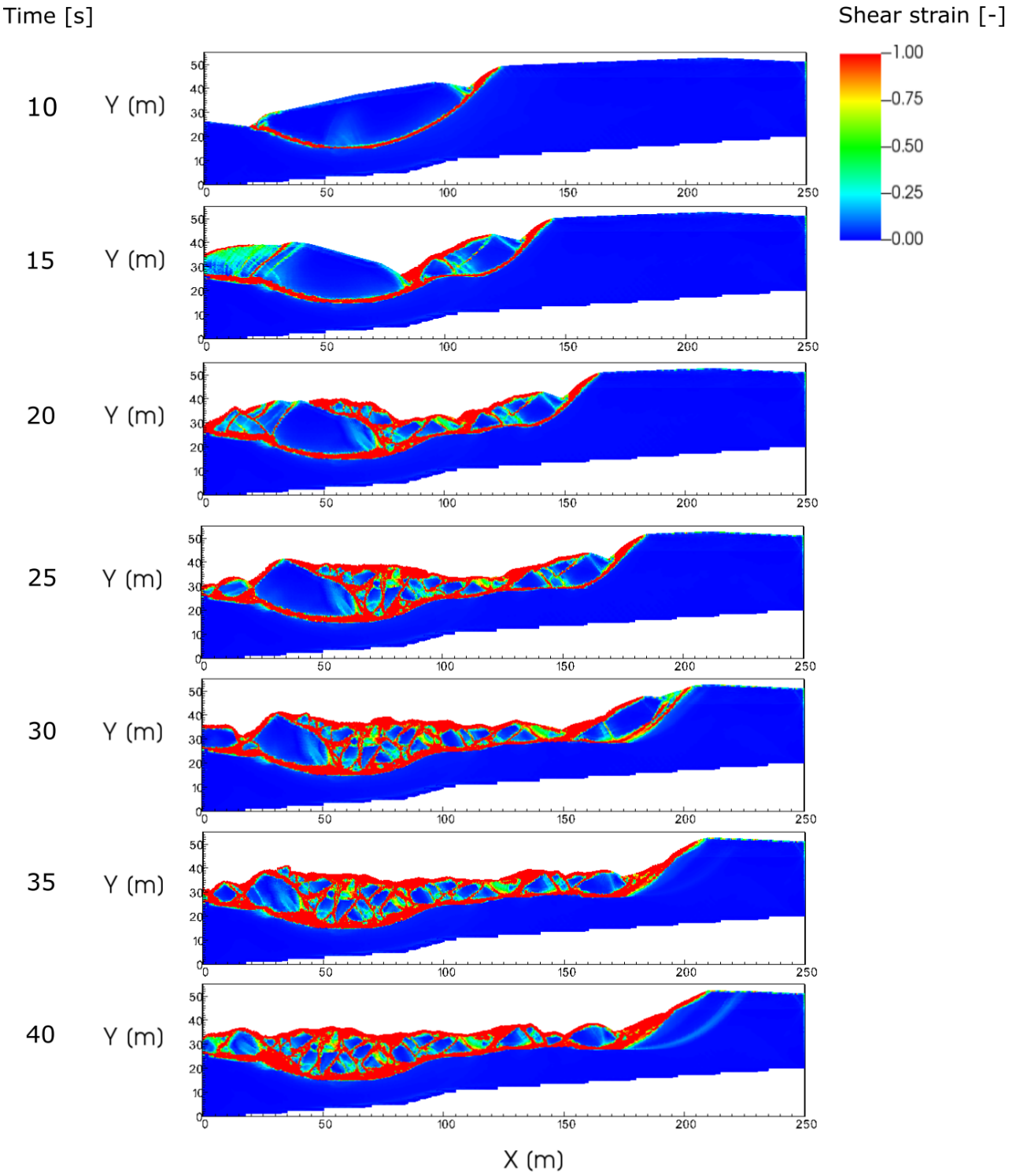

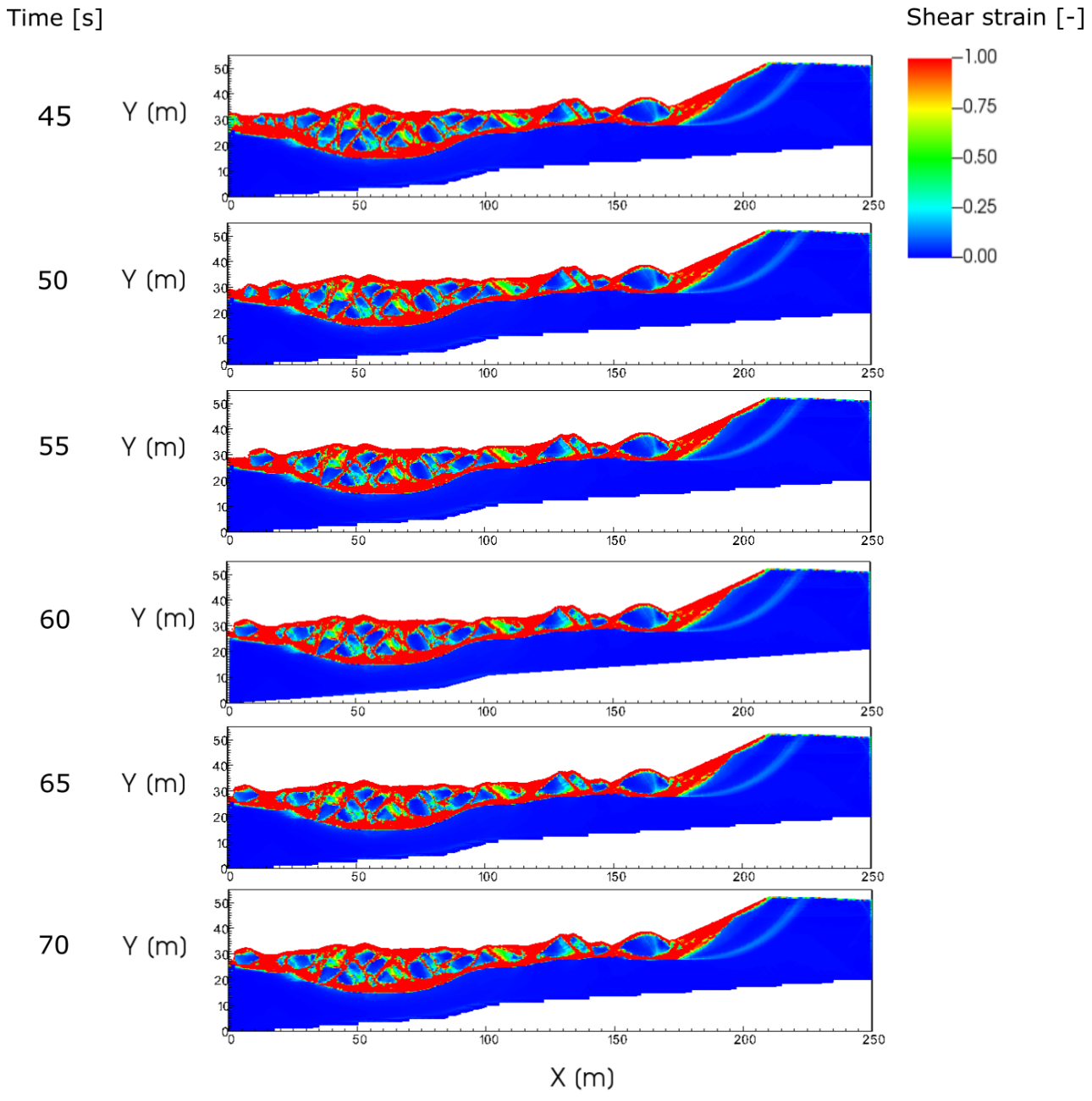
Time [s]
Shear strain [-]
1.00
0.75
0.50
0.25
0.00
45
50
55
60
65
70
Y (m)
X (m)
0
50
100
150
200
250
10
20
30
40
50

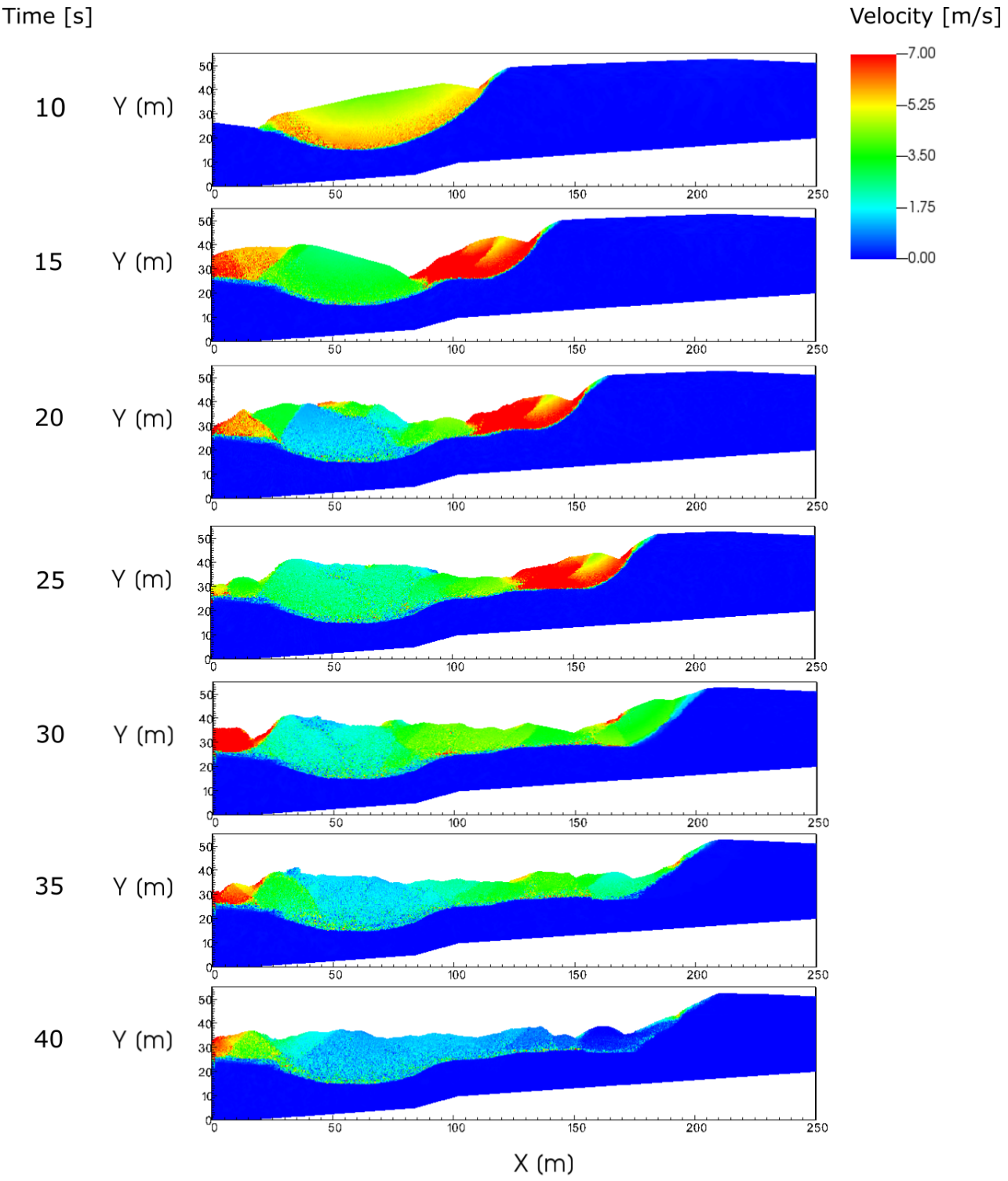
Time [s]
Velocity [m/s]
7.00
5.25
3.50
1.75
0.00
10
15
20
25
30
35
40
Y (m)
X (m)
0
50
100
150
200
250
10
20
30
40
50

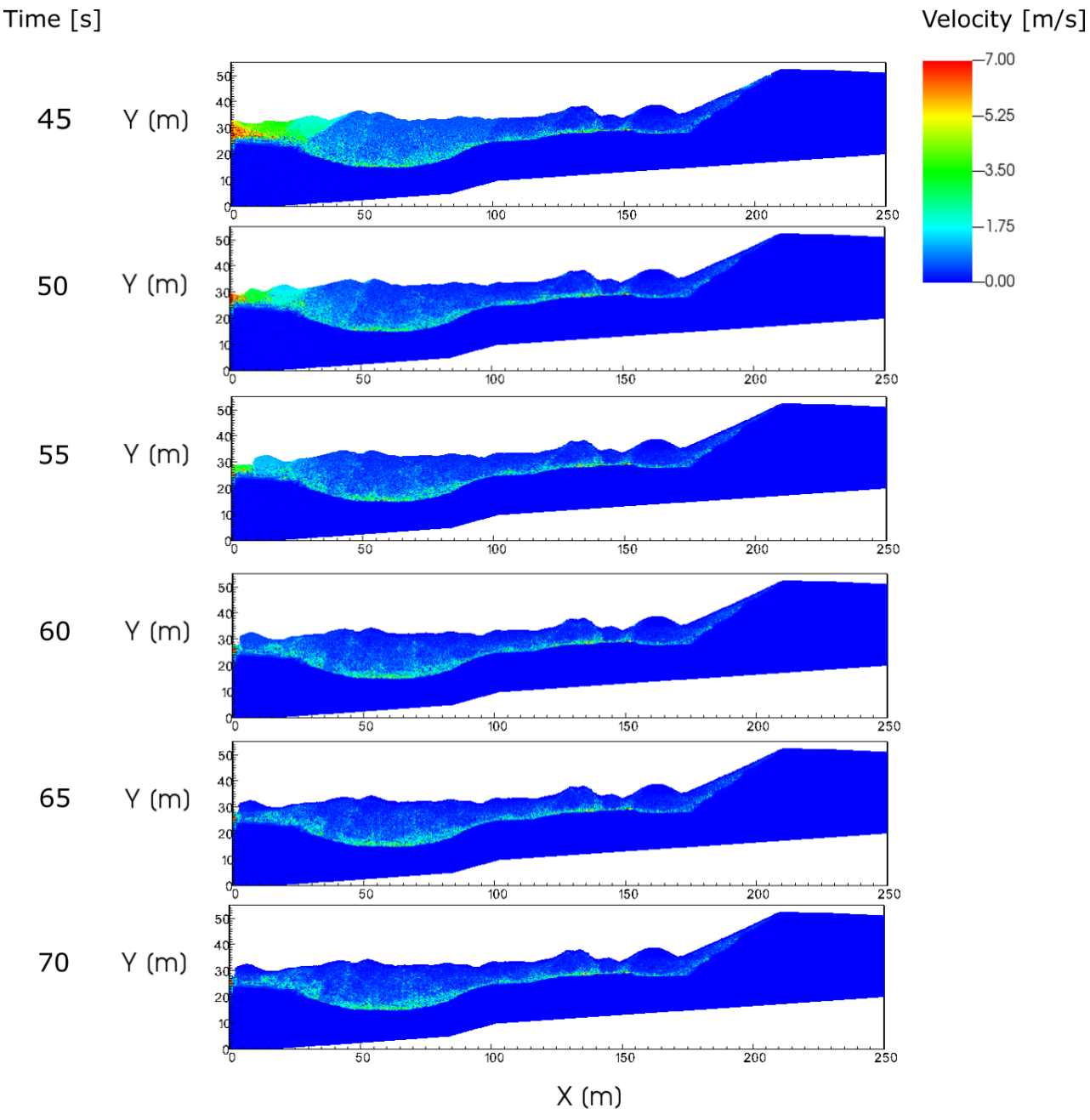
Time [s]
Velocity [m/s]
7.00
5.25
3.50
1.75
0.00
45
50
55
60
65
70
Y (m)
X (m)
0
50
100
150
200
250
10
20
30
40

Simulation 3

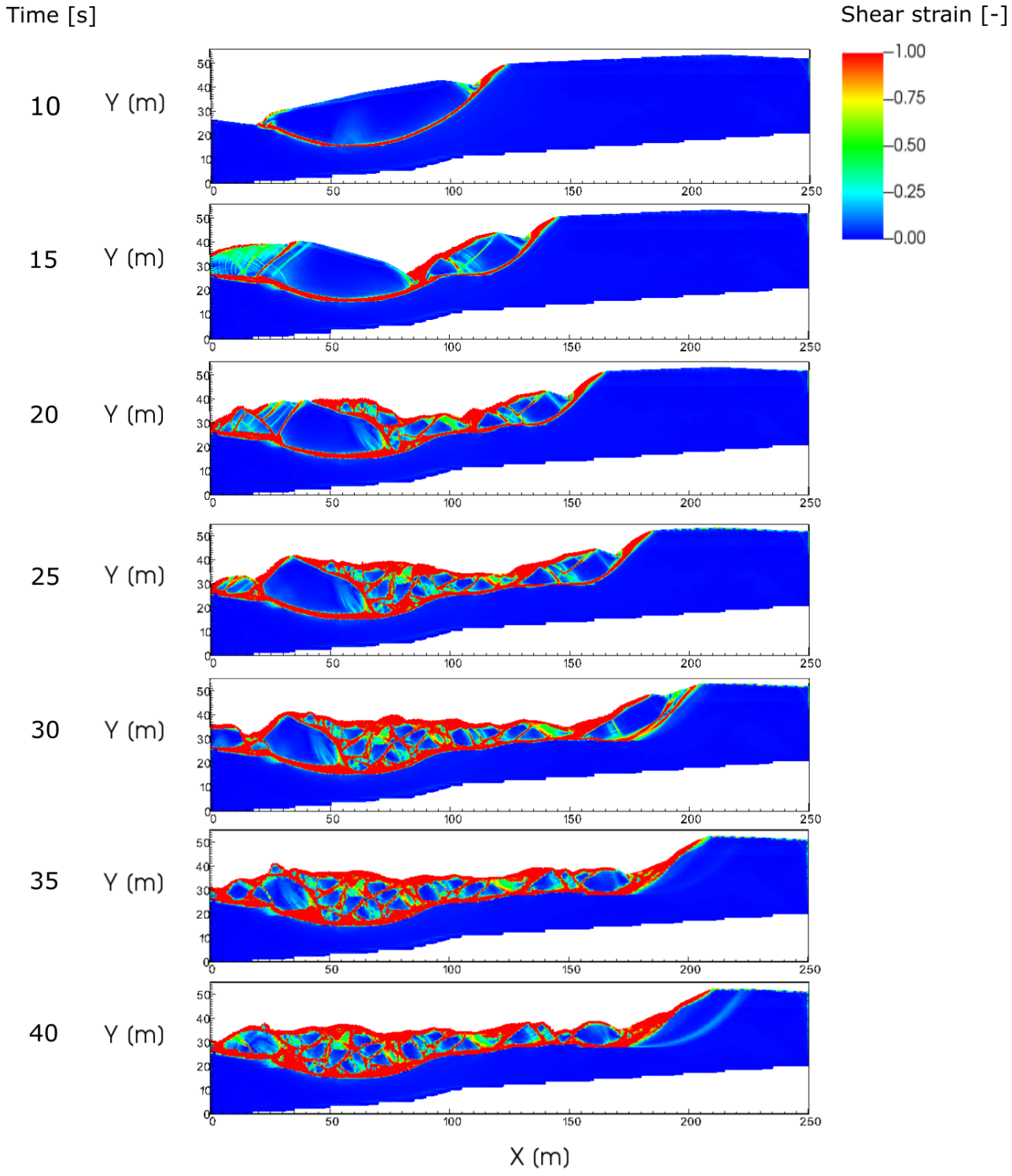

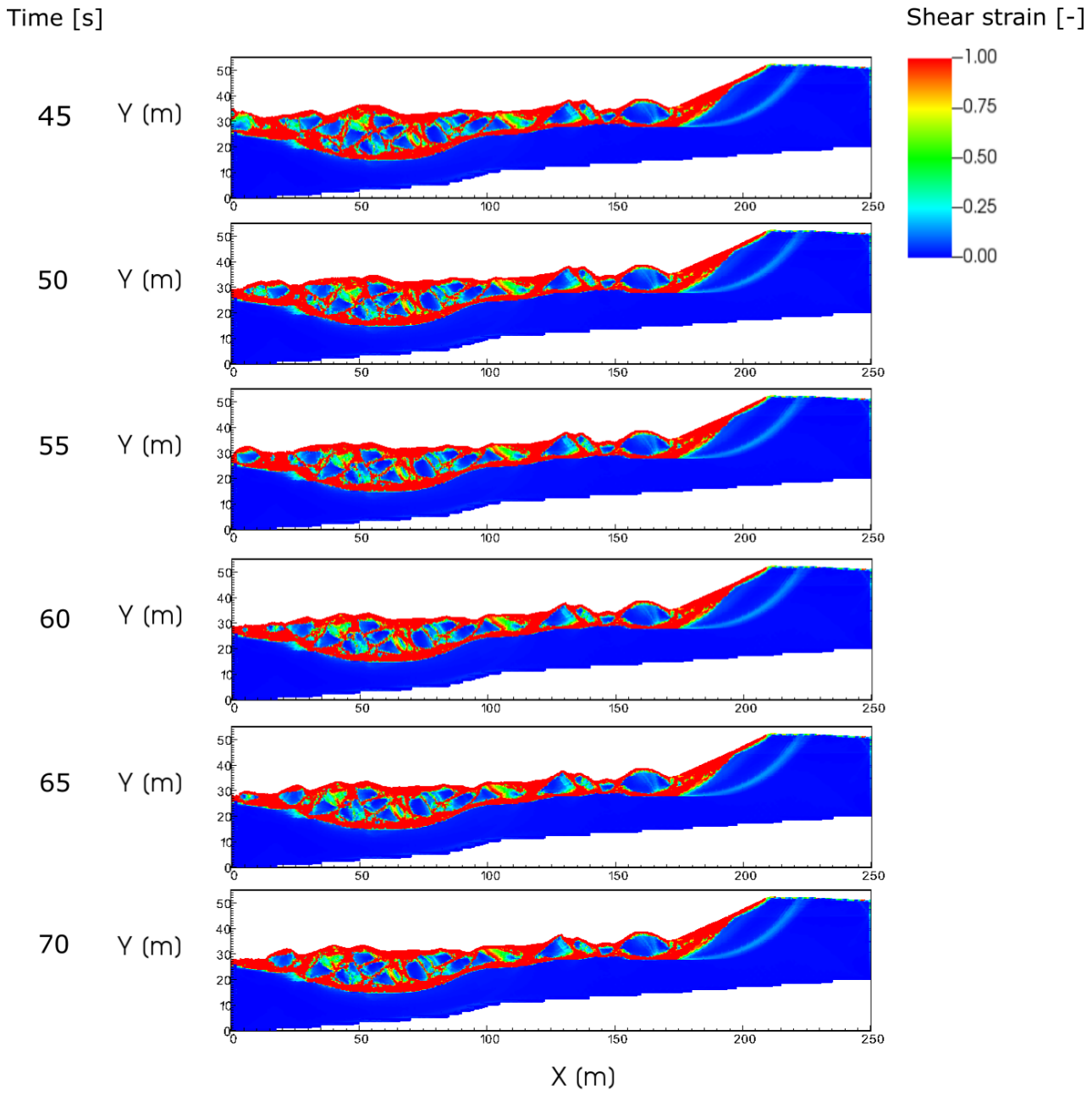
Time [s]
Shear strain [-]
1.00
0.75
0.50
0.25
0.00
45
50
55
60
65
70
Y (m)
X (m)
0
50
100
150
200
250
10
20
30
40

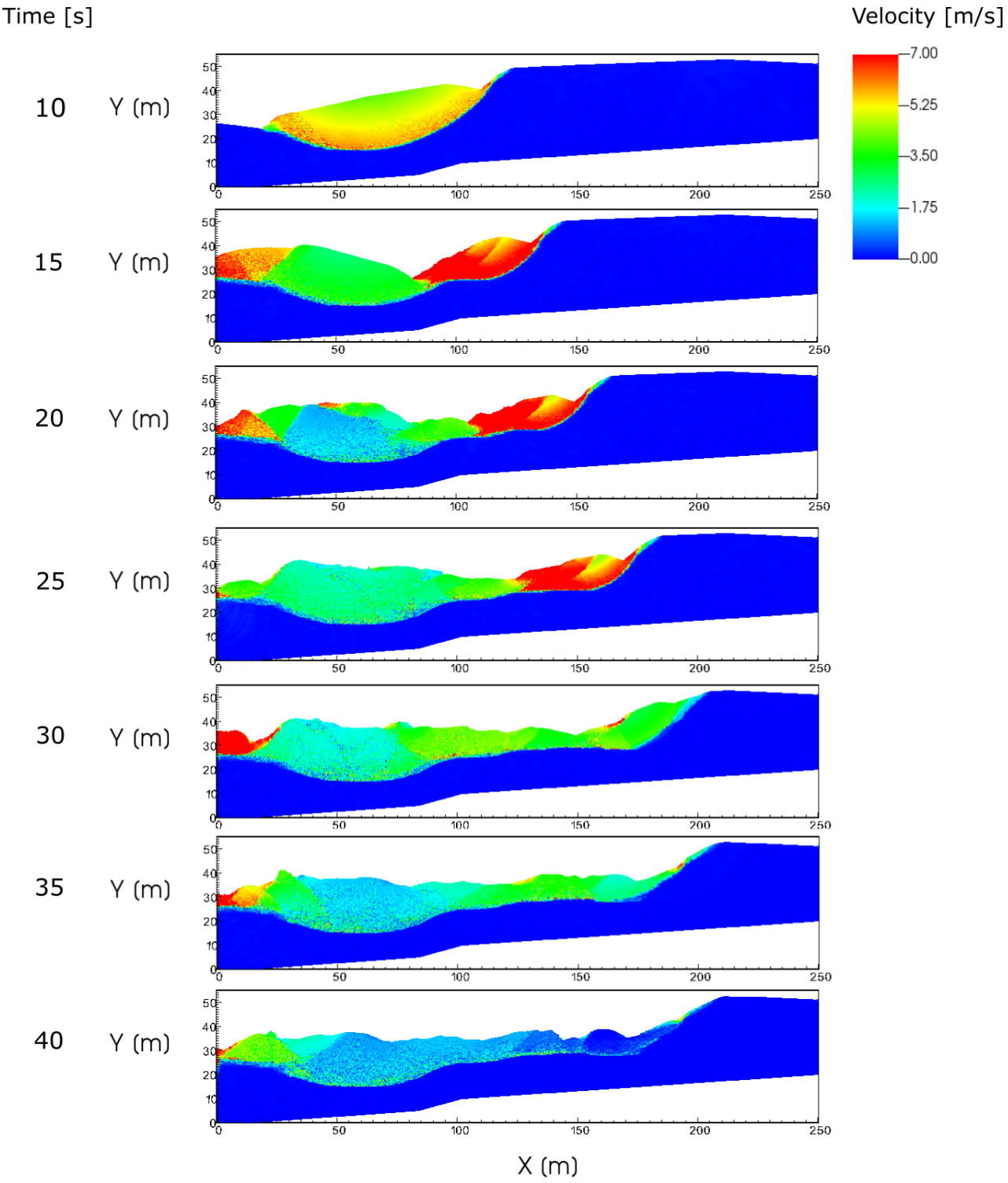
Time [s]
Velocity [m/s]
7.00
5.25
3.50
1.75
0.00
10
15
20
25
30
35
40
Y (m)
X (m)
0
50
100
150
200
250
10
20
30
40
50

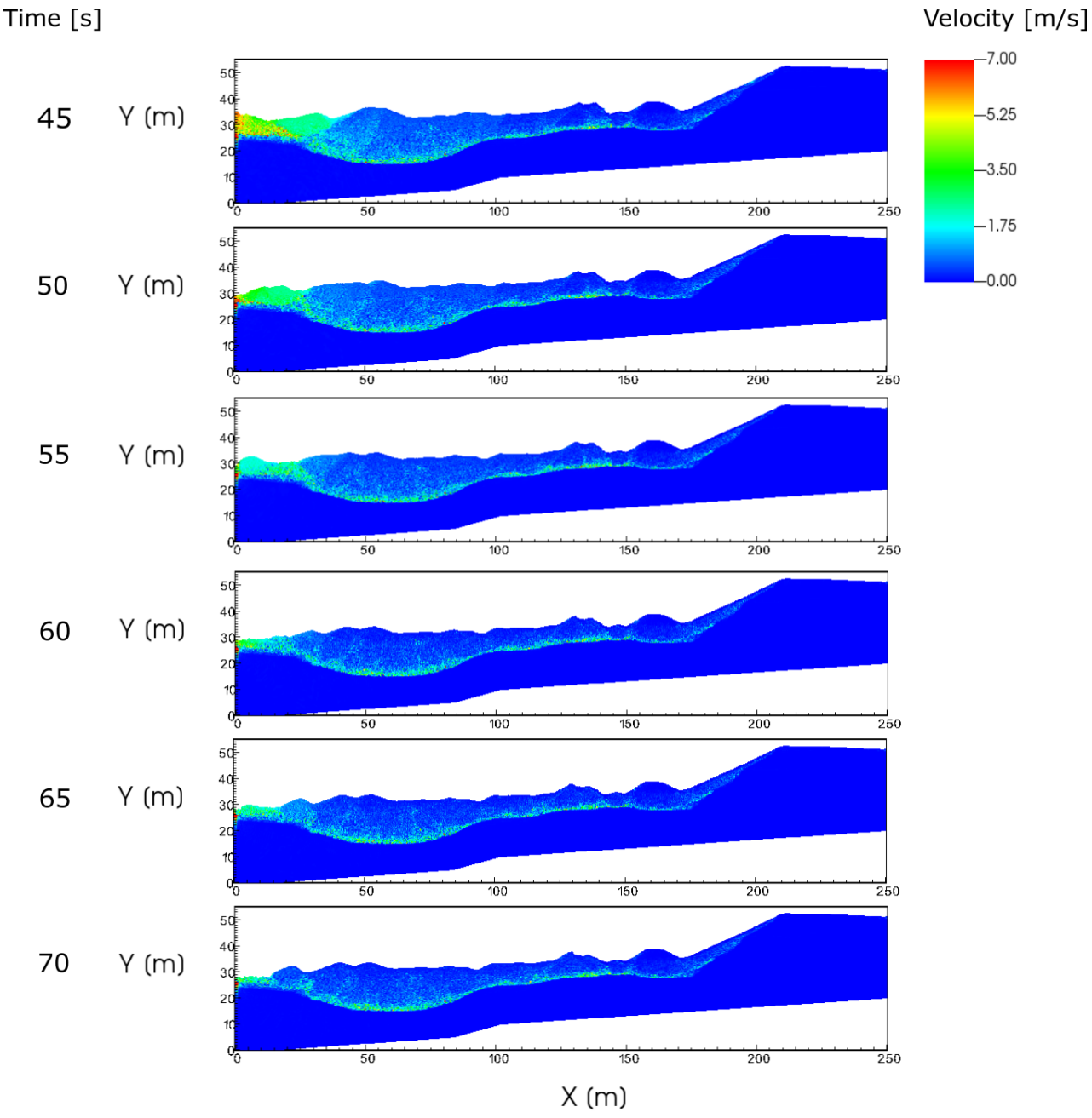
Time [s]
Velocity [m/s]
7.00
5.25
3.50
1.75
0.00
45
50
55
60
65
70
Y (m)
X (m)
0
50
100
150
200
250
10
20
30
40
50

Simulation 4

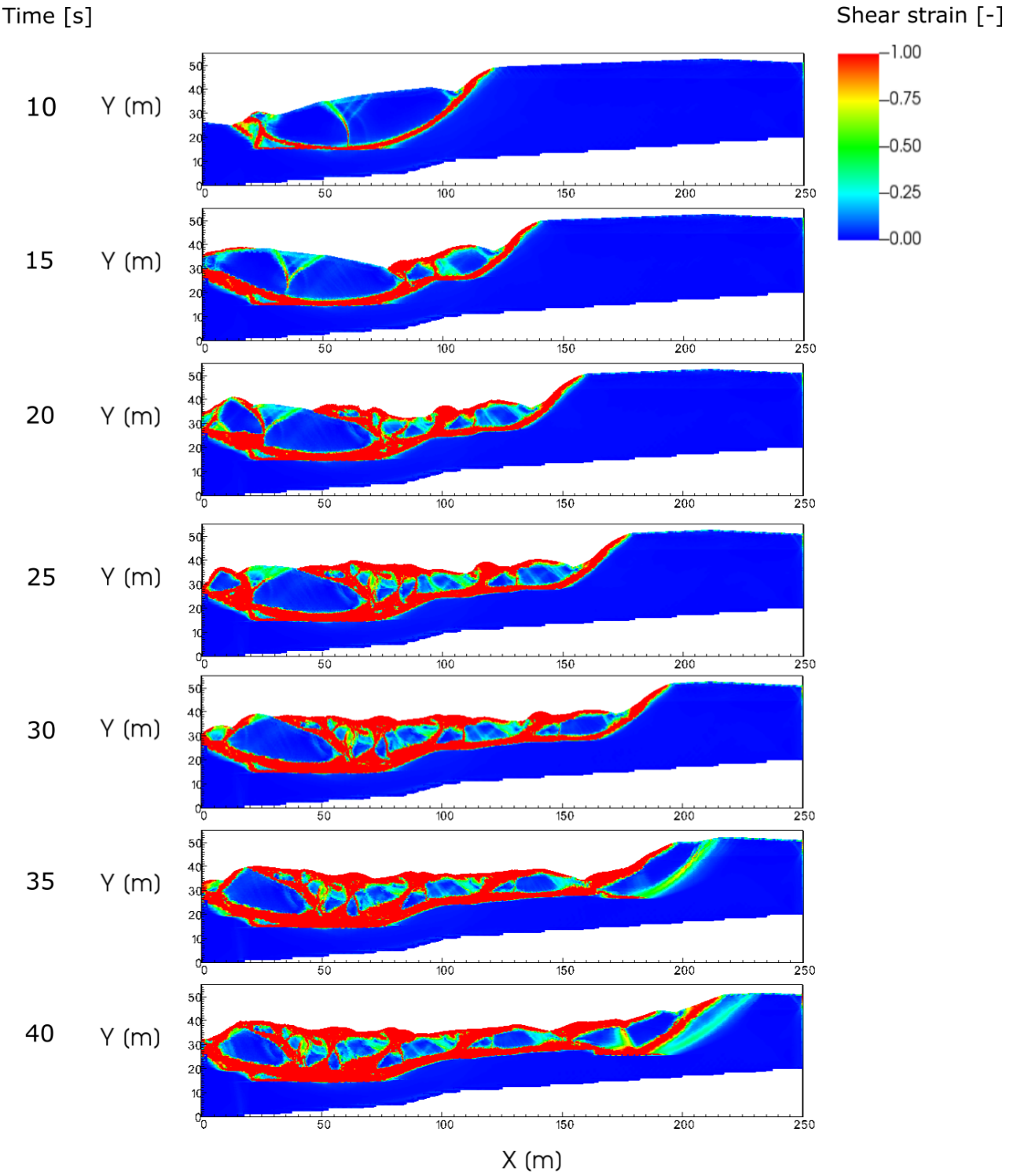

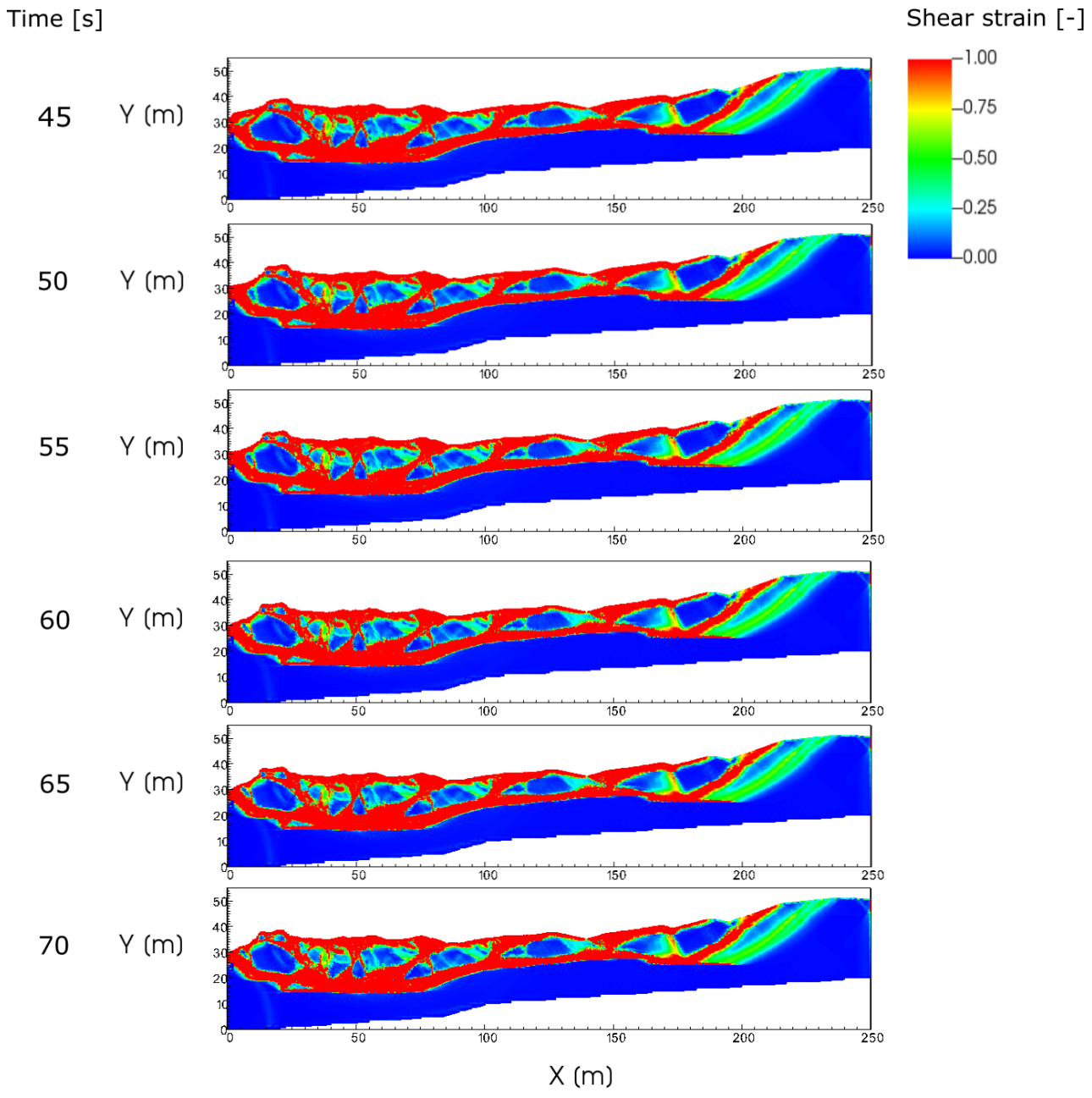
Time [s]
Shear strain [-]
1.00
0.75
0.50
0.25
0.00
45
50
55
60
65
70
Y (m)
X (m)
0
50
100
150
200
250
10
20
30
40
50

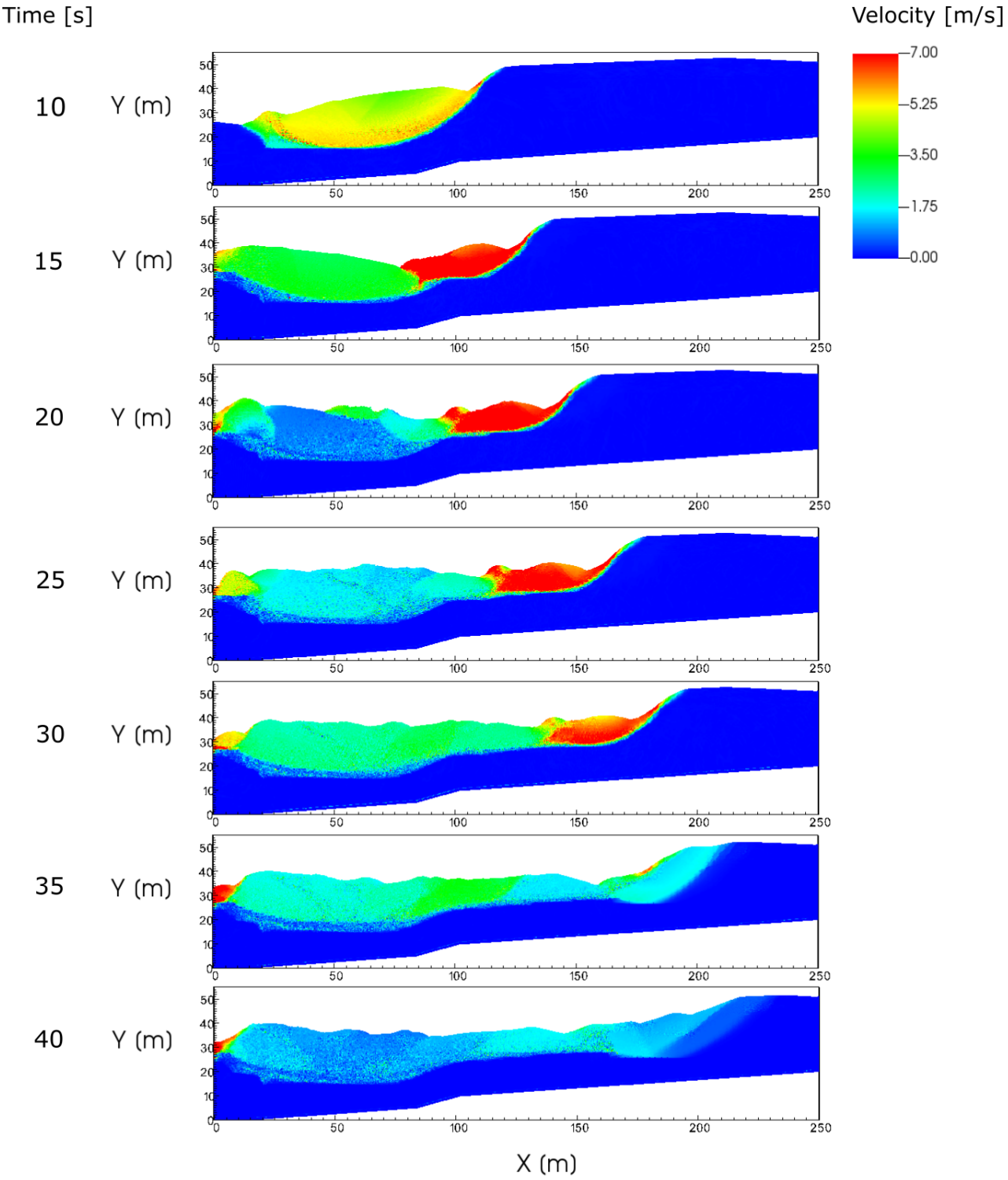
Time [s]
Velocity [m/s]
7.00
5.25
3.50
1.75
0.00
10
15
20
25
30
35
40
Y (m)
X (m)
0
50
100
150
200
250
10
20
30
40
50

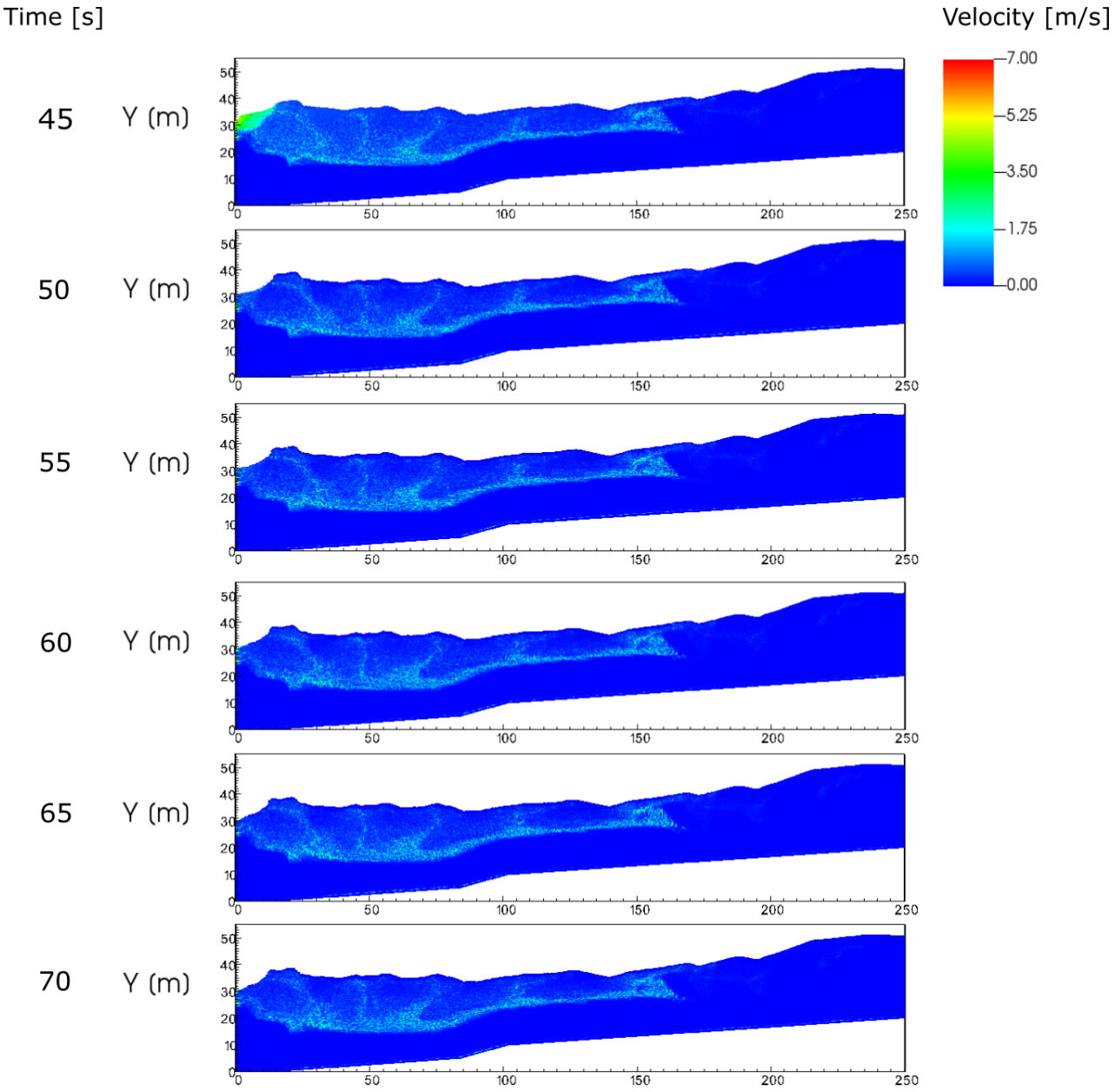
Time [s]
Velocity [m/s]
7.00
5.25
3.50
1.75
0.00
45
50
55
60
65
70
Y (m)
0
10
20
30
40
50
0
50
100
150
200
250

Simulation 5

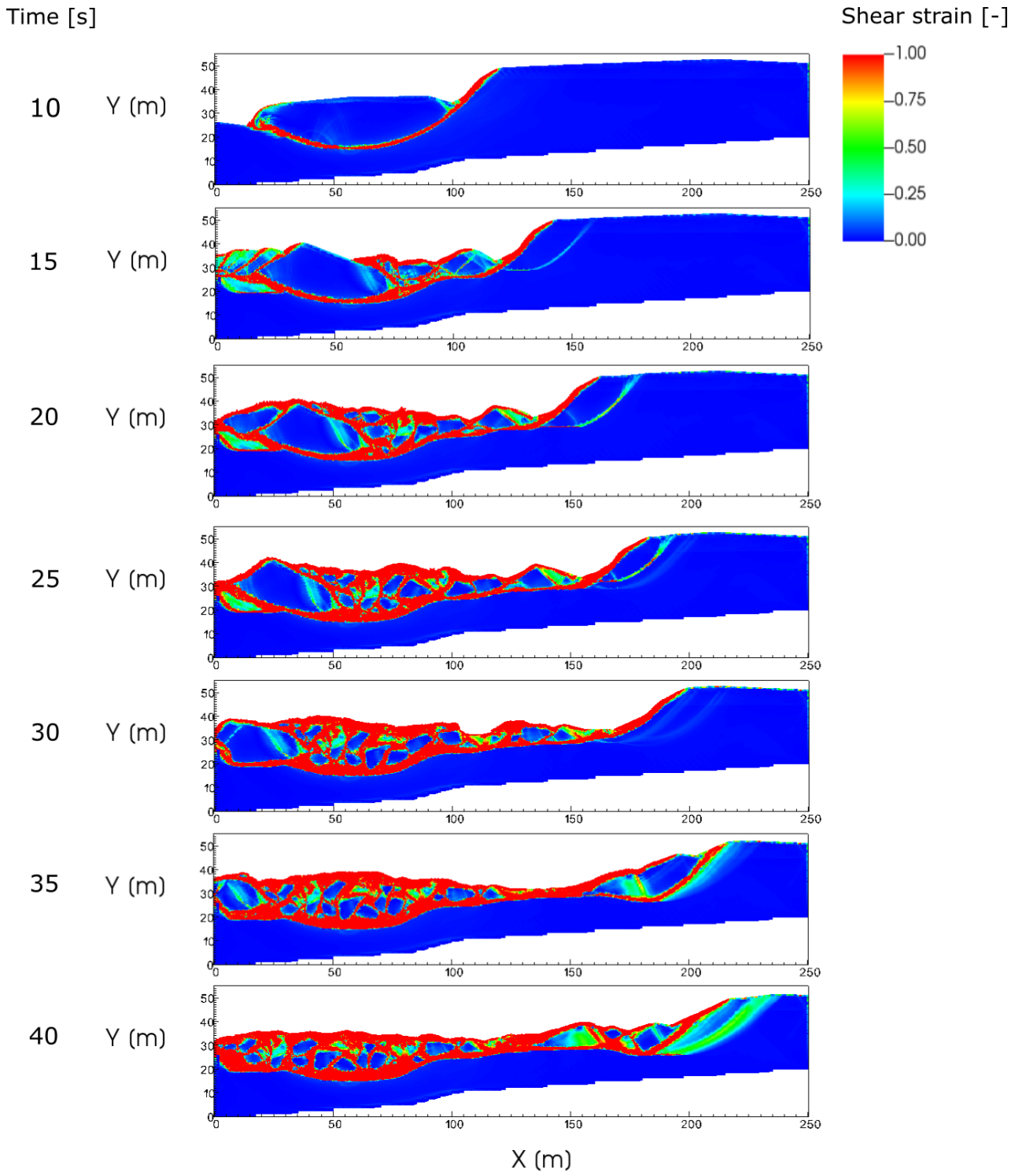

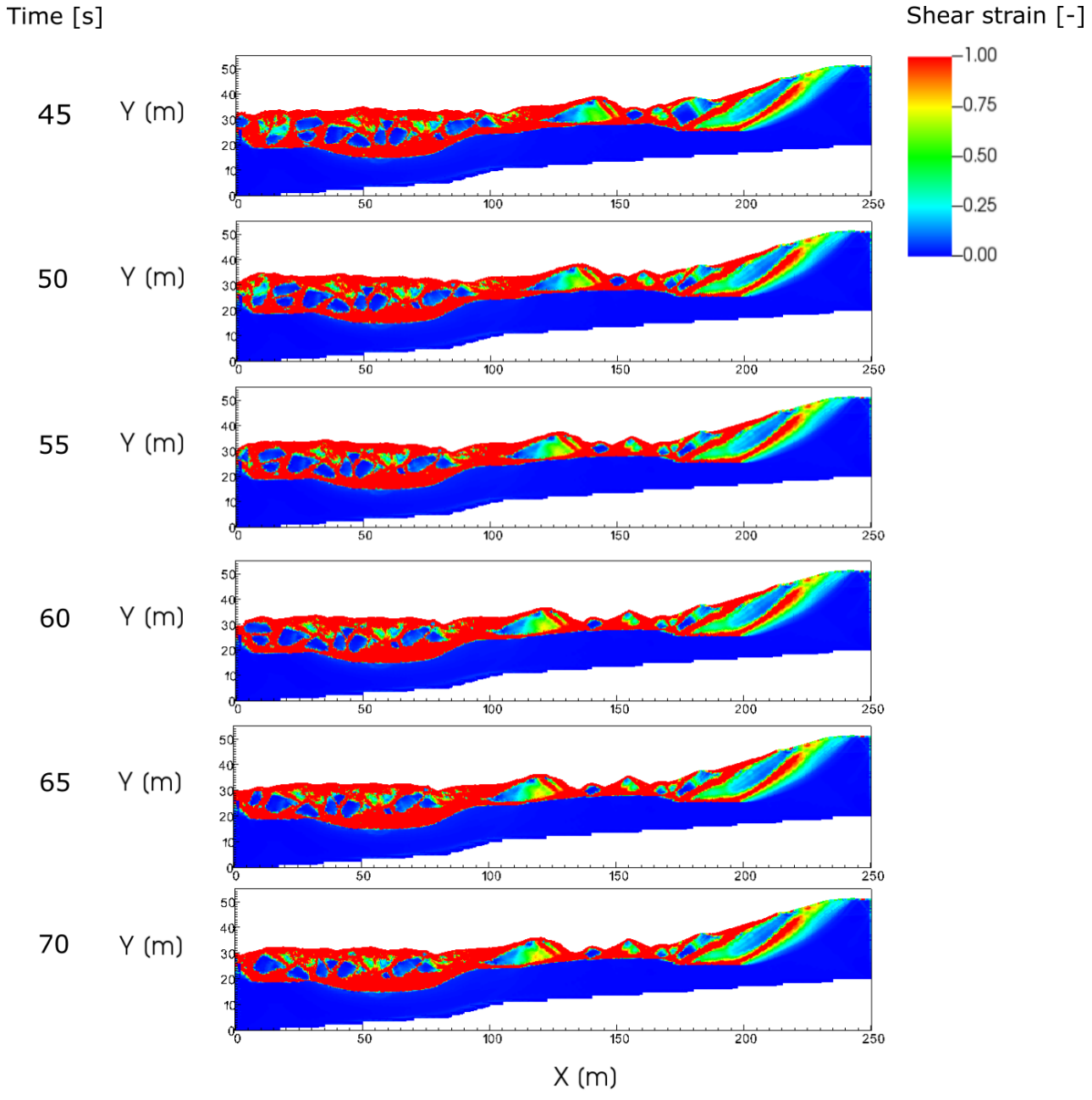
Time [s]
Shear strain [-]
1.00
0.75
0.50
0.25
0.00
45
50
55
60
65
70
Y (m)
X (m)
0
50
100
150
200
250
10
20
30
40

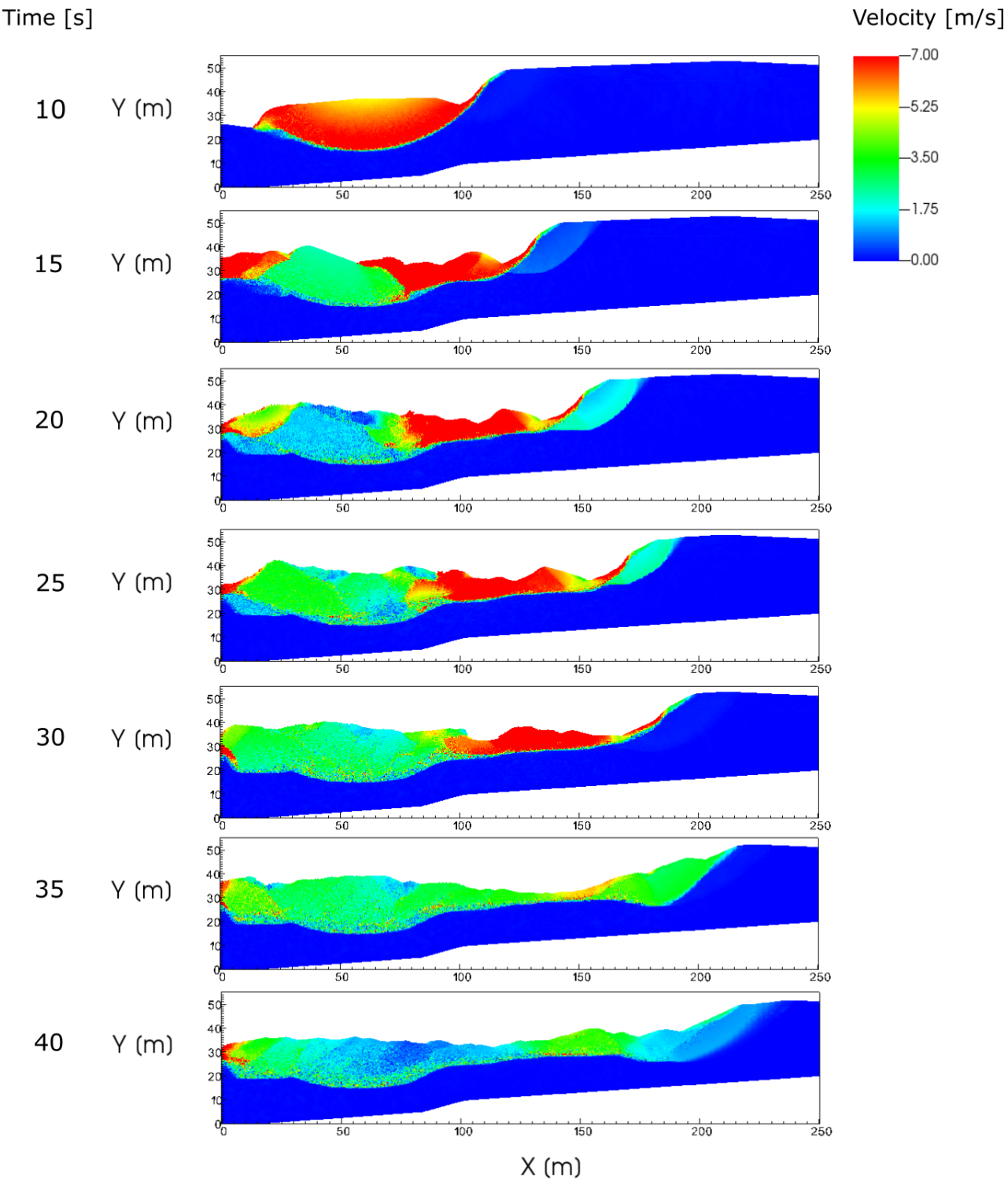
Time [s]
Velocity [m/s]
7.00
5.25
3.50
1.75
0.00
10
15
20
25
30
35
40
Y (m)
X (m)
0
50
100
150
200
250
10
20
30
40
50

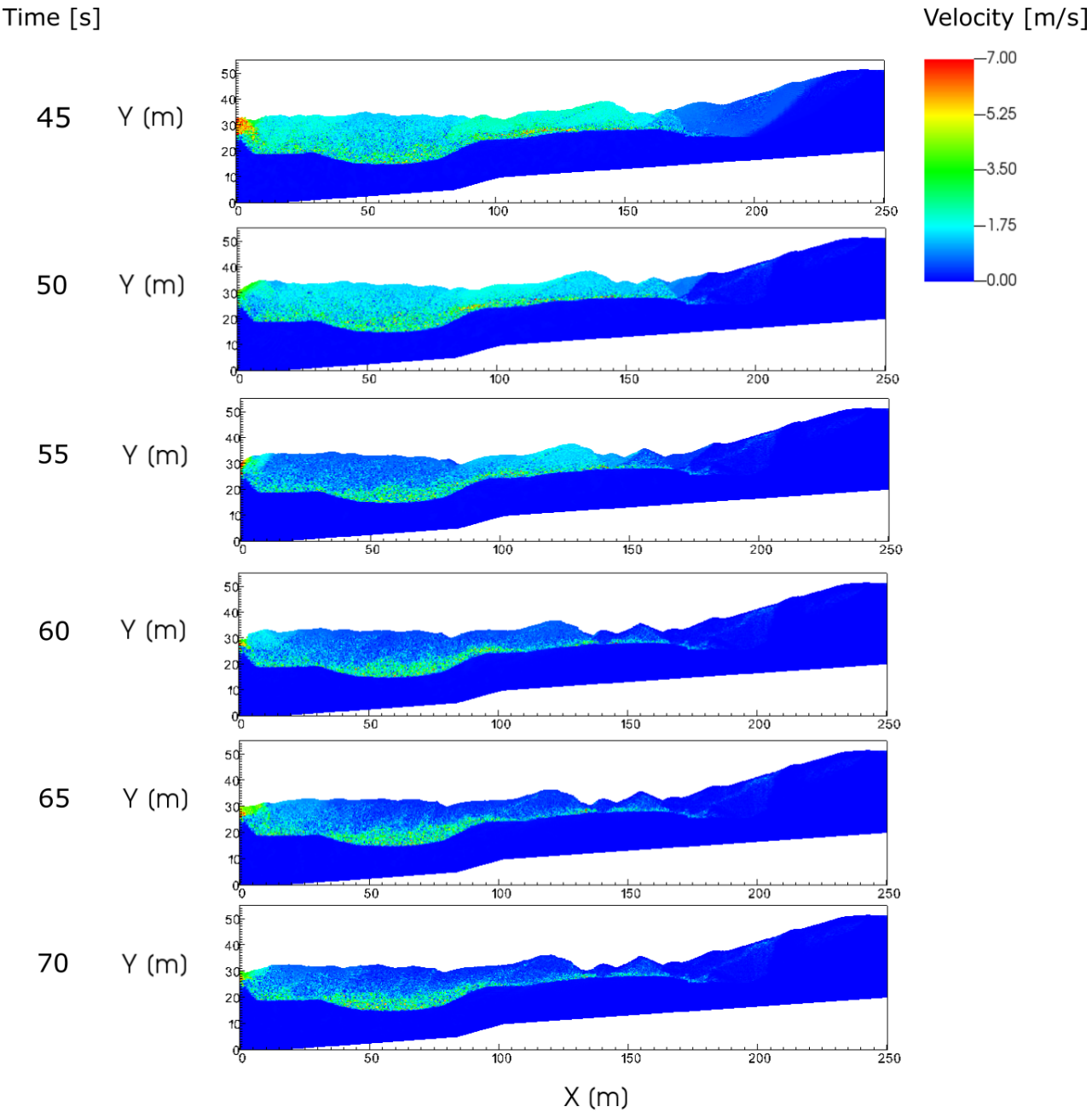
Time [s]
Velocity [m/s]
7.00
5.25
3.50
1.75
0.00
45
Y (m)
50
Y (m)
55
Y (m)
60
Y (m)
65
Y (m)
70
Y (m)
0
50
100
150
200
250
10
20
30
40
50
X (m)

Appendix D

3D Empirical Results

Profiles A - H with the retrogression distances for the three empirical criteria.

Profile A

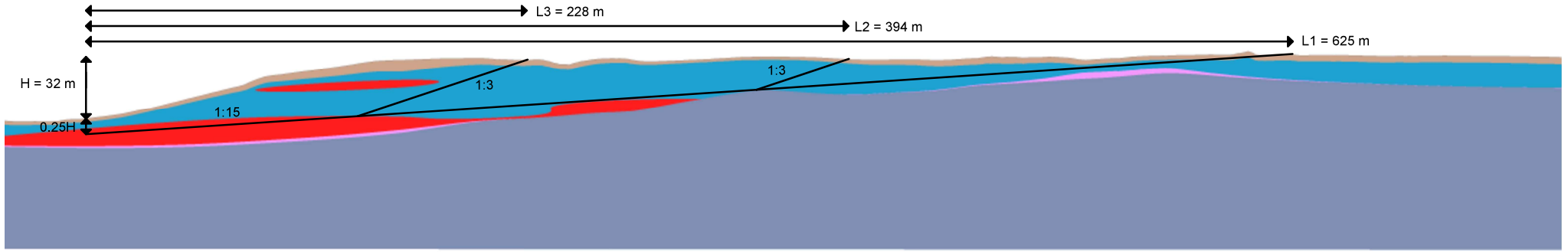

Profile B

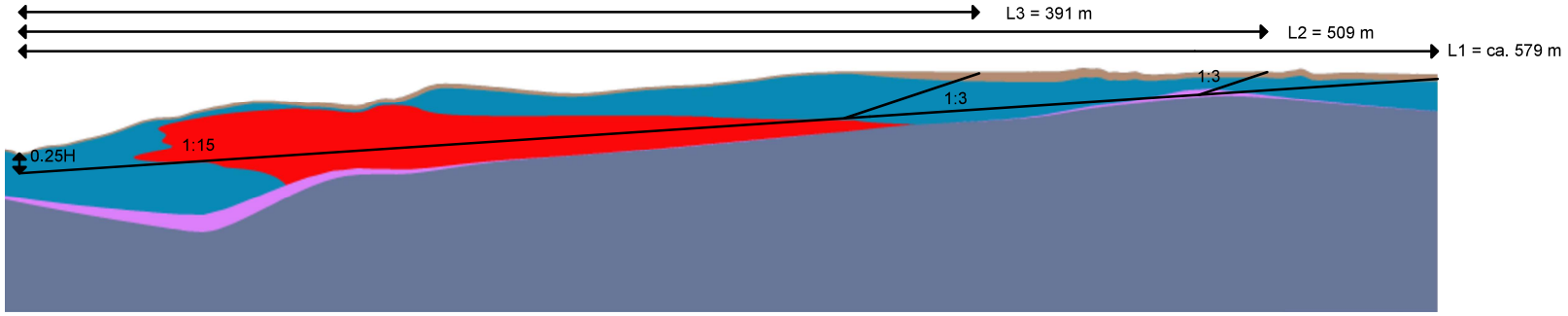

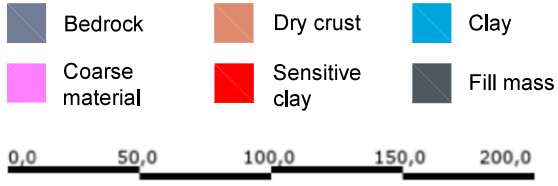

Profile C

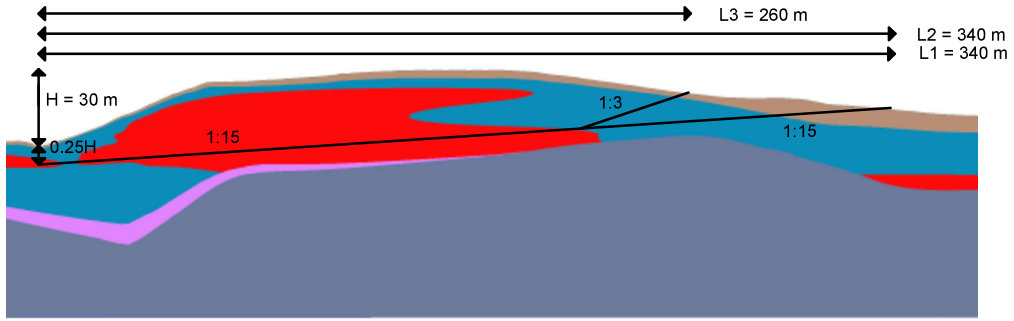

Profile D

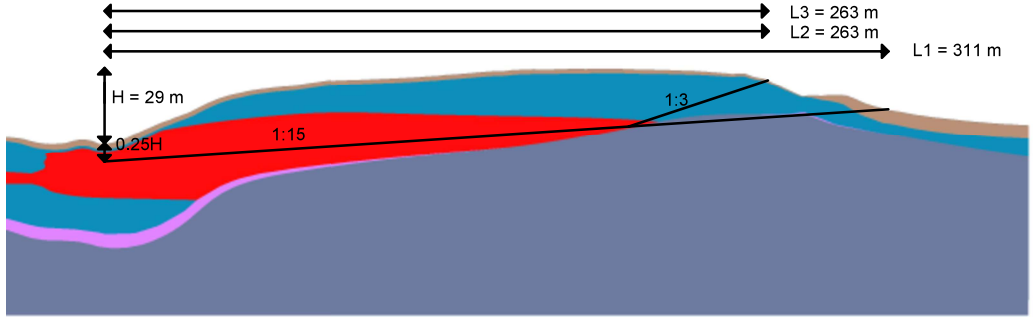

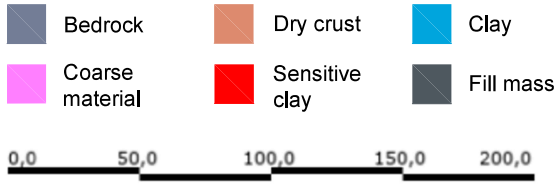

Profile E

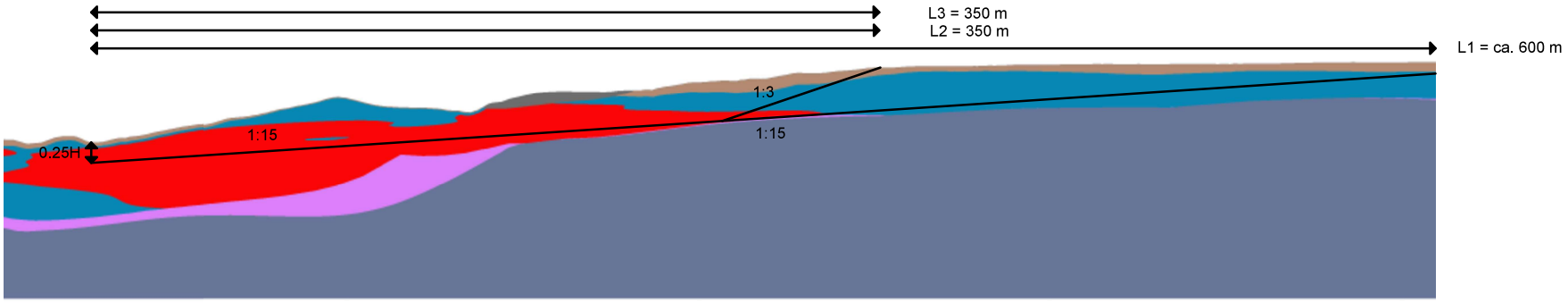

Profile F

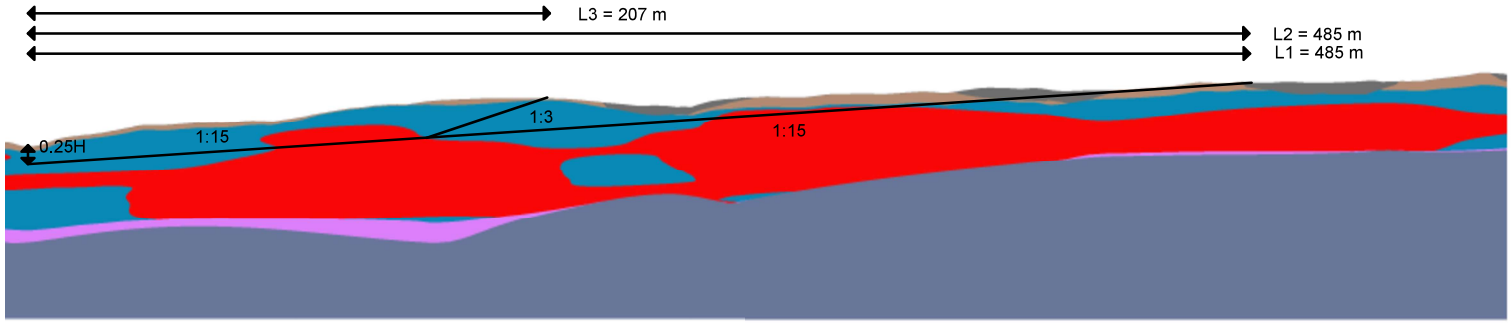

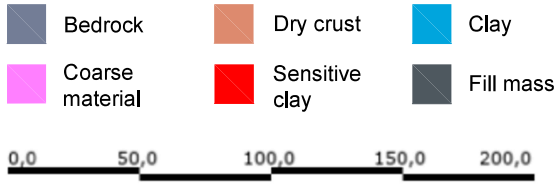

Profile G

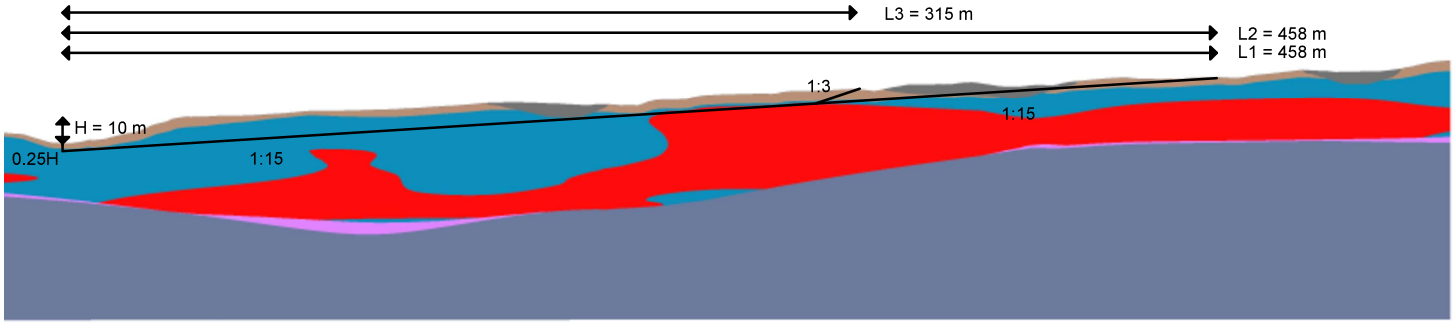

Profile H

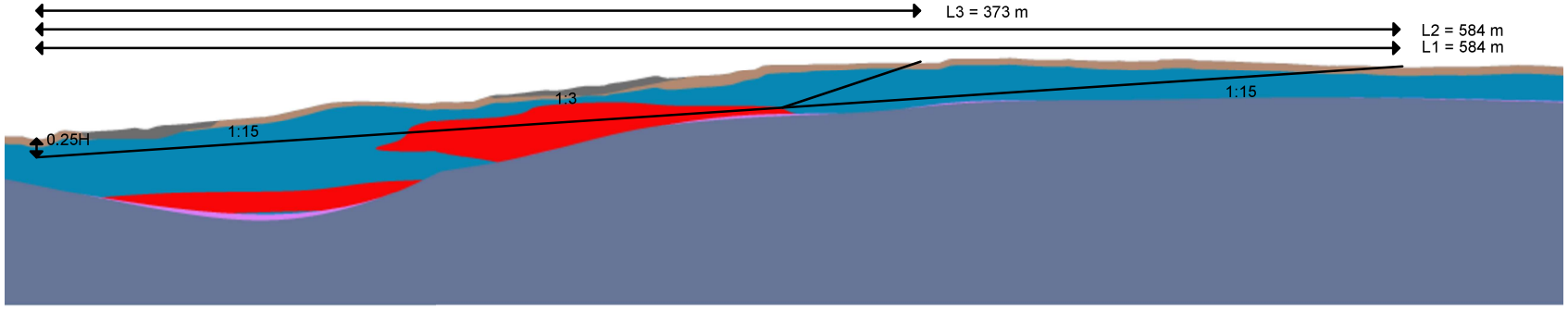

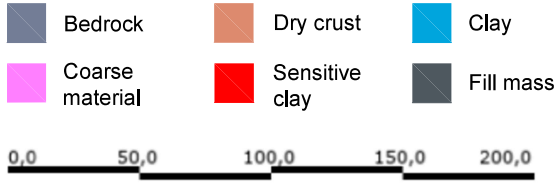

Appendix E

3D MPM Results

Shear strain and velocity for every time step for the three simulations. All time steps are in seconds. Time step t = 110 seconds is missing for the first simulation. All shear strain larger than 1 is displayed as black. All velocity higher than 20 m/s is displaced as red.

Simulation 1: Terrain and Bedrock

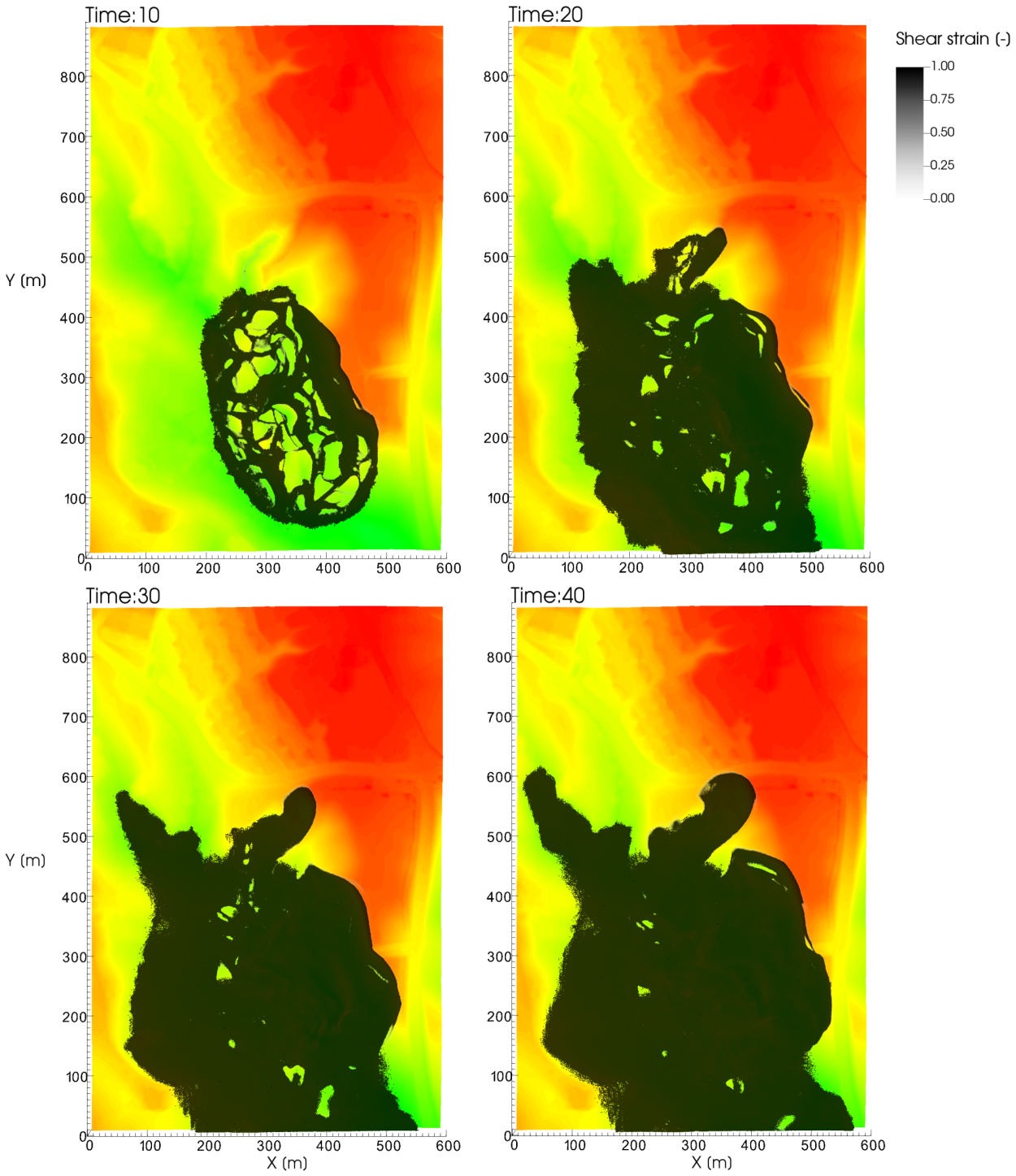

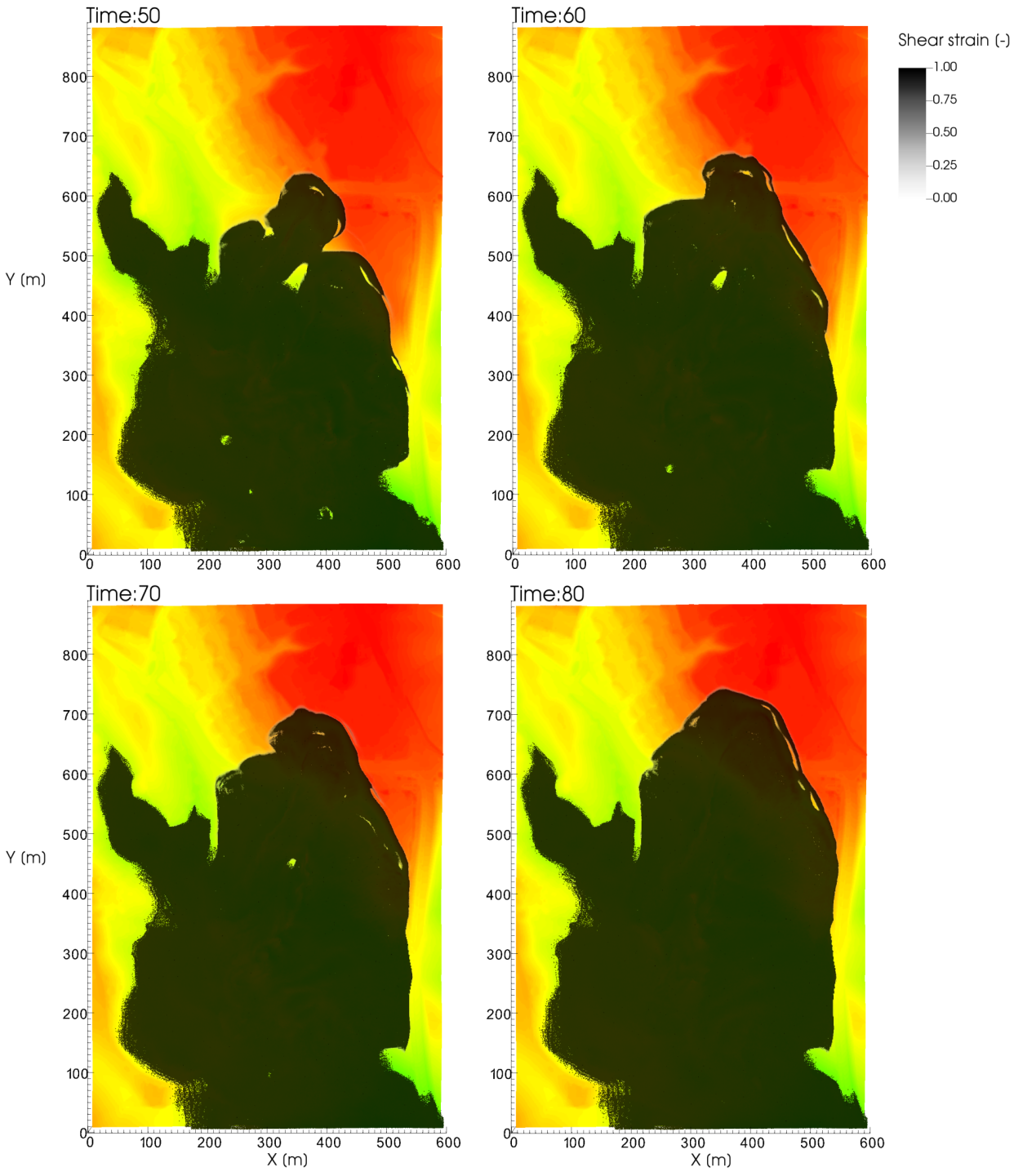
Time:50
Time:60
Time:70
Time:80
Shear strain (-)
1.00
0.75
0.50
0.25
0.00
Y (m)
X (m)
0
100
200
300
400
500
600
700
800

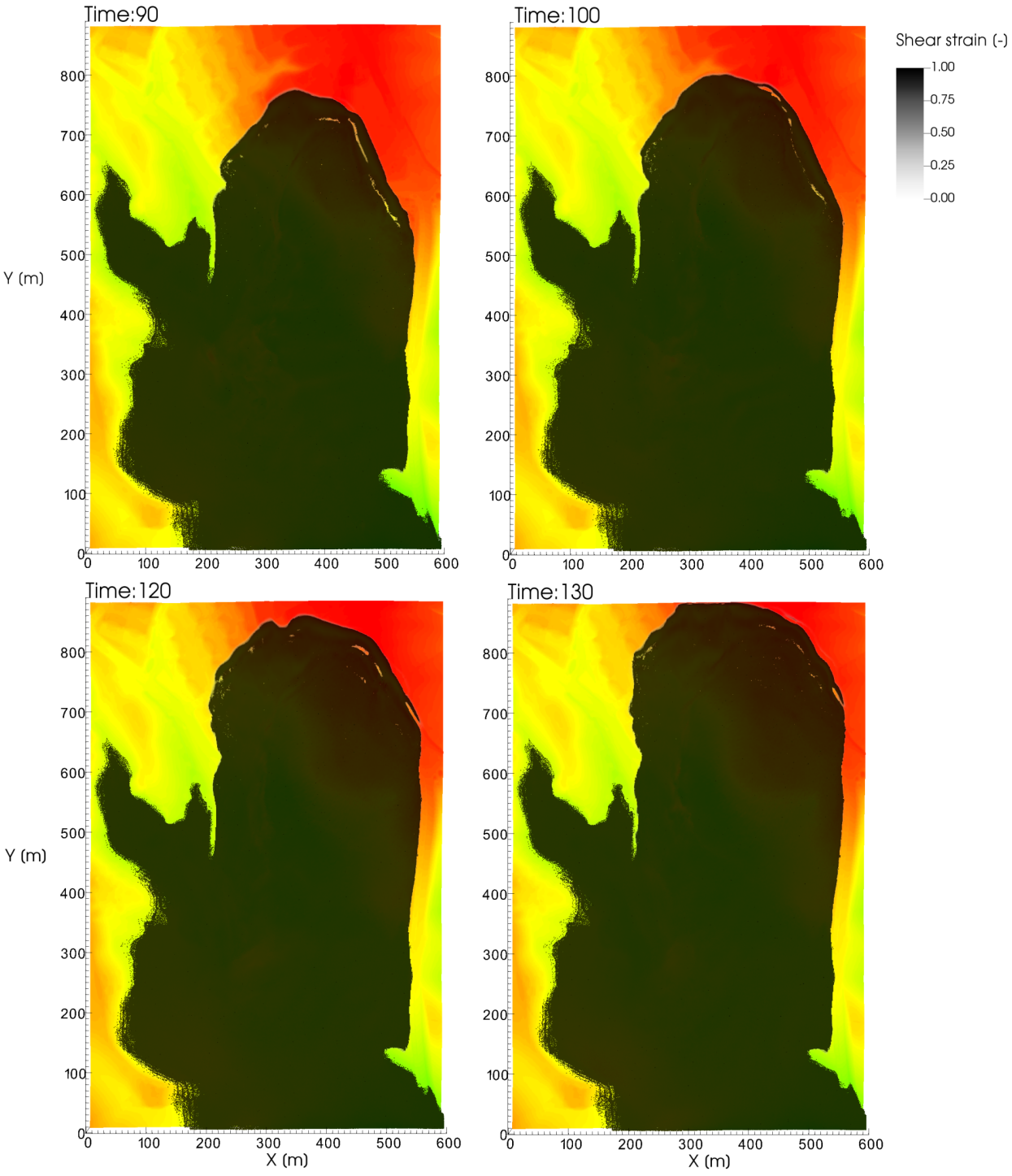
Time:90
Time:100
Time:120
Time:130
Shear strain (-)
1.00
0.75
0.50
0.25
0.00
Y (m)
X (m)
0
100
200
300
400
500
600
700
800

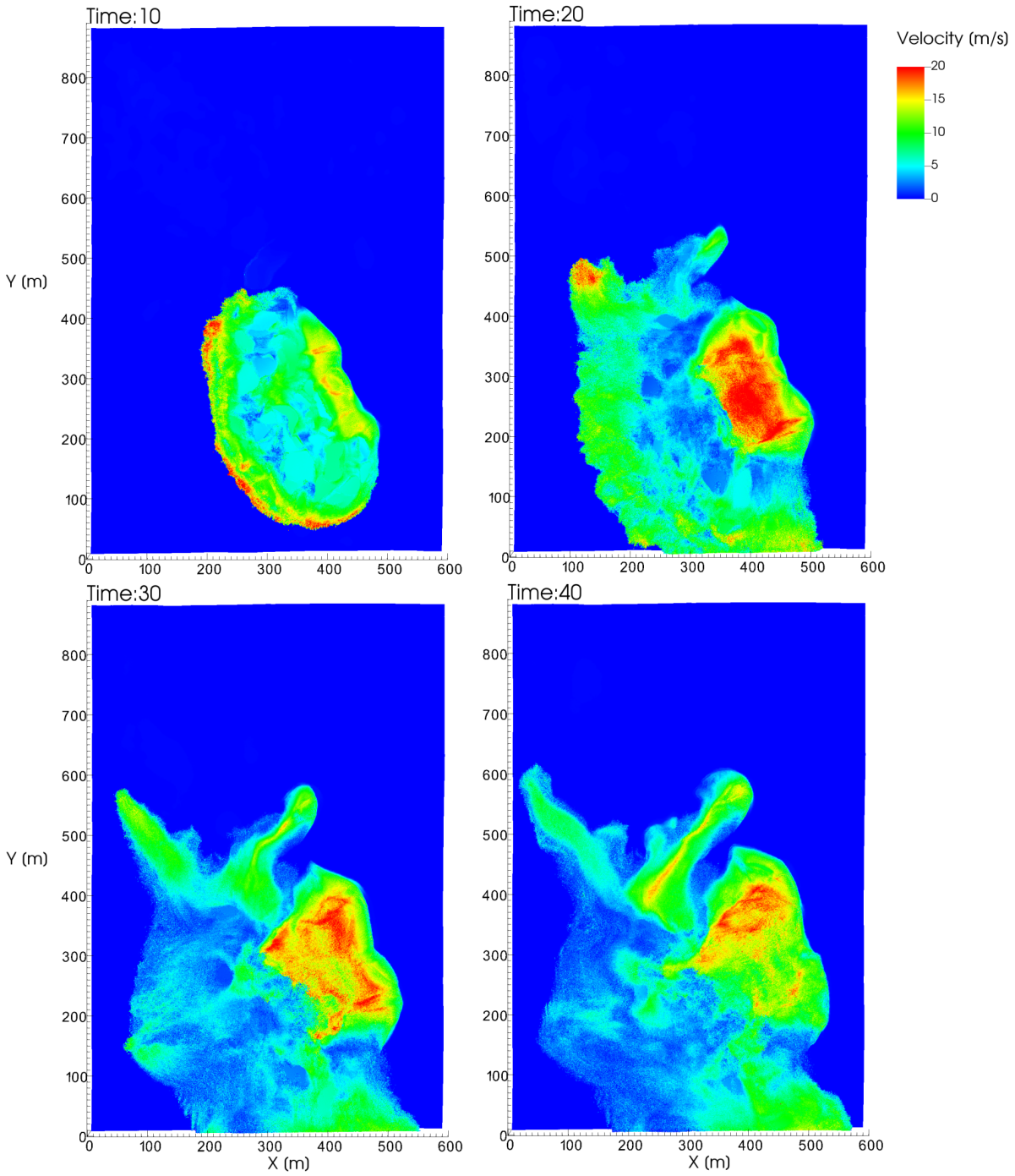
Time:10
Time:20
Time:30
Time:40
Velocity (m/s)
20
15
10
5
0
Y (m)
X (m)
0
100
200
300
400
500
600
700
800

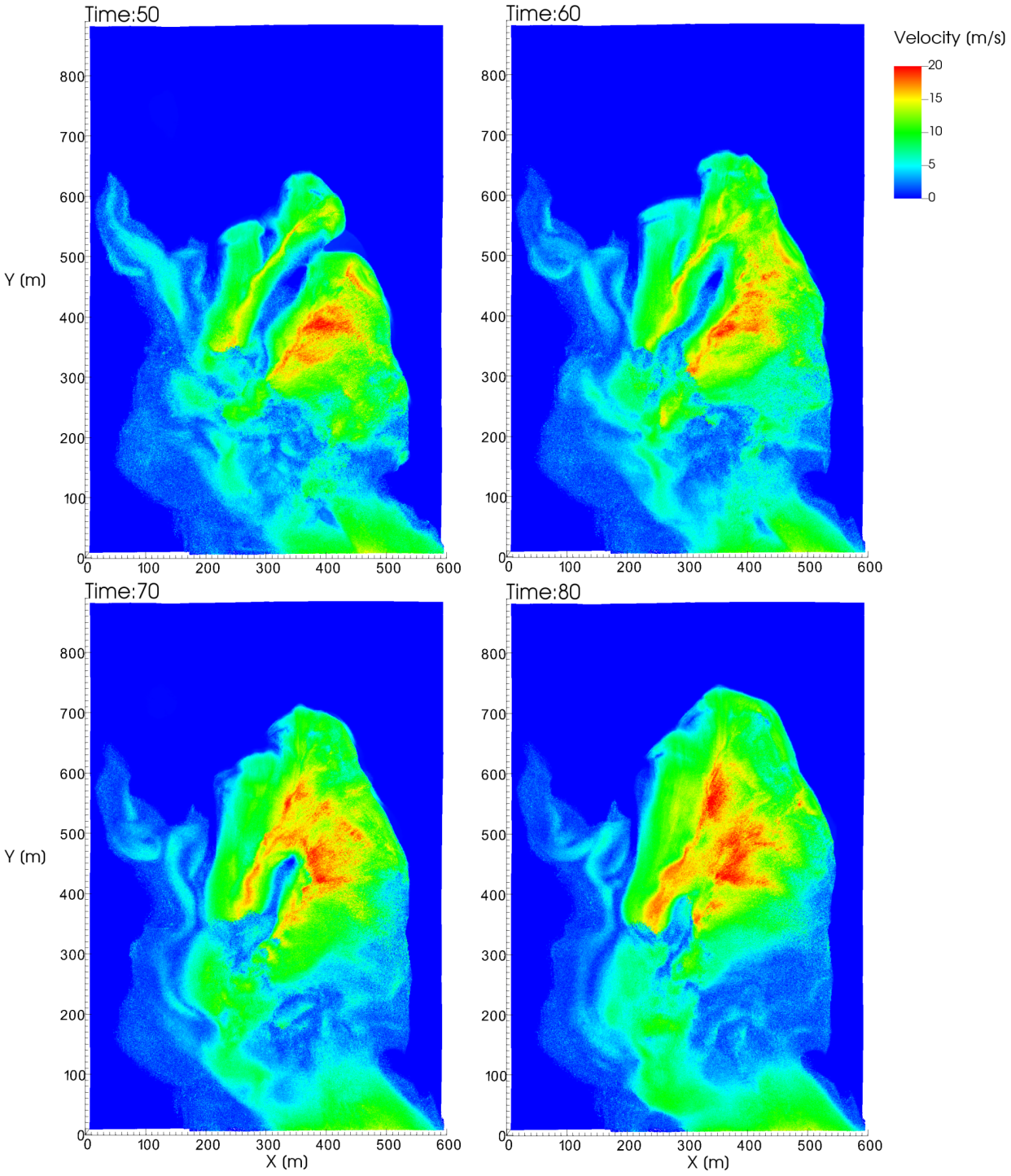
Time:50
Time:60
Time:70
Time:80
Velocity (m/s)
20
15
10
5
0
Y (m)
X (m)
0
100
200
300
400
500
600
700
800

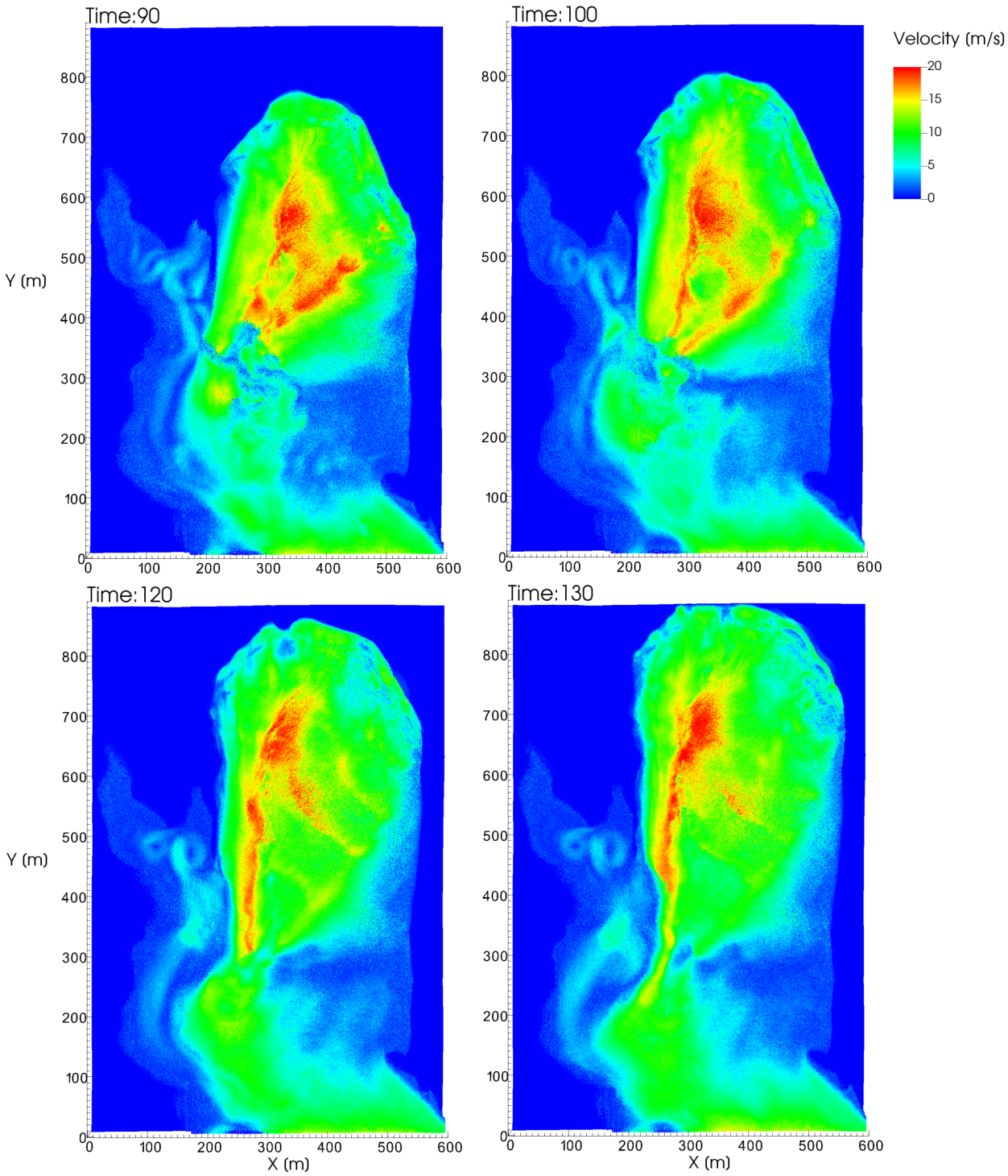
Time:90
Time:100
Time:120
Time:130
Velocity (m/s)
20
15
10
5
0
Y (m)
X (m)
0
100
200
300
400
500
600
700
800

Simulation 2: Terrain, Bedrock and Sensitive Clay Layer, Clay ($S_t = 1$)

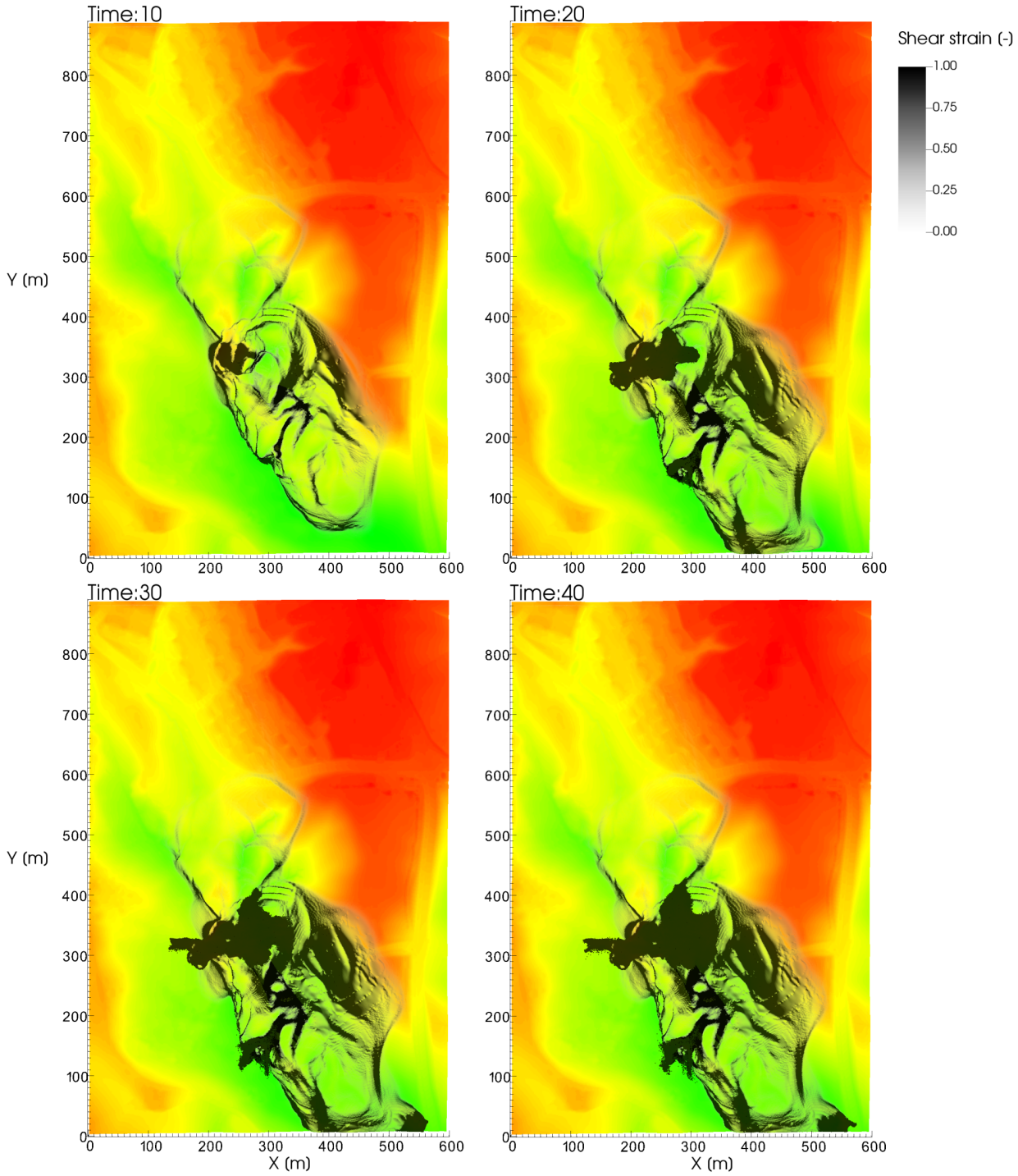

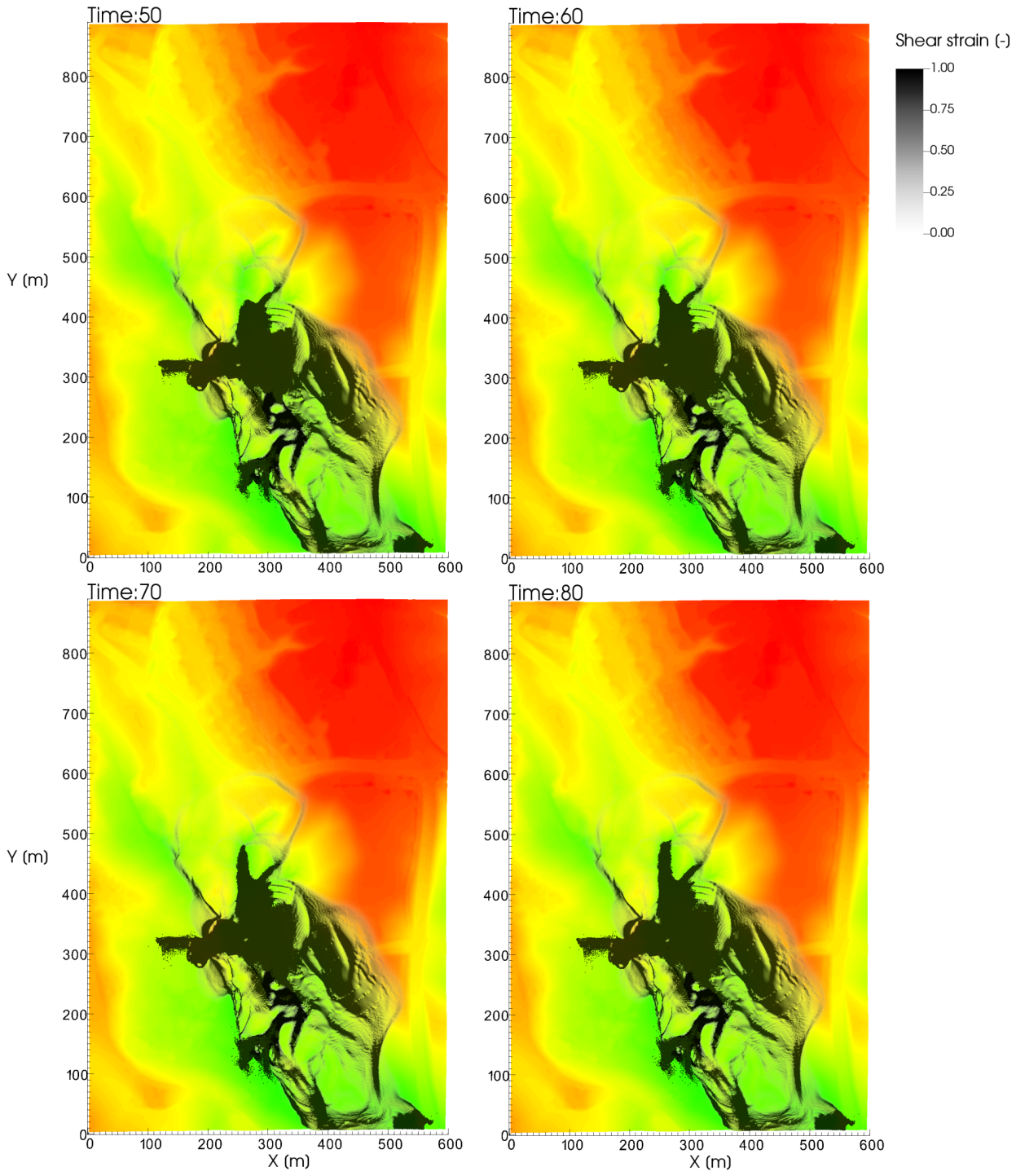
Time:50
Time:60
Time:70
Time:80
Shear strain (-)
1.00
0.75
0.50
0.25
0.00
Y (m)
X (m)
0
100
200
300
400
500
600
700
800

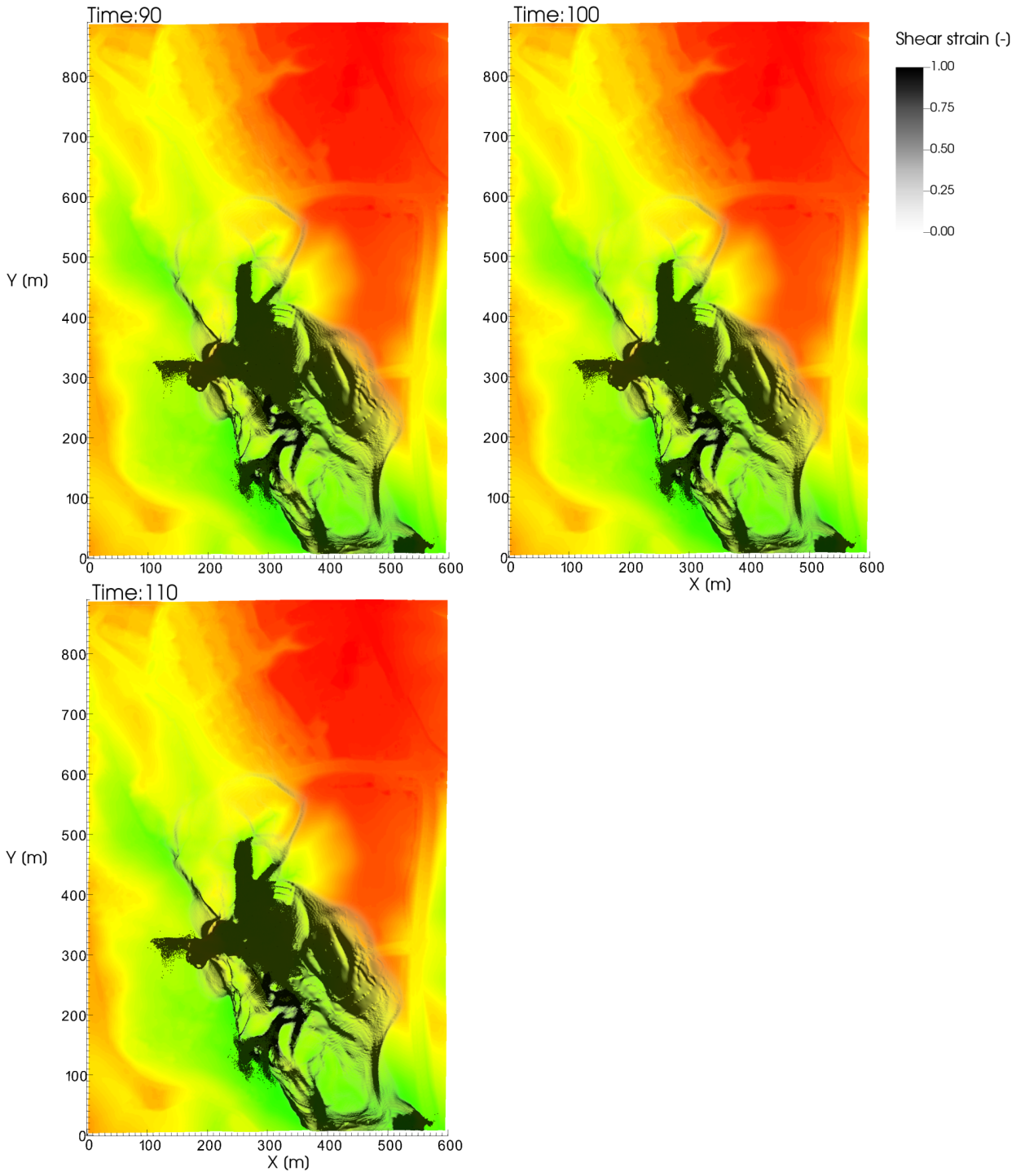
Time:90
Time:100
Time:110
Shear strain (-)
1.00
0.75
0.50
0.25
0.00
Y (m)
X (m)
0
100
200
300
400
500
600
700
800

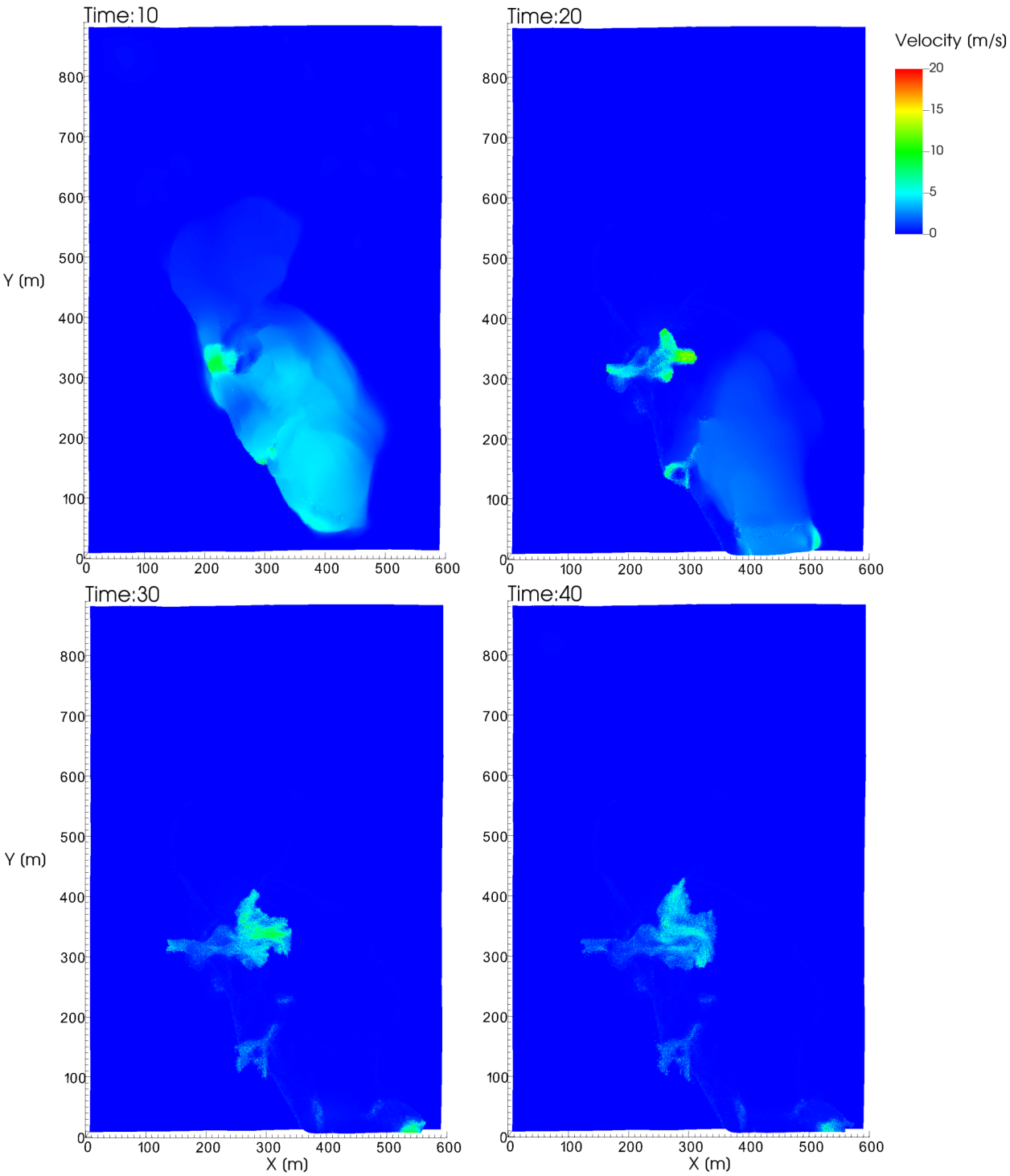
Time:10
Time:20
Time:30
Time:40
Velocity (m/s)
20
15
10
5
0
Y (m)
X (m)
0
100
200
300
400
500
600
700
800

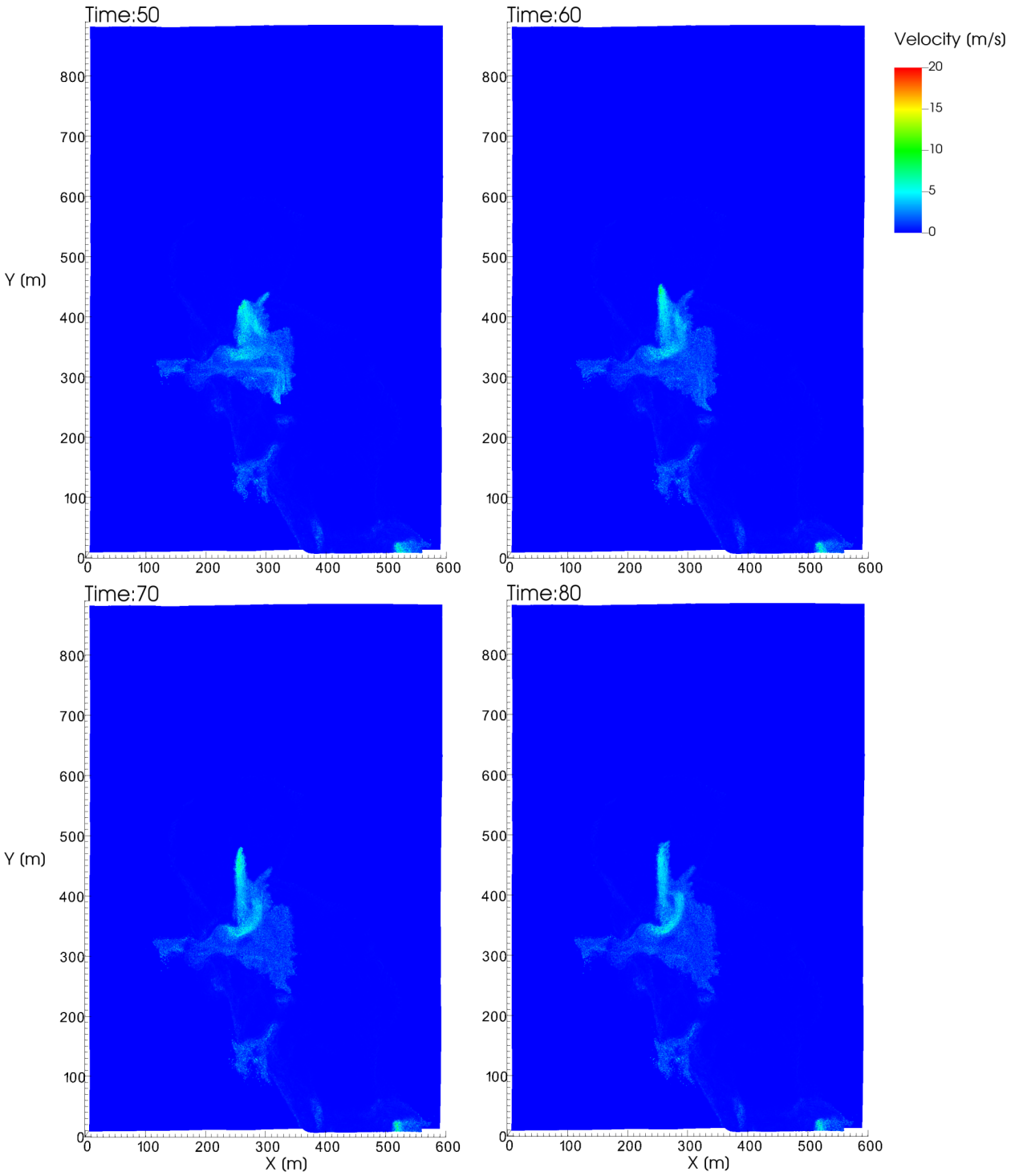
Time:50
Time:60
Time:70
Time:80
Velocity (m/s)
20
15
10
5
0
Y (m)
X (m)
0
100
200
300
400
500
600
700
800

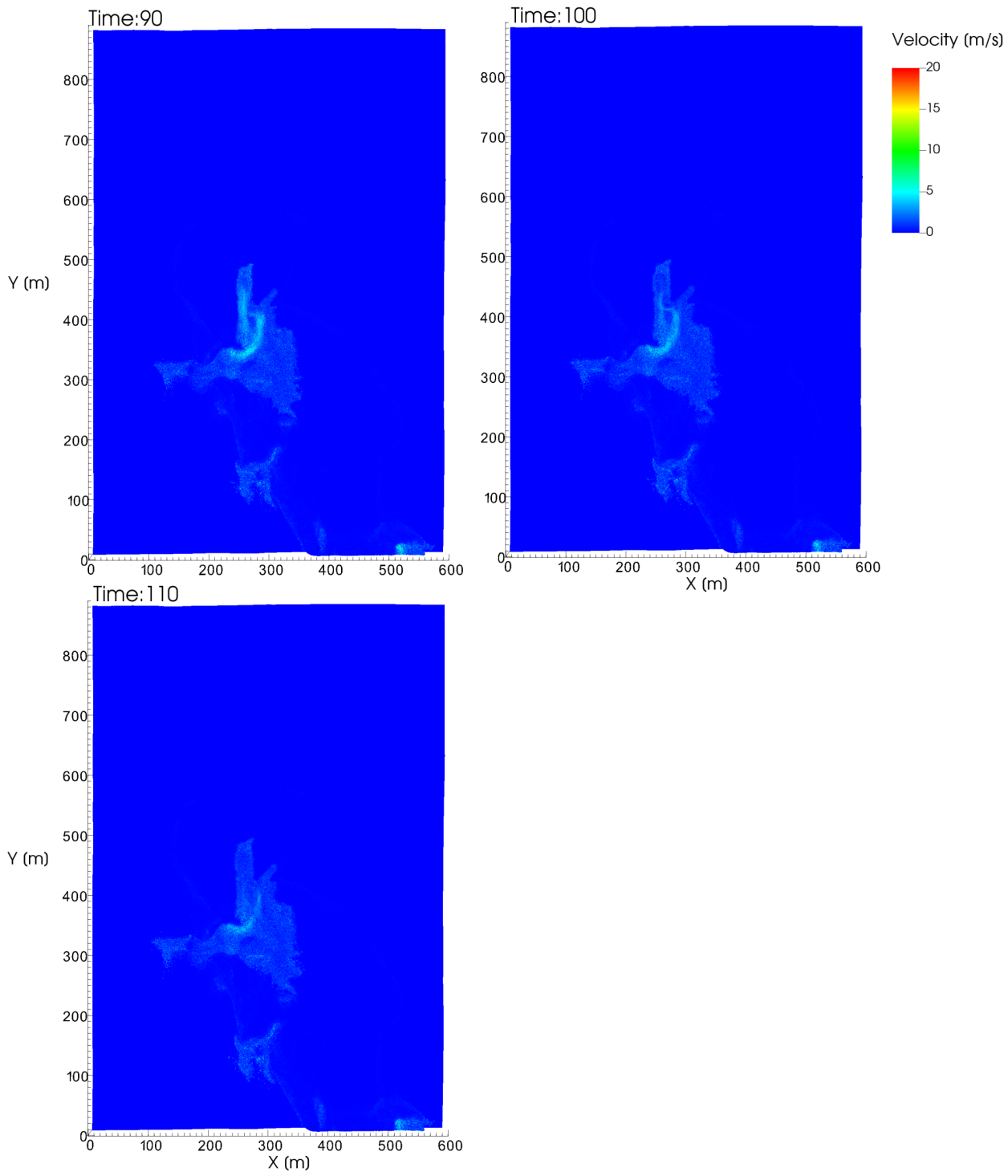
Time:90
Time:100
Time:110
Velocity (m/s)
20
15
10
5
0
Y (m)
X (m)
0
100
200
300
400
500
600
700
800

Simulation 3: Terrain, Bedrock and Sensitive Clay Layer, Clay ($S_t = 2$)

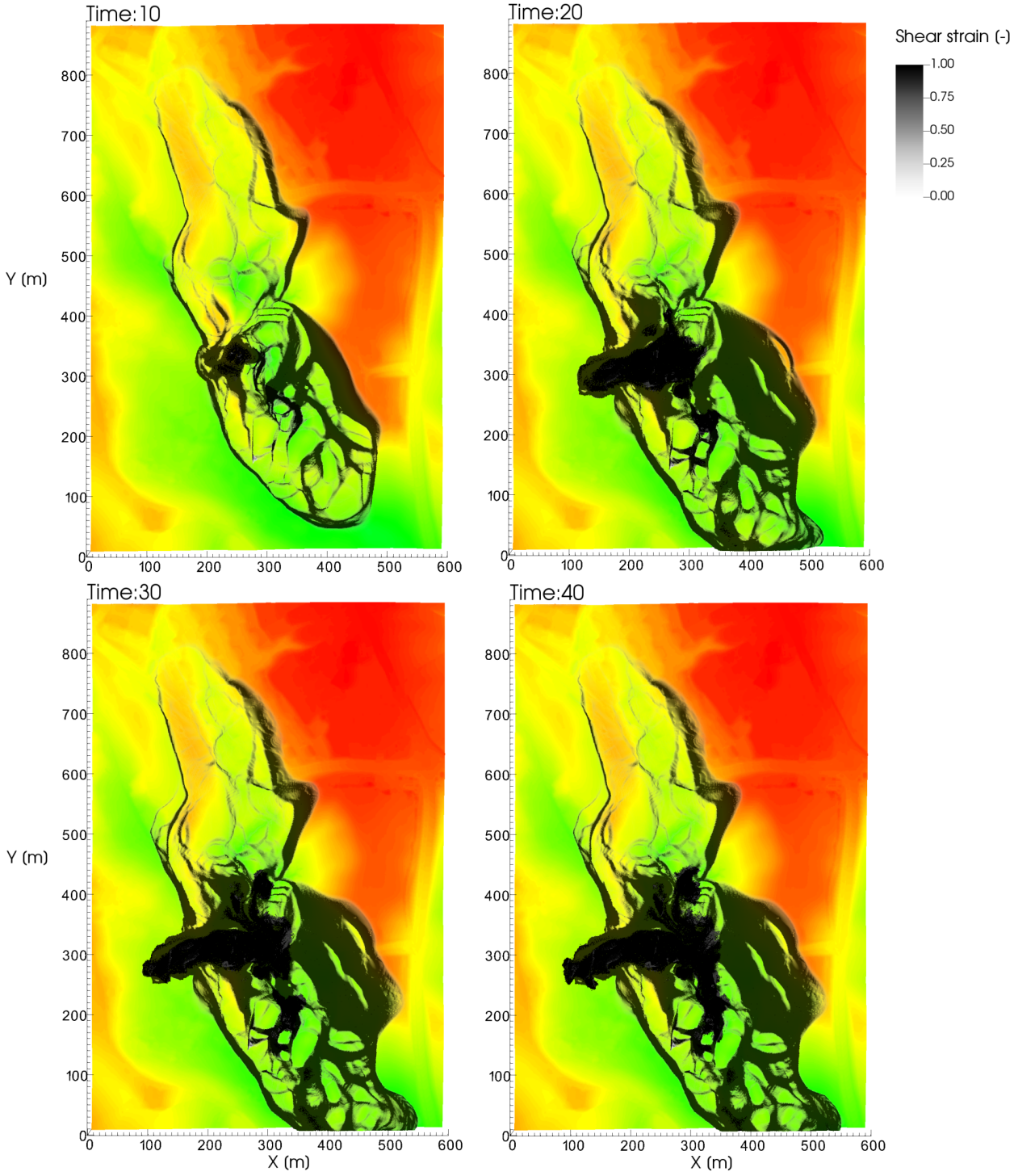

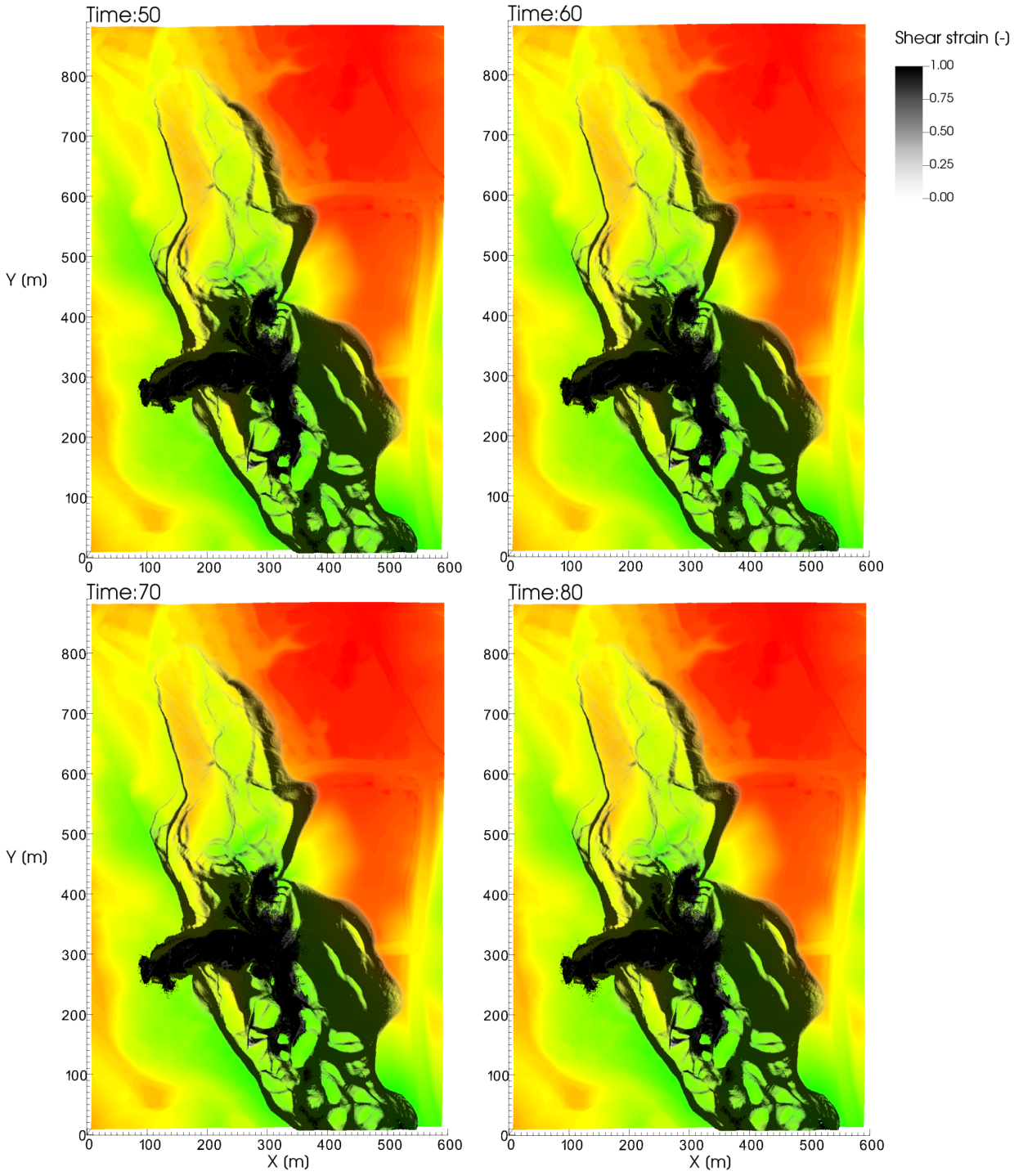
Time:50
Time:60
Time:70
Time:80
Shear strain (-)
1.00
0.75
0.50
0.25
0.00
Y (m)
X (m)
0
100
200
300
400
500
600
700
800

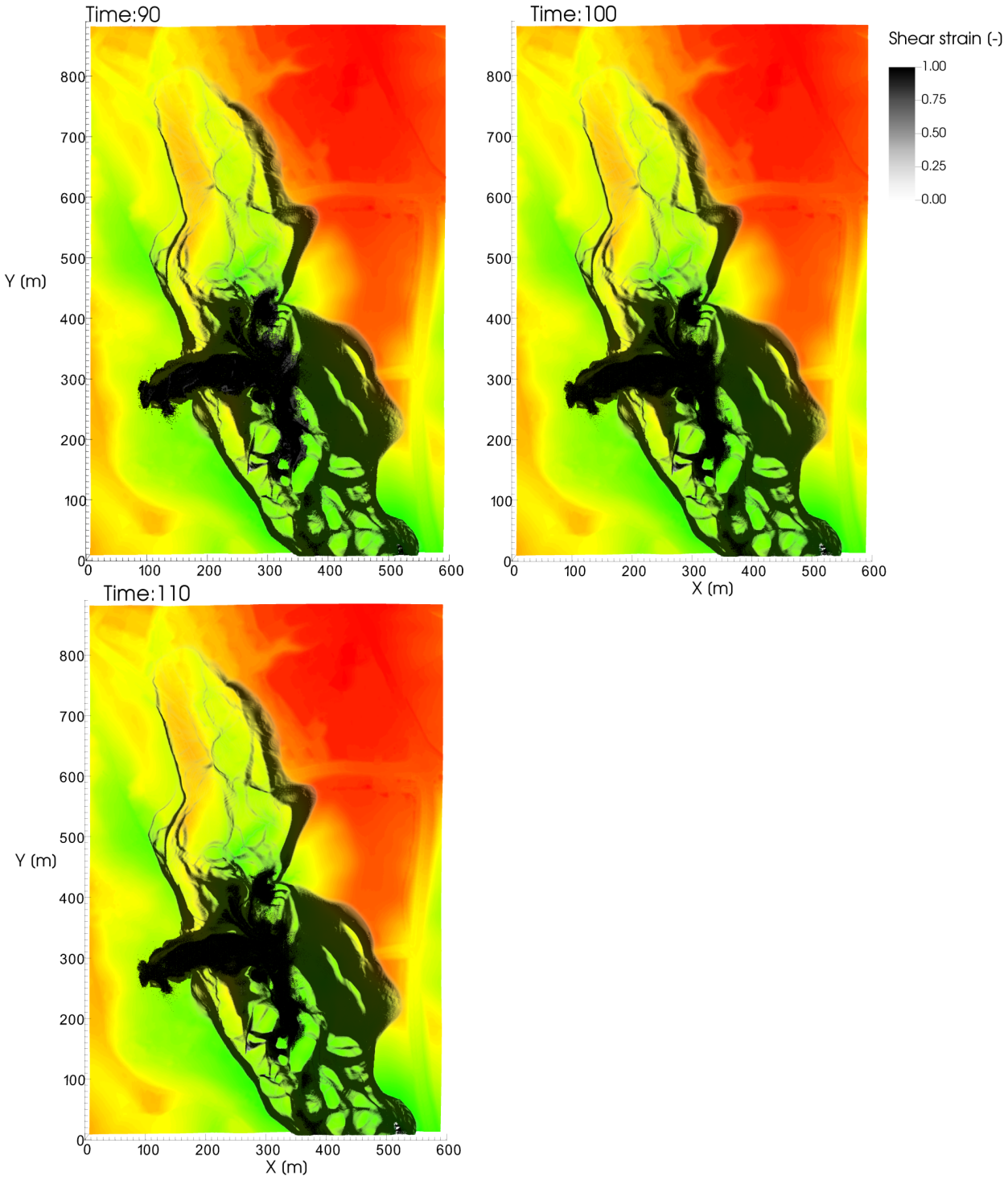
Time:90
Time:100
Time:110
Shear strain (-)
1.00
0.75
0.50
0.25
0.00
Y (m)
X (m)
0
100
200
300
400
500
600
700
800

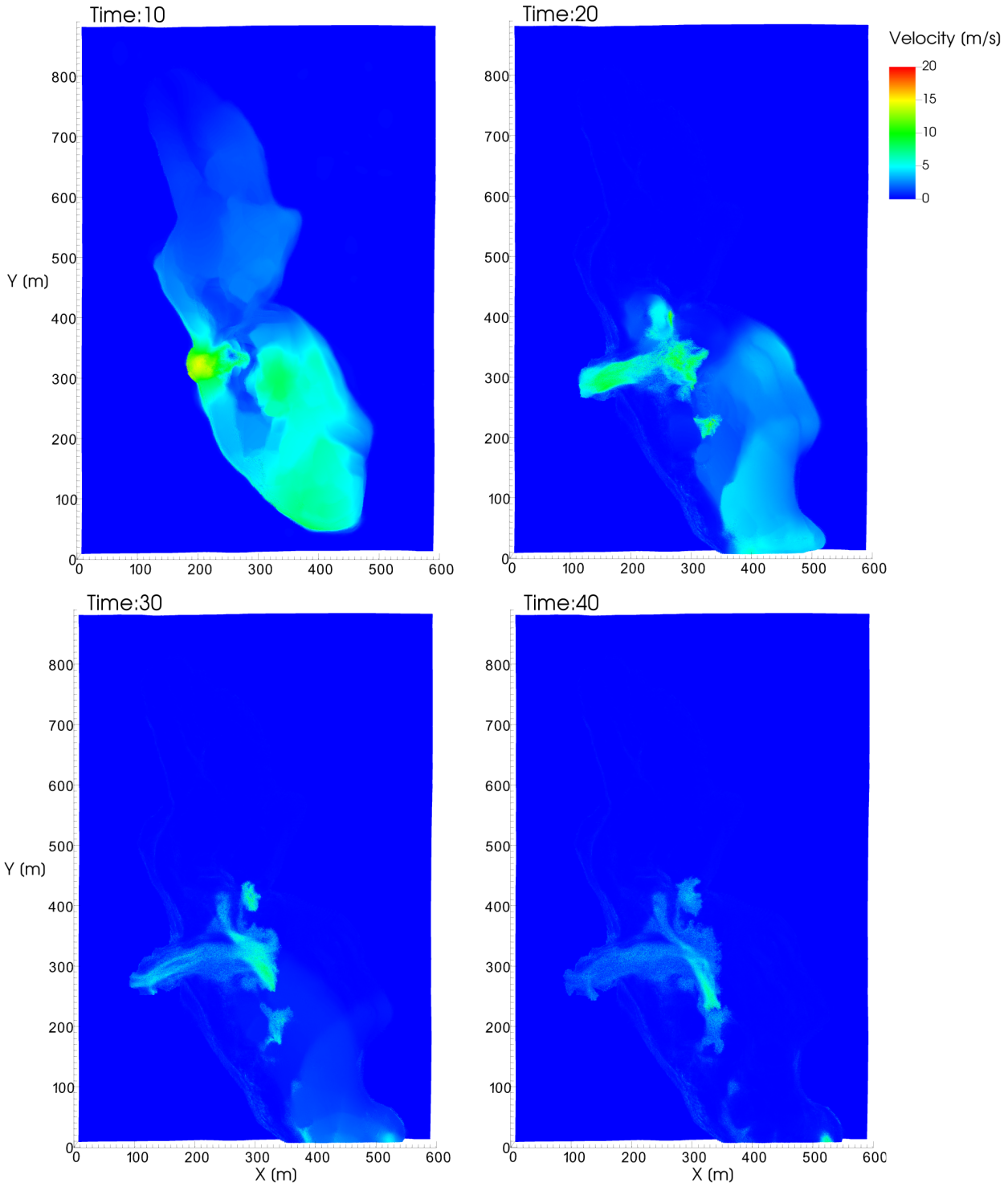
Time:10
Time:20
Time:30
Time:40
Velocity (m/s)
20
15
10
5
0
Y (m)
X (m)
0
100
200
300
400
500
600
700
800

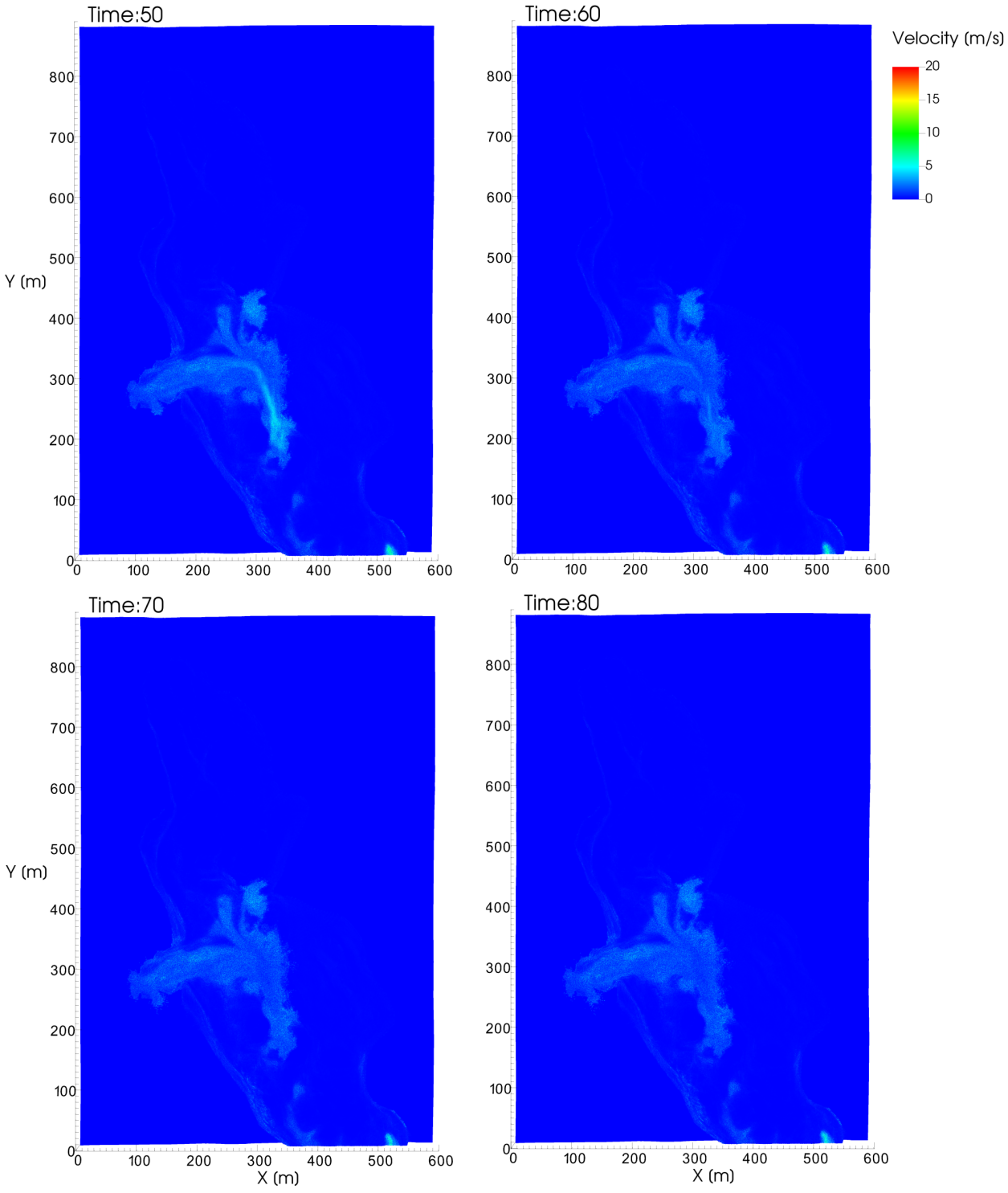
Time:50
Time:60
Time:70
Time:80
Velocity (m/s)
20
15
10
5
0
Y (m)
X (m)
0
100
200
300
400
500
600
700
800

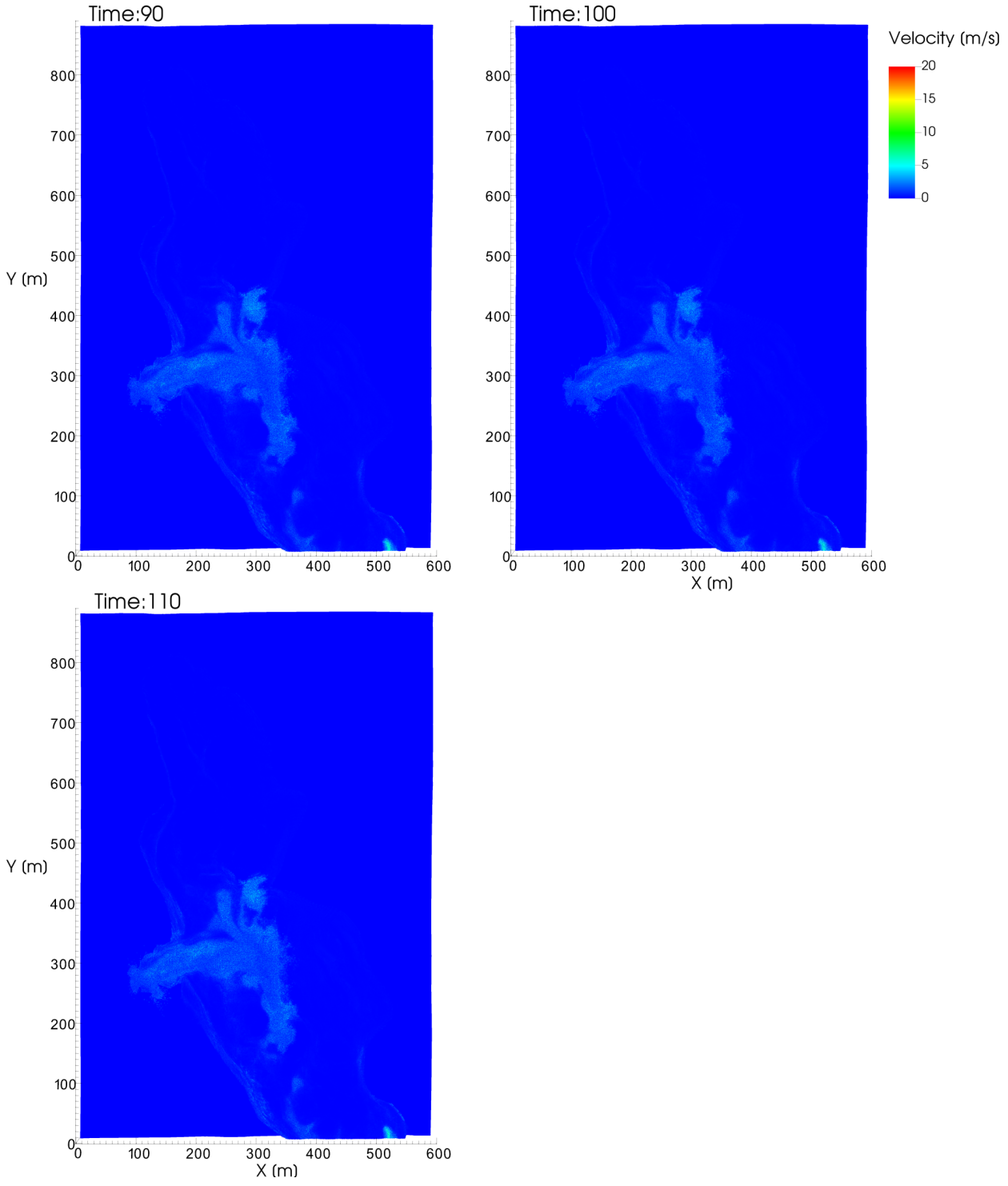
Time:90
Time:100
Time:110
Velocity (m/s)
20
15
10
5
0
Y (m)
X (m)
0
100
200
300
400
500
600
700
800

Agnete Rogstad

Empirical and Numerical Analysis of the Retrogression in the Gjerdrum Landslide

NTNU
Norwegian University of
Science and Technology